arXiv:2512.05117v3 [cs.LG] 5 Oct 2026

The Universal Weight Subspace Hypothesis

Prakhar Kaushik* *pkaushi1@jhu.edu*
Department of Computer Science
Johns Hopkins University, Baltimore, MD, USA

Shravan Chaudhari† *schaud35@jhu.edu*
Department of Computer Science
Johns Hopkins University, Baltimore, MD, USA

Ankit Vaidya† *avaidya7@jhu.edu*
Department of Computer Science
Johns Hopkins University, Baltimore, MD, USA

Rama Chellappa *rchella4@jhu.edu*
Department of Computer Science
Johns Hopkins University, Baltimore, MD, USA

Alan Yuille *ayuille1@jhu.edu*
Department of Computer Science
Johns Hopkins University, Baltimore, MD, USA

Abstract

We show that many deep neural networks trained across diverse tasks exhibit remarkably similar low-dimensional parametric subspaces. We provide the first large-scale empirical evidence that demonstrates that many neural networks systematically converge to shared spectral subspaces regardless of initialization, task, or domain. Through mode-wise spectral analysis of over 1200 models - including 500 Mistral-7B LoRAs, 500 ViTs, and 50 LLaMA models - we identify universal subspaces capturing information in just a few principal directions. Via spectral decomposition of the weight matrices of various architectures trained on a wide range of tasks and datasets, we identify sparse, joint subspaces that are consistently exploited within shared architectures across diverse tasks and datasets. Our findings offer new insights into the intrinsic organization of information within deep networks and raise important questions about the possibility of discovering these universal subspaces without the need for extensive data and computational resources. Furthermore, this inherent structure has significant implications for model reusability, multi-task learning, model merging, and the development of training- and inference-efficient algorithms, potentially reducing the carbon footprint of large-scale neural models.

*Corresponding author: prakhark2@gmail.com
†Equal contribution.
Project page

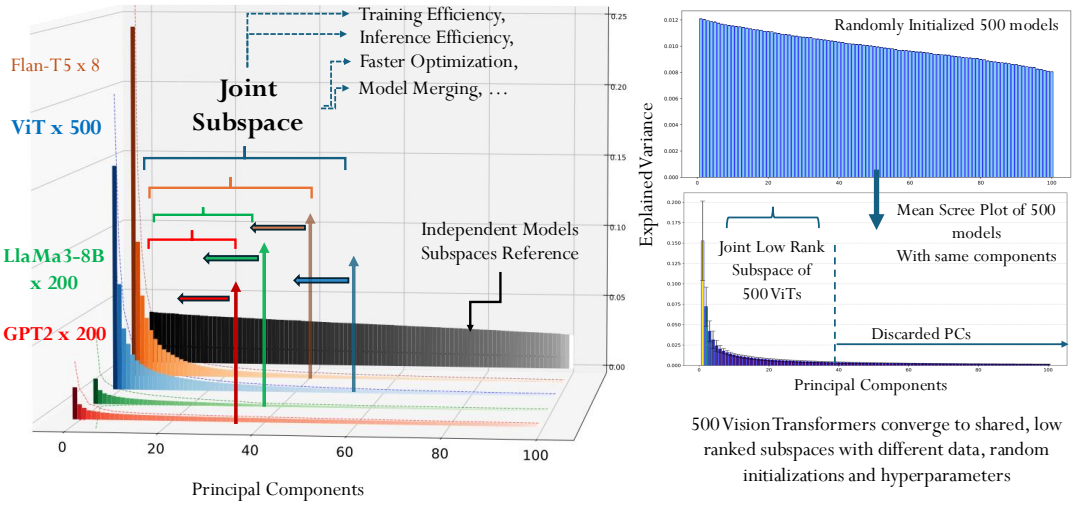


Figure 1: **Deep Networks Exhibit Shared, Low-Rank (Universal) Subspaces.** Across distinct architectures and modalities, neural networks systematically learn to operate within remarkably similar low-dimensional parameter subspaces. **Left:** PCA of ∼200 GPT2, 500 ViTs, 50 LLaMA-8B, & 8 Flan-T5 models reveals consistent sharp spectral decay - strong evidence that a few weight directions capture dominant variance despite vast differences in training data, objectives, and initialization. The black baseline (independent subspaces reference) represents the naive expectation that models would learn distinct directions; our empirical findings contradict this. **Right:** Strikingly, 500 distinct ViT models exhibit a shared low-rank subspace across diverse datasets, training configurations, and domains. This emergent structure unlocks powerful applications: parameter-efficient adaptation, efficient model merging, compressed storage, and accelerated training and inference. Further discussion in Section A.

1 Introduction

We show that many backpropagated neural networks trained on a variety of datasets - which could be disjoint and unrelated, diverse hyper-parameter settings, initializations and regularization methods, often learn an architecture-specific, layer-wise similar, low-rank joint subspace (we refer to this as the Universal Subspace). We provide the first large-scale empirical analysis - across a diverse set of models - that neural networks tend to converge to these joint subspaces, largely independent of their initialization or the specific data used for training. Our study encompasses different model architectures trained on a variety of datasets, even with different loss functions and tasks. Our spectral subspace analysis of the weights of these models (Fig.1) suggests that although individual tasks appear to induce distinct subspaces, individually, they are all part of an unusually low-ranked joint subspace. Our work extends our understanding of what neural networks learn. This universality could explain several puzzling neural properties: why overparameterized models with millions more parameters than training samples still generalize; how different initializations converge to similar representations; and why techniques like weight sharing and parameter-efficient fine-tuning succeed across architectures. If networks indeed learn within shared subspaces, this would provide a supporting explanation for implicit regularization, transferability, and the effectiveness of sparse training methods, while also opening up avenues for applications like merging, new optimization techniques, faster and more efficient learning and inference.

Some prior works have hinted at phenomena consistent with our joint (universal) subspace hypothesis. For example, in the infinite - width limit, training dynamics are governed by a limiting kernel determined by the architecture and initialization distribution (Jacot et al., 2018). Similarly, research into mechanistic interpretability - specifically its own universality hypothesis (Olah et al., 2020; Chughtai et al., 2023) - has uncovered recurring circuits and patterns within specific layers of toy or vision networks, lending indirect support to the concept of universality. Other phenomena, such as the lottery ticket hypothesis (Frankle & Carbin, 2019) and mode connectivity (Garipov et al., 2018), provide further evidence of structure and redundancy in neural-network parameter spaces. Notably, Krizhevsky et al. (2012) observed that the first layer of convolutional networks consistently learns Gabor-like filters on ImageNet. More recently, studies by Guth & Ménard (2024); Guth et al. (2024) have shown initial evidence of recurring eigendirections in certain layers of convolutional neural networks trained on natural images. While Mao et al. (2024) study low-dimensional structure in prediction space, we examine shared subspaces in model weights. Importantly, in contrast to the abstract or speculative notions of universality presented in earlier works like Chughtai et al. (2023); Olah et al. (2020) - which focus primarily on representations and are arguably easier to demonstrate due to direct data dependency - ours is the first work to provide rigorous empirical evidence and a clear universal hypothesis at the *neural parameter* level.

In our analysis, we present compelling empirical evidence for the existence of universal subspaces within model architectures across different modalities and tasks. We initially focus on LoRA adapters due to their ease of training and the ability to collect a large number of adapters for diverse tasks, models, and datasets, which enables robust evaluation of our hypothesis. E.g., we demonstrate the emergence of a universal subspace across approximately 500 LoRA adapters for the Mistral-7B (Jiang et al., 2023) model. We further extend our investigation to the full weight space, where we observe similar universality, extracting sparse, low-rank universal subspaces from about 500 Vision Transformer models and 50 LLaMA3-8B models, each trained on different datasets and initializations. Additional experiments with a trained from scratch ResNet-50, StyleGAN2, and 3D generative models further verify the hypothesis. Although the underlying causes and broader implications of this universal property remain an open area of investigation, even an initial understanding of parameter subspace universality has profound implications for neural network efficiency and interpretability. Shared subspaces could enable: (1) massive model compression by storing only subspace coefficients rather than full weights; (2) rapid adaptation to new tasks within learned subspaces; (3) theoretical insights into generalization bounds and optimization landscapes; and (4) environmental benefits through reduced computational requirements for training and inference.

This geometric universality offers a novel vantage point for investigating fundamental neural properties, including generalization, catastrophic forgetting, and dataset efficiency. Crucially, the pervasive nature of this universal property may underscore the relative primacy of model architecture over other factors in shaping the learned parameter space. We leave open the question of cross-architectural comparison: how do the universal subspaces of distinct architectures differ, and can we explicitly design architectures to optimize the geometry of this subspace? Furthermore, a fundamental question emerges from our results regarding the implications of convergence: if neural networks systematically collapse into the same subspace - thereby inheriting shared biases, capabilities, and failure modes - is this lack of diversity a fundamental bottleneck, and should we develop methods specifically designed to break this convergence? The remainder of this paper is organized as follows. Section 2 explains our analysis methodology and Section 4 presents the comprehensive empirical evidence of the Universal subspaces, including their application to new tasks in Section

4.0.1. Section 3 then gives a conditional analysis of when a shared subspace can be estimated consistently. Section 5 briefly discusses the analysis, providing useful insights and addressing the fundamental questions raised in the introduction. We discuss related work in appendix C.1 and discuss limitations and scope for future work in Section C.6. Our primary contributions include: (1) We empirically demonstrate the existence of a lower-dimensional shared universal subspace in backpropagated neural networks and give a conditional analysis of when such a subspace can be estimated consistently. (2) We illustrate how to learn an approximate low-dimensional shared subspace from available tasks and introduce a data-free metric for assessing the suitability of available models and layers. (3) We show that the universal subspace enables efficient and faster learning, model scaling, and model compression.

2 Universal Subspace Analysis

This analysis constitutes the core contribution of our work. We demonstrate that architecture-specific, layer-wise **universal subspaces** consistently emerge across a diverse array of neural models. In our experiments, adherence to the universal subspace hypothesis appears robust, showing no significant deviation regardless of whether models are trained from scratch, fully finetuned, or adapted via low-rank methods. Furthermore, this phenomenon remains invariant across differing initialization strategies, modalities, data formats, and dataset contents. Notably, however, the fidelity of the extracted subspace correlates with the quantity and quality of the available models. This observation leads us to postulate the existence of an "ideal" universal subspace intrinsic to each architecture, towards which individual model instances converge. We hypothesize that superior algorithms, cleaner data, and more effective optimization strategies enable models to approximate this ideal more closely. While we do not formally verify the "ideal universal subspace" hypothesis in the present work, leaving it for future investigation, we suggest that this subspace represents the most stable configuration for contemporary neural networks trained via backpropagation. Consequently, exceptions to this rule may offer fertile ground for further research.

Analysis methodology We introduce a data-free heuristic to assess whether the available models support a reliable universal subspace approximation. Following Martin & Hinrichs (2025), we use the layer-wise heavy-tail exponent α as a proxy for training quality. Our layer score q_l combines the number of models, the fraction with $2 \leq \alpha \leq 6$, and the variability of α across models. Geometric means over all and selected layers give the architecture-level scores q_{all} and q_{arch}, respectively. Higher scores favor larger, better-trained, spectrally consistent collections. These scores guide layer selection and flag potentially unreliable approximations; details are in Section B.1.

Since there is no current method that enables us to compare subspaces of models with different architectures, we focus on large number of models trained on the same architecture. To this end, we perform analysis using Low rank adapters (Hu et al., 2021) (LoRA) as well as classical weights of transformer and CNN (Convolutional Neural Network) architectures. For all our experiments, unless stated otherwise, we perform Order 1-2 HOSVD De Lathauwer et al. (2000) only (i.e., $|\mathcal{P}| \in \{1, 2\}$ in Algorithm 1), to ensure that our methodology works even in the simplest case. Algorithm 1 provides the algorithm we implement. Refer to Section C.3 for discussion regarding secondary subspace and how to choose the number of top components. Throughout the paper, *Universal Subspace* refers to the shared linear subspace of the zero-centered weights. In the original parameter coordinates, the corresponding reconstruction set is the affine space obtained by adding the mean $\boldsymbol{\mu}$ of Algorithm 1, broadcast to the weight shape.

Algorithm 1 Truncated Zero-Centered Shared HOSVD

Require: M aligned model weight tensors $\{W^{(m)}\}_{m=1}^{M}$, $W^{(m)} \in \mathbb{R}^{I_1 \times \cdots \times I_P}$; set of decomposed parameter modes $\mathcal{P} \subseteq \{1, \ldots, P\}$; explained-variance threshold τ.

Ensure: Mean $\boldsymbol{\mu}$; shared factors $U^{(p)} \in \mathbb{R}^{I_p \times \hat{r}_p}$ (orthonormal columns) for $p \in \mathcal{P}$; model-specific cores $\{\mathcal{C}^{(m)}\}_{m=1}^{M}$.

Stack the models: $\mathcal{X} \in \mathbb{R}^{M \times I_1 \times \cdots \times I_P}$.
Zero-centering: $\boldsymbol{\mu} \leftarrow$ mean of $\mathcal{X}$ over the model axis and all modes $j \notin \mathcal{P}$ ▷ feature-wise mean
$X_c^{(m)} \leftarrow W^{(m)} - \boldsymbol{\mu}$ for $m = 1, \ldots, M$ ▷ broadcast $\boldsymbol{\mu}$ to $I_1 \times \cdots \times I_P$
for $p \in \mathcal{P}$ **do**
    $X_{c,(p)} \leftarrow$ mode-p unfolding of the centered stacked tensor ▷ $X_{c,(p)} \in \mathbb{R}^{I_p \times M \prod_{j \neq p} I_j}$
    Compute thin SVD: $X_{c,(p)} = \tilde{U}^{(p)} \Sigma^{(p)} \tilde{V}^{(p)\top}$
    $\hat{r}_p \leftarrow$ smallest rank whose cumulative explained variance is at least τ
    $U^{(p)} \leftarrow \tilde{U}^{(p)}(:, 1{:}\hat{r}_p)$
end for
for $m = 1$ **to** M **do**
    $\mathcal{C}^{(m)} \leftarrow X_c^{(m)} \times_p U^{(p)\top}$ for all $p \in \mathcal{P}$ ▷ project onto the shared factors
end for
return $\boldsymbol{\mu}$, $\{U^{(p)}\}_{p \in \mathcal{P}}$, $\{\mathcal{C}^{(m)}\}_{m=1}^{M}$

A model is reconstructed as $\widehat{W}^{(m)} = \boldsymbol{\mu} + \mathcal{C}^{(m)} \times_p U^{(p)}$ for all $p \in \mathcal{P}$, where $\times_p$ denotes mode-p tensor–matrix multiplication and modes not in $\mathcal{P}$ are left uncompressed. The model/task axis is used only to estimate the shared factors and is not itself compressed. With a single decomposed mode ($|\mathcal{P}| = 1$), the procedure is PCA on the mode-p fibers of all models (Section B.5).

3 Conditional Analysis of Shared-Subspace Estimation

This section gives conditional theoretical motivation for our methodology; it does not prove universality for the networks we study, which is an empirical claim (Section 4). Following kernel analyses of deep networks (Ortiz-Jimenez et al., 2023; Wei et al., 2019; Chen & Xu, 2021; Belfer et al., 2024; Bietti et al., 2019), we model each task's ground-truth predictor $f_t^\star$ as an element of a Hilbert space, e.g., a reproducing kernel Hilbert space (RKHS). We ask when the dominant subspace of the task second-moment operator $\mathcal{S}$ can be estimated consistently from predictors $\hat{f}_t$ learned on finitely many tasks with finitely many samples each, and then when this function-space object corresponds to what Algorithm 1 computes on weights.

Setup. Let $(\mathcal{H}, \langle \cdot, \cdot \rangle)$ be a separable Hilbert space with norm $\|\cdot\| = \|\cdot\|_{\mathcal{H}}$. For $a, b \in \mathcal{H}$, the rank-one operator $a \otimes b : \mathcal{H} \to \mathcal{H}$ is $(a \otimes b)g = \langle b, g \rangle\, a$; in particular $\|a \otimes b\|_{\mathrm{op}} = \|a\|\,\|b\|$. Tasks $t \in \{1, \ldots, T\}$ are drawn i.i.d. from a distribution $\mathcal{T}$, and each task dataset $S_t = \{(x_{t,i}, y_{t,i})\}_{i=1}^{n_t}$ with n_t samples is drawn independently from D_t. Let $f_t^\star \in \mathcal{H}$ denote the (unknown) ground-truth predictor for task t and $\hat{f}_t \in \mathcal{H}$ be the learned predictor for the task.

Definition 3.1 (Task second-moment operator)**.** The *population*, *true empirical*, and *learned empirical* task second-moment operators are respectively,

$$\mathcal{S} := \mathbb{E}_{t\sim\mathcal{T}}[\, f_t^\star \otimes f_t^\star \,], \qquad \hat{\mathcal{S}} := \frac{1}{T}\sum_{t=1}^{T} f_t^\star \otimes f_t^\star, \qquad \tilde{\mathcal{S}} := \frac{1}{T}\sum_{t=1}^{T} \hat{f}_t \otimes \hat{f}_t.$$

where $\mathcal{S}, \hat{\mathcal{S}}, \tilde{\mathcal{S}}$ are self-adjoint and positive semi-definite such that $\mathrm{tr}(\mathcal{S}) < \infty$. Its top-$k$ eigenspace $\mathcal{H}_k^\star$ is the population rank-k *shared subspace* of tasks.

Remark 3.2. Algorithm 1 centers the weights; all results below extend to the centered covariance $\mathcal{S} - m \otimes m$, $m := \mathbb{E} f_t^\star$, at the same rates (Corollary 3.8).

Let $\lambda_1 \geq \lambda_2 \geq \cdots$ be the eigenvalues of $\mathcal{S}$ with orthonormal eigenvectors $\{\phi_i\}_{i\geq 1}$. Write $P_k = \sum_{i=1}^{k} \phi_i \otimes \phi_i$ for the projector onto the population top-k subspace $\mathcal{H}_k^\star = \mathrm{span}\{\phi_1, \ldots, \phi_k\}$, and let $\tilde{P}_k$ be the projector onto the top-k eigenspace of $\tilde{\mathcal{S}}$ (the learned shared subspace). Define the eigengap $\gamma_k := \lambda_k - \lambda_{k+1} > 0$.

Assumption 3.3 (Realizability and bounded second moment)**.** *For a constant $B > 0$ and for all tasks, $f_t^\star \in \mathcal{H}$ almost surely and $\|f_t^\star\| \leq B$ a.s. In particular, $\mathbb{E}_{t\sim\mathcal{T}} \|f_t^\star\|^2 = \mathrm{tr}(\mathcal{S}) \leq B^2 < \infty$.*

Assumption 3.4 (Per-task estimation accuracy in $\mathcal{H}$)**.** *For each task t and confidence level $\delta_t \in (0,1)$, the learning procedure satisfies*

$$\Pr\Big(\Big\|\hat{f}_t - f_t^\star\Big\| \leq \eta_t(n_t, \delta_t)\Big) \;\geq\; 1 - \delta_t,$$

where the probability is over the draw of S_t. We write $\eta_t := \eta_t(n_t, \delta_t)$.

We keep η_t abstract; its rate in n_t depends on the learning procedure (see the remark in Section A.1).

The main result combines two ingredients: concentration of the empirical task operator across tasks, and a Davis–Kahan perturbation bound that transfers operator error to subspace error (proofs in Section A.1).

Lemma 3.5 (Concentration of the empirical second-moment operator)**.** *Under Assumption 3.3, for any $\delta_T \in (0,1)$, with probability at least $1 - \delta_T$,*

$$\Big\|\hat{\mathcal{S}} - \mathcal{S}\Big\|_{\mathrm{op}} \;\leq\; \frac{B^2}{\sqrt{T}}\left(1 + \sqrt{2\ln(1/\delta_T)}\right).$$

Lemma 3.6 (Davis–Kahan, sin-Θ)**.** *Let $\gamma_k > 0$. Then*

$$\big\|\tilde{P}_k - P_k\big\|_{\mathrm{op}} \;\leq\; \frac{2}{\gamma_k}\,\big\|\tilde{\mathcal{S}} - \mathcal{S}\big\|_{\mathrm{op}}.$$

using definition of γ_k from definition 3.1.

Theorem 3.7 (Two-level convergence to the shared subspace)**.** *Assume 3.3–3.4. There exist absolute constants $c_1, c_2 > 0$ (e.g., $c_1 = 3$, $c_2 = 2$) such that the following holds. For any $\delta \in (0,1)$, choose $\delta_t = \delta/(2T)$ and set $\delta_T = \delta/2$. With probability at least $1 - \delta$ (over tasks and all per-task samples),*

$$\big\|\tilde{\mathcal{S}} - \mathcal{S}\big\|_{\mathrm{op}} \;\leq\; c_1 B^2 \sqrt{\frac{\log(c_2/\delta)}{T}} \;+\; (2B\bar{\eta} + \overline{\eta^2}) \tag{1}$$

If moreover $\gamma_k > 0$, then

$$\left\|\tilde{P}_k - P_k\right\|_{\mathrm{op}} \;\le\; \frac{2}{\gamma_k}\left(c_1 B^2\sqrt{\frac{\log(c_2/\delta)}{T}} + (2B\bar{\eta} + \overline{\eta^2})\right). \tag{2}$$

where $\bar{\eta} = \frac{1}{T}\sum_{t=1}^{T}\eta_t$, $\overline{\eta^2} = \frac{1}{T}\sum_{t=1}^{T}\eta_t^2$, and η_t is as in Assumption 3.4.

Theorem 3.7 (proof in Section A.1) separates across-task error, which decays as $T^{-1/2}$, from per-task error ($\bar{\eta}$, $\overline{\eta^2}$); a larger eigengap γ_k stabilizes recovery. The theorem concerns estimation only: it does not imply that the spectral tail $\sum_{i>k}\lambda_i$ is small, i.e., that a low-rank shared subspace exists. That is the empirical question of Section 4; Corollary 3.11 keeps the tail as irreducible error.

Since Algorithm 1 centers the weights, we also state the analogous guarantee for the centered covariance.

Corollary 3.8 (Centered covariance)**.** *Let $m := \mathbb{E}_{t\sim\mathcal{T}} f_t^\star$, $\mathcal{C} := \mathbb{E}_{t\sim\mathcal{T}}[(f_t^\star - m)\otimes(f_t^\star - m)] = \mathcal{S} - m\otimes m$, and $\tilde{\mathcal{C}} := \frac{1}{T}\sum_{t=1}^{T}(\hat{f}_t - \bar{f})\otimes(\hat{f}_t - \bar{f})$ with $\bar{f} := \frac{1}{T}\sum_{t=1}^{T}\hat{f}_t$. Under Assumptions 3.3–3.4, for any $\delta\in(0,1)$ and with $\delta_t = \delta/(2T)$, with probability at least $1-\delta$,*

$$\left\|\tilde{\mathcal{C}} - \mathcal{C}\right\|_{\mathrm{op}} \;\le\; \left(9B^2 + 3B\bar{\eta}\right)\sqrt{\frac{\ln(4/\delta)}{T}} \;+\; 4B\bar{\eta} + 2\,\overline{\eta^2}.$$

Lemma 3.6, applied to $\mathcal{C}$ with its own eigengap, then bounds the distance between the top-k eigenspaces of $\tilde{\mathcal{C}}$ and $\mathcal{C}$ at the same rate.

From functions to weights. The theorem concerns predictors, whereas Algorithm 1 decomposes weights. Proposition 3.9 shows that the two coincide in an idealized regime matching collections fine-tuned from shared pretrained weights θ_0: for models linearized around θ_0, with $\mathcal{H}$ the RKHS of the tangent kernel at θ_0, the centered covariance of the predictors is unitarily equivalent to the covariance of the function-relevant part of the weights, which is all of it under gradient training from θ_0. PCA of model-wise centered weights then estimates the centered operator of Theorem 3.7, and centering removes θ_0. Algorithm 1 departs from this regime in three ways: it decomposes each mode separately, which captures the top eigenspace of the full weight covariance only under extra structure (e.g., separability across modes); it centers feature-wise; and several of our collections are trained from scratch, without a shared θ_0. We therefore use the analysis as conditional motivation, not as a proof of universality.

Proposition 3.9 (Weight-space correspondence in the linearized regime)**.** *Let all models share reference weights $\theta_0\in\mathbb{R}^p$ and be linearized around them, $f_\theta(x) = f_{\theta_0}(x) + \langle\phi(x), \theta-\theta_0\rangle$ with $\phi(x) := \nabla_\theta f_\theta(x)|_{\theta=\theta_0}$. Let $\mathcal{H}$ be the RKHS of the tangent kernel $K(x,x') := \langle\phi(x),\phi(x')\rangle$, let $V := \mathrm{span}\{\phi(x) : x\in\mathcal{X}\}\subseteq\mathbb{R}^p$ with orthogonal projector P_V, and define $\Phi:\mathbb{R}^p\to\mathcal{H}$ by $(\Phi u)(x) := \langle\phi(x), u\rangle$. Then:*

(i) $\|\Phi u\|_{\mathcal{H}} = \|P_V u\|$ for all $u\in\mathbb{R}^p$, and Φ restricted to V is an isometry onto $\mathcal{H}$.

(ii) For weights $\theta_1,\dots,\theta_T$ with mean $\bar{\theta}$, and $\bar{f} := \frac{1}{T}\sum_t f_{\theta_t}$,

$$\frac{1}{T}\sum_{t=1}^{T}(f_{\theta_t} - \bar{f})\otimes(f_{\theta_t} - \bar{f}) = \Phi\,\hat{\Sigma}_V\,\Phi^*, \qquad \hat{\Sigma}_V := \frac{1}{T}\sum_{t=1}^{T}P_V(\theta_t - \bar{\theta})(\theta_t - \bar{\theta})^\top P_V,$$

and the same identity holds for the population covariances. Hence the two have the same nonzero eigenvalues, and $u \mapsto \Phi u$ maps the corresponding eigenvectors of $\hat{\Sigma}_V$ onto those of the predictor covariance.

(iii) If $\theta_t - \theta_0 \in V$ for all t, then $\hat{\Sigma}_V = \frac{1}{T}\sum_t (\theta_t - \bar{\theta})(\theta_t - \bar{\theta})^\top$ is the ordinary covariance of the weights. This holds, e.g., for gradient-based training of the linearized model from θ_0 without weight decay.

Finally, the learned subspace is near-optimal for representing tasks, up to the irreducible spectral tail.

Definition 3.10 (Population projection risk)**.** For a k-dimensional subspace $\mathcal{U} \subset \mathcal{H}$ with orthogonal projector $P_{\mathcal{U}}$, define

$$\mathcal{R}(\mathcal{U}) := \mathbb{E}_{t\sim\mathcal{T}} \|f_t^\star - P_{\mathcal{U}} f_t^\star\|^2 .$$

Corollary 3.11 (Excess projection risk of the learned subspace)**.** *Let $\tilde{\mathcal{H}}_k$ denote the range of $\tilde{P}_k$. Under the event of Theorem 3.7,*

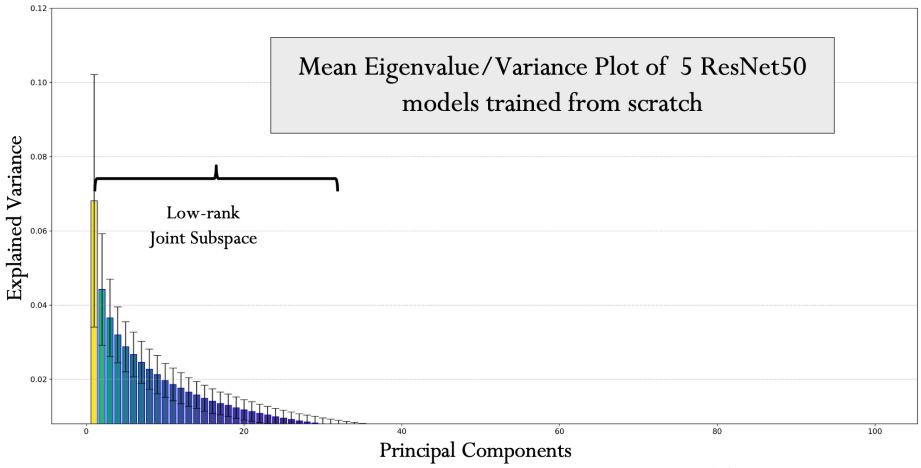
$$\mathcal{R}(\tilde{\mathcal{H}}_k) \;\le\; \sum_{i>k} \lambda_i \;+\; \frac{2\,\mathrm{tr}(\mathcal{S})}{\gamma_k}\left(c_1 B^2 \sqrt{\frac{\ln(c_2/\delta)}{T}} + 2B\,\bar{\eta} + \overline{\eta^2} \right).$$

Why do these universal subspaces emerge? While the precise mechanisms driving this phenomenon remain an open area of investigation, several theoretical factors likely contribute to the emergence of these shared structures. First, spectral analyses of neural tangent kernels show polynomially decaying eigenvalues and a preference for learning low-frequency functions in certain architectures (Belfer et al., 2024; Bietti et al., 2019). Second, modern architectures impose strong inductive biases that constrain the solution space: convolutional structures inherently favor local, Gabor-like patterns (Krizhevsky et al., 2012; Guth et al., 2024), while mechanistic interpretability studies identify recurring computational circuits (Olah et al., 2020; Chughtai et al., 2023). Third, the ubiquity of gradient-based optimization - governed by kernels that are largely invariant to task specifics in the infinite-width limit (Jacot et al., 2018) - inherently prefers smooth solutions, channeling diverse learning trajectories toward shared geometric manifolds (Garipov et al., 2018). If these hypotheses hold, the universal subspace likely captures fundamental computational patterns that transcend specific tasks, potentially explaining the efficacy of transfer learning and why diverse problems often benefit from similar architectural modifications. Under explicit spectral-selection, covariance-concentration, eigengap, and layer-stability assumptions, Theorem A.5 formalizes one version of this argument for models trained on a common data distribution (Section A.2).

4 Results across Modalities, Tasks, Architectures, and Training Mechanisms

We present empirical results using method shown in Section 2, extracting our layer wise universal subspace approximations using thousands of publicly available models for most of our experiments. This keeps the additional training cost low. Spectral analysis relies on efficient spectral decomposition libraries, and can even be run on CPUs. We run all our analysis and experiments on one Nvidia A5000 GPU. The presented large scale empirical results forms the crux of our work and provide strong evidence for the presence of such low ranked joint subspaces across a wide range

Method	ImageNet	EuroSAT	Cifar10	Cifar100	Pets	Avg.
ResNet50	80.86	98.96	97.35	83.82	93.48	90.89
Universal R50	77.89	98.83	95.89	81.49	83.81	87.58



Note. The eigenvalue plot summarizes all model weights, averaged across all layers of five ResNet50 models. "Mean" denotes this layer-wise averaging. The vertical axis shows explained variance across all models and the horizontal axis shows principal components. We use this plotting convention throughout the paper. We refer to the low-rank shared subspace as the *Universal* subspace and a model constructed from its extracted basis as a *Universal variant*.

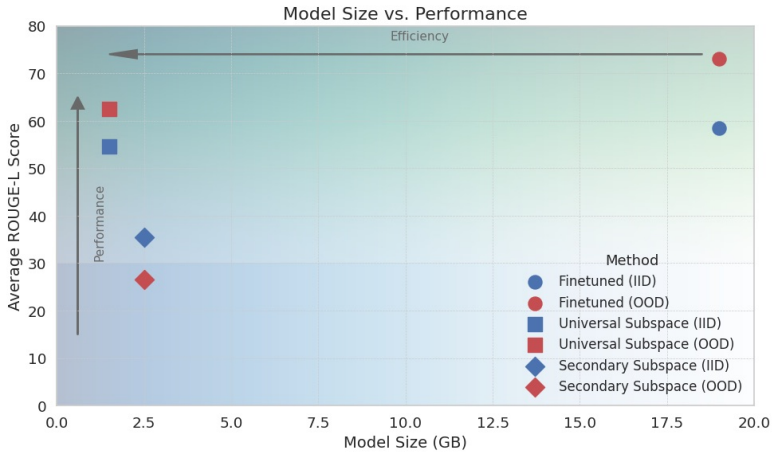
Figure 2: **Universal subspaces in CNNs.** Decomposing 5 ResNet50 models trained on different tasks reveals a low-rank shared subspace, with most information concentrated in top fewer directions across layers.

of task, architecture and modalities. In summary, we present **ten** sets of analyses and applications spanning image classification, language understanding and generation, text-to-image and 3D generation, model merging, and adaptation to new tasks.

These experiments cover architectures including CNNs and transformers; vision, language, and multimodal data; discriminative and generative objectives; full model weights and low-rank adapters; and models trained from scratch or finetuned. Together, this diversity provides strong empirical evidence for shared low-rank subspaces within architectures. Further controlled experiments could isolate the effects of individual factors, that remains future work.

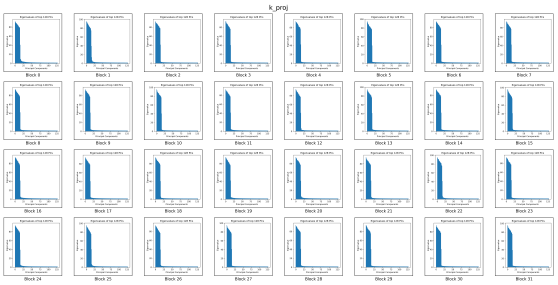
Lower-rank joint subspaces in CNNs, LoRA and Finetuned models In smaller and conventional architectures such as CNNs, evidence for universal structure has been more limited but suggestive. Early work observed that the first convolutional layer often learns Gabor-like filters on ImageNet (Krizhevsky et al., 2012). More recently, works report recurring eigendirections in certain CNN layers trained on natural images (Guth et al., 2024; Guth & Ménard, 2024). We extend these observations and examine whether a shared low-rank joint subspace emerges across tasks. Specifically, we use a mix of finetuned and scratch-trained ResNet-50 models for image classification on five disjoint datasets (CIFAR-10, CIFAR-100, ImageNet, Oxford-IIIT Pets, and EuroSAT). The small number of available models leads to a poor approximation of the joint subspace, but we still observe a low-rank structure in the eigenvalue spectrum of the weight matrices (Figure 2). We also find that projecting the original weights into this subspace preserves competitive performance across all five datasets, providing evidence for a shared subspace.

Figure 3: Lots of LoRA model size vs. performance.

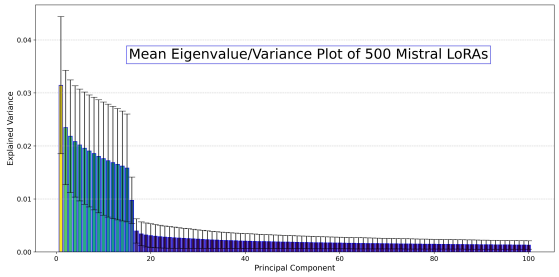


We further analyze nine ResNet-50 models trained independently from scratch on different datasets. Despite the low suitability score ($q_{\text{all}} = 0.0183$), a shared subspace retains 77.91% mean top-1 accuracy on OOD tasks (compared with 81.00% for the original models) (Table 6) - it is a significant result for a relatively poor-quality universal space approximation and without any fine-tuning. More details and results are given in Section B.2. To test the hypothesis in CNNs beyond image classification, we analyze 20 StyleGAN2 Karras et al. (2020) generative models. Despite a low suitability score ($q_{\text{all}} = 0.0572$), reconstruction using the universal shared basis preserves comparable image quality (Figure 9). This holds for both IID and OOD(leave-one-model-out) reconstruction, where the basis is estimated from the other 19 models, without finetuning (Table 8), providing strong evidence for our hypothesis. Further details in Section B.3.

A recurring limitation of the above experiments is the relatively small number of independently trained models available for testing our hypothesis. To address this, we turn to LoRA Hu et al. (2021), for which large collections of task-specific adapters are publicly available. LoRA updates are particularly suitable for this analysis because they encode task-specific directions and exhibit limited alignment with the pretrained weights Hu et al. (2021), providing a meaningful alternative parameterization for testing whether a shared low-dimensional structure still emerges. Following Section 2, we spectrally decompose each LoRA submatrix after concatenating the corresponding matrices across all available adapters, and retain the top-k spectral bases. The scale and task diversity of this setting provide a substantially stronger stress test of the Universal Subspace hypothesis. In our first experiment, we use LoRA models trained on 500 natural instruction tasks (Wang et al., 2022) using Mistral-7B-Instruct-v0.2 (Jiang et al., 2023) as the base (Brüel-Gabrielsson et al., 2024). Figure 4 shows the results of our analysis. Figure 4a shows the subspace analysis of individual layers of the Mistral model. Each bar corresponds to the Eigenvalue or explained variance of every unique component (unique for all models, trained in disjoint/different datasets), showing that the parameters of all 500 models can be well approximated by a finite low-rank subspace for all layers. Note that for visualization purposes, the graphs only show the top 100 components, but there exists a significantly larger number of basis. Figure 4b gives a summary of this analysis, (summarized)



(a) Eigenvalue/variance plot for spectral components across 500 Mistral-7B LoRAs.



(b) Summarized eigenvalue plot across all 31 layers and 500 LoRAs.

Figure 4: **Proving existence of universal subspaces in deep networks.** Decomposing 500 LoRAs trained on different tasks using Mistral-7B reveals a low-rank universal subspace, with most information concentrated in 16 or fewer directions across all layers. Additional layer-wise plots are provided in Section B.5.

for all of the layers of the 500 Mistral models, further validating the idea of a layer-wise universal subspace.

To test the expressiveness of this universal subspace, we analytically reconstruct the LoRA parameters of randomly chosen seen (IID) and unseen (OOD) tasks by projecting it onto the universal subspace. Figure 3 shows the result of our experiment, and as can be seen, that the Universal subspace model perform robustly for both seen and unseen cases. In order to verify the importance of this chosen subspace, we redo the experiment with the *leftover* components from our spectral decomposition (called *Secondary Subspace*). As can be seen from the results, the performance of this model lags drastically behind our chosen subspace. We note that our universal subspace model is 19× **more memory efficient** since it is no longer necessary to save all 500 LoRAs.

We extend our analysis to **text-to-image generation** using Stable Diffusion-XL (Podell et al., 2023). A universal subspace is extracted from publicly available LoRAs on HuggingFace (von Platen et al., 2022). When projecting individual LoRAs into this subspace, the resulting generations preserve visual quality and style (Figure 5). CLIP-based evaluations (Table 1) show that the universal subspace even outperforms individual LoRAs in some cases, possibly due to denoising effects similar to those observed in (Sharma et al., 2023).

Table 1: CLIP scores (higher is better) of images generated using SDXL.

Method	Style 1	Style 2	Style 3	Style 4	Style 5	Style 6	Style 7	Style 8	Style 9	Style 10	Avg
LoRA	21.95	15.59	22.18	18.84	16.65	17.99	24.66	17.47	22.07	19.93	19.73
Universal SDXL LoRA	21.96	16.07	22.07	18.79	16.68	17.99	24.66	17.56	22.46	20.09	**19.83**

In order to test the ability of condensing many models into a single universal subspace, we compare our method with model merging/combination methods in Table 18. We compare our universal subspace inspired combination approach against six gradient-free baselines: RegMean (Jin et al., 2023), Task Arithmetic (TA) (Ilharco et al., 2023), TIES (Yadav et al., 2023), DARE-TIES (Yu et al., 2024), KnOTS-TIES, and KnOTS-DARE-TIES (Stoica et al., 2025). RegMean merges layer weights through a least-squares objective using precomputed layer-input Gram matrices. TA



Figure 5: Text-to-Image Generation Results for Individual models vs. Universal Subspace model. We observe no significant reduction in visual quality despite huge reduction in total model size.

combines task vectors obtained by subtracting the common pretrained weights from each finetuned model. DARE-TIES randomly drops and rescales task-vector entries before applying TIES. KnOTS-TIES and KnOTS-DARE-TIES further apply SVD-based subspace alignment before merging, but still inherit the need for coefficient or pruning hyperparameter selection. In contrast, our universal subspace method, analytically computes the merging coefficients based solely on the geometry of a shared, low-rank universal subspace identified across models, requiring no iterative tuning or validation data-although optional finetuning is possible if data is available. Furthermore, because our subspace is intrinsically low-rank, the merged universal model (plus task specific coefficients) contains significantly fewer parameters than any individual models, offering both computational efficiency and alignment quality. Empirically, our approach achieves higher average accuracy, while reducing parameter count.

In summary, these experiments provide strong empirical support for our universal subspace hypothesis and demonstrate its practical advantages in terms of memory efficiency, model merging, model reusability, and scalable deployment across diverse tasks and modalities.

Low rank shared universal subspaces in classical weights While aforementioned experiments on CNNs trained from scratch, and LoRAs, provide strong evidence for the presence of the joint subspace, we further rigorously test on large scale MLP and transformer models (500 pretrained ViT, 50 LLaMA3-8B models, 177 GPT-2 and Flan-T5).

First, we collect ∼500 pretrained ViT from HuggingFace, spanning diverse domains - medical imaging, satellite data, and synthetic - and trained with varying losses, optimizers, and initializations. Importantly, we did not filter or curate these models in any way and had no access to the original training data, ensuring our analysis reflects real-world diversity. Details are provided in Section B.6. We spectrally decompose (Section 2) all layers (excluding first and last) and observe, in Figure 6, that the majority of variance is captured by the top few spectral components, revealing a highly compressible, shared subspace across layers. Only the top 100 components are visualized for clarity.

To further validate the universality of this subspace, we selected five additional, previously unseen pretrained ViT models for which we had access to evaluation data. These models, considered out-of-domain relative to the initial set, had all their weights reconstructed by projecting onto the identified 16-dimensional universal subspace. We then evaluate their classification accuracy. As shown Table 2,

Table 2: Image Classification

Method	**IID**	**OOD**
Full Training	94.4 ± 1.7	91.3 ± 2.1
Universal ViT	94.1 ± 2.0	87.8 ± 1.5

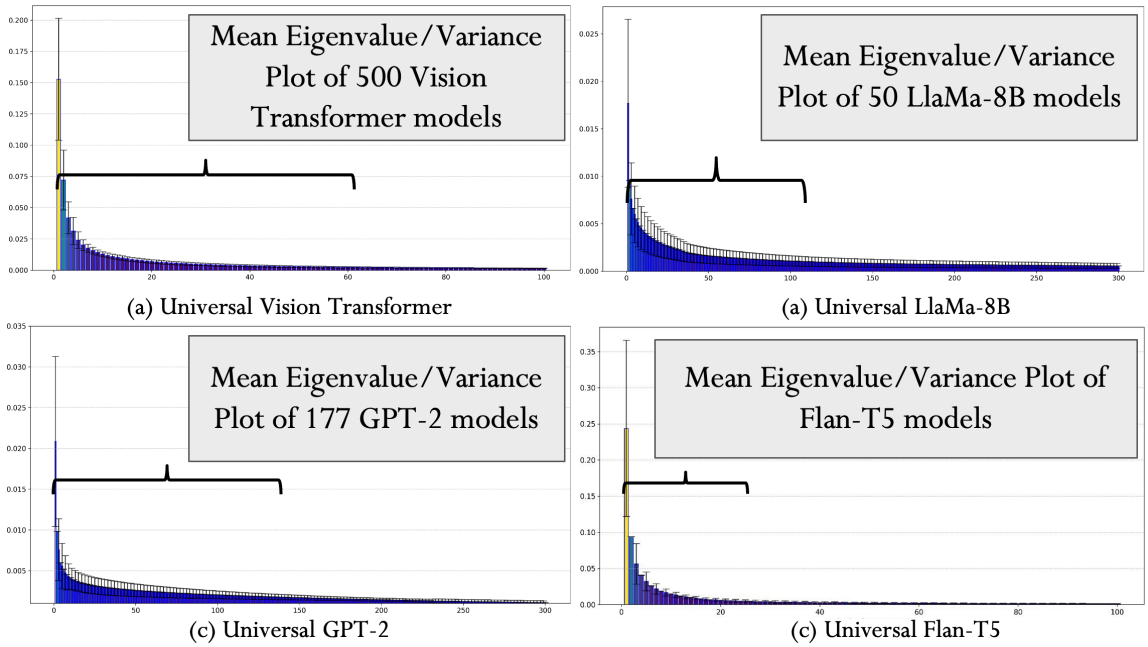


Figure 6: **Universal Subspaces in Classical Weights.** Spectral decomposition of weights from (1) ∼500 Vision Transformers, (2) 50 LLaMA-8B models, (3) 177 GPT-2 models, and (4) GLUE Flan-T5 models reveals a consistent low-rank structure, with most variance captured by the top few spectral bases. Despite diverse tasks, datasets, and training configurations, learned weights consistently align with a shared low-dimensional subspace. Only a subset of bases is shown; extended plots are provided in Section B.6.

the Universal ViT retains performance close to full training, achieving 94.1% versus 94.4% in IID evaluation and 87.8% versus 91.3% in OOD evaluation.

A major outcome of this experiment is that we can replace these 500 ViT models with a single Universal Subspace model. Ignoring the task-variable first and last layer (weight matrices vary due to different number of categories and input size and formats), we observe a requirement of **100× less memory**, and these savings are prone to increase as the number of trained models increases. We note that we are, to the best of our knowledge, the first work, to be able to *merge* 500 (and theoretically more) ViT into a single universal subspace model. This result implies that hundreds of ViTs can be represented using a single subspace model - excluding task-specific layers - yielding up to **100× memory reduction**. To our knowledge, this is the first demonstration of merging over 500 ViTs into a single universal representation. We further extend this analysis to 50 finetuned LLaMA3-8B models, 177 GPT-2 models, and Flan-T5 models (trained on GLUE Wang et al. (2019) datasets) again sourced from HuggingFace without filtering. As shown in Figure 6, a small number of directions capture dominant structure across models spanning diverse and distinct datasets and tasks. Further details in Section B.6. We also test the hypothesis on 3D generation using 20 Geometry Distributions models (Zhang et al., 2025), each trained from scratch to represent a single shape. These models use a coordinate-denoising MLP and generate point clouds by iterative sampling, extending our analysis to a different architecture, modality, and inference procedure. Despite a low suitability score ($q_{\text{all}} = 0.1501$), reconstruction through the shared subspace preserves

Table 3: Performance on the GLUE Benchmark.

Method	Speedup	CoLA	MRPC	RTE	QNLI	SST-2	STS-B	Avg.
LoRA	1×	59.56	86.76	77.61	92.53	94.72	90.81	83.67
Universal order-2	2×	61.82	87.25	77.62	92.71	94.15	90.48	84.01
Universal order-3	1.8×	62.06	86.52	75.81	92.98	94.26	90.39	83.67

the learned geometry without any fine-tuning (Figure 10 and Table 9). Details are in Section B.4. This is, to our knowledge, the first instance of compressing such a large and diverse collection of foundation models into a unified subspace, highlighting its potential for large-scale model reuse and environmental efficiency.

4.0.1 Finding universal subspaces and applying them to future tasks

In this section, the low-rank shared subspaces estimated from a set of available tasks are leveraged to adapt to new, previously unseen tasks. While we do not make theoretical guarantees about reuse on unseen tasks, our experiments show that the approximate shared subspace is empirically reusable across a wide range of practical settings. Concretely, we reuse the shared principal directions and learn only their task-specific coefficients for the new task. Learning these low-rank coefficients is substantially cheaper than optimizing full-rank weights of size, reducing both computation and memory. The resulting trainable parameter counts are reported in Table 4. We find our universal subspace models can have significant impact on the carbon footprint issues of large AI models by making the training, inference and scaling of these models efficient and cheap. As shown in the previous section, we can effectively recycle and replace available pretrained models with a universal subspace model with every individual being represented by a sparse set of coefficients. In this section, we show a set of experiments where we utilize the universal subspaces to learn new tasks by freezing the components and simply learning the coefficients using gradient descent. We find that since we are only learning the coefficients, it drastically cuts down the number of parameters required to train the new models. Because only the coefficients are optimized, substantially fewer trainable parameters are required.

We present two experiments - Image Classification using ViT-base and Natural Language Understanding using GLUE benchmark Wang et al. (2019) with RoBERTa-base model. Both involve creating a universal subspace using publicly available models. Details are in Section C.4. For the GLUE benchmark, we follow the same setup as (Kopiczko et al., 2023) -considering the 6 tasks - CoLA, MRPC, SST-2, QNLI, RTE and STS-B while omitting the time-intensive MNLI and QQP tasks. We initialize our universal subspace using a leave-one-out-setup, where the subspace is calculated using components of all but one model for which the coefficients are learned. We also compare second- and third-order HOSVD to evaluate how decomposition order affects adaptation performance and training speed for the GLUE experiment. For image classification, we utilize publicly available models to extract our shared subspaces taking care that the data any of these pretrained LoRAs have not seen the data we will be training our coefficients on. Table 4 and Table 3 show that our universal subspace enables significantly more efficient and effective learning since only compact coefficients are trained. The storage required to save all these models is also drastically reduced. The ViTs require 150 GB and LLaMA models require 1.6TB of memory total. Our universal subspace reduces that memory requirement by more than **100**×.

Table 4: Image Classification with Vision Transformer.

	Params	CIFAR100	Food101	Flowers	CIFAR10	Pets
Full Training	86M	92.8	90.7	98.82	99.0	91.2
Universal ViT	10K	90.1	89.1	90.1	96.7	89.4

5 Discussion

This work provides, to the best of our knowledge, the first large-scale, cross-domain analysis showing that many neural networks trained across diverse tasks, modalities, initializations, and hyperparameters consistently exhibit an architecture-specific shared low-rank universal subspace at the layer level. Concretely, by performing layer-wise spectral decompositions and retaining only the leading principal directions, an accurate approximation of these universal subspaces can be extracted. Empirically, this behavior emerges broadly: in fully finetuned models and LoRA-based adapters, in models trained from scratch, in both generative and discriminative settings, and in multimodal configurations, as shown in our experiments. Moreover, the approximated subspaces generalize to out-of-distribution tasks, where projecting models and learning only a small set of coefficients suffices to recover strong performance. This enables adapting to new tasks without retraining or storing full weights, and supports robust multi-task learning (Han et al., 2026), scalable fine-tuning, and principled model merging within a single unifying framework. The practical implications are substantial. By reusing a common set of layer-wise principal directions and learning only lightweight coefficients per task, large models can be extended and served with dramatically reduced computational, memory, and engineering overhead. This directly lowers both the financial and environmental costs of training and deployment, aligning with the broader goals of sustainable and accessible AI.

References

Sanjeev Arora, Nadav Cohen, Wei Hu, and Yuping Luo. Implicit regularization in deep matrix factorization, 2019. URL https://arxiv.org/abs/1905.13655.

Randall Balestriero and Richard Baraniuk. Mad max: Affine spline insights into deep learning, 2018. URL https://arxiv.org/abs/1805.06576.

Peter L. Bartlett and Shahar Mendelson. Rademacher and gaussian complexities: risk bounds and structural results. *J. Mach. Learn. Res.*, 3:463–482, March 2003. ISSN 1532-4435.

Yuval Belfer, Amnon Geifman, Meirav Galun, and Ronen Basri. Spectral analysis of the neural tangent kernel for deep residual networks. *Journal of Machine Learning Research*, 25(184):1–49, 2024. URL http://jmlr.org/papers/v25/22-0597.html.

Alberto Bietti, Grégoire Mialon, Dexiong Chen, and Julien Mairal. A kernel perspective for regularizing deep neural networks, 2019. URL https://arxiv.org/abs/1810.00363.

Lukas Bossard, Matthieu Guillaumin, and Luc Van Gool. Food-101 – mining discriminative components with random forests. In *European Conference on Computer Vision*, 2014.

Rickard Brüel-Gabrielsson, Jiacheng Zhu, Onkar Bhardwaj, Leshem Choshen, Kristjan Greenewald, Mikhail Yurochkin, and Justin Solomon. Compress then serve: Serving thousands of lora adapters with little overhead, 2024. URL https://arxiv.org/abs/2407.00066.

Shravan S Chaudhari, Yoav Wald, and Suchi Saria. Open-set domain adaptation under background distribution shift: Challenges and a provably efficient solution. *Transactions on Machine Learning Research*, 2026. ISSN 2835-8856. URL https://openreview.net/forum?id=uAJDta7VaQ.

Lin Chen and Sheng Xu. Deep neural tangent kernel and laplace kernel have the same {rkhs}. In *International Conference on Learning Representations*, 2021. URL https://openreview.net/forum?id=vK9WrZ0QYQ.

Zirui Chen and Michael F. Bonner. Universal dimensions of visual representation. *Science Advances*, 11(27):eadw7697, 2025. doi: 10.1126/sciadv.adw7697. URL https://www.science.org/doi/abs/10.1126/sciadv.adw7697.

Gong Cheng, Junwei Han, and Xiaoqiang Lu. Remote sensing image scene classification: Benchmark and state of the art. *Proceedings of the IEEE*, 105(10):1865–1883, October 2017. ISSN 1558-2256. doi: 10.1109/jproc.2017.2675998. URL http://dx.doi.org/10.1109/JPROC.2017.2675998.

Bilal Chughtai, Lawrence Chan, and Neel Nanda. A toy model of universality: Reverse engineering how networks learn group operations, 2023. URL https://arxiv.org/abs/2302.03025.

Mircea Cimpoi, Subhransu Maji, Iasonas Kokkinos, Sammy Mohamed, and Andrea Vedaldi. Describing textures in the wild, 2013. URL https://arxiv.org/abs/1311.3618.

Lieven De Lathauwer, Bart De Moor, and Joos Vandewalle. A multilinear singular value decomposition. *SIAM Journal on Matrix Analysis and Applications*, 21(4):1253–1278, 2000. doi: 10.1137/S0895479896305696. URL https://doi.org/10.1137/S0895479896305696.

Amil Dravid, Yossi Gandelsman, Alexei A. Efros, and Assaf Shocher. Rosetta neurons: Mining the common units in a model zoo, 2023. URL https://arxiv.org/abs/2306.09346.

Jonathan Frankle and Michael Carbin. The lottery ticket hypothesis: Finding sparse, trainable neural networks. In *International Conference on Learning Representations (ICLR)*, 2019.

Timur Garipov, Pavel Izmailov, Dmitrii Podoprikhin, Dmitry Vetrov, and Andrew Gordon Wilson. Loss surfaces, mode connectivity, and fast ensembling of dnns. In *Advances in Neural Information Processing Systems*, volume 31, pp. 8789–8798, 2018.

Matan Gavish and David L. Donoho. The optimal hard threshold for singular values is 4/sqrt(3), 2014. URL https://arxiv.org/abs/1305.5870.

Aaron Grattafiori, Abhimanyu Dubey, Abhinav Jauhri, Abhinav Pandey, et al. The llama 3 herd of models, 2024. URL https://arxiv.org/abs/2407.21783.

Suriya Gunasekar, Blake Woodworth, Srinadh Bhojanapalli, Behnam Neyshabur, and Nathan Srebro. Implicit regularization in matrix factorization, 2017. URL https://arxiv.org/abs/1705.09280.

Florentin Guth and Brice Ménard. On the universality of neural encodings in cnns, 2024. URL https://arxiv.org/abs/2409.19460.

Florentin Guth, Brice Ménard, Gaspar Rochette, and Stéphane Mallat. A rainbow in deep network black boxes. *Journal of Machine Learning Research*, 25(350):1–59, 2024. URL http://jmlr.org/papers/v25/23-1573.html.

Xing Han, Shravan Chaudhari, Tanvi Ranade, Rama Chellappa, and Suchi Saria. Flame: Adaptive mixture-of-experts for continual multimodal multi-task learning, 2026. URL https://arxiv.org/abs/2605.09355.

Patrick Helber, Benjamin Bischke, Andreas Dengel, and Damian Borth. Eurosat: A novel dataset and deep learning benchmark for land use and land cover classification, 2019. URL https://arxiv.org/abs/1709.00029.

Edward J Hu, Yelong Shen, Phillip Wallis, Zeyuan Allen-Zhu, Yuanzhi Li, Shean Wang, Lu Wang, and Weizhu Chen. Lora: Low-rank adaptation of large language models. *arXiv preprint arXiv:2106.09685*, 2021.

Gabriel Ilharco, Marco Tulio Ribeiro, Mitchell Wortsman, Ludwig Schmidt, Hannaneh Hajishirzi, and Ali Farhadi. Editing models with task arithmetic. In *The Eleventh International Conference on Learning Representations*, 2023. URL https://openreview.net/forum?id=6t0Kwf8-jrj.

Arthur Jacot, Franck Gabriel, and Clément Hongler. Neural tangent kernel: Convergence and generalization in neural networks. In *Advances in Neural Information Processing Systems*, volume 31, 2018.

Albert Q. Jiang, Alexandre Sablayrolles, Arthur Mensch, Chris Bamford, Devendra Singh Chaplot, Diego de las Casas, Florian Bressand, Gianna Lengyel, Guillaume Lample, Lucile Saulnier, Lélio Renard Lavaud, Marie-Anne Lachaux, Pierre Stock, Teven Le Scao, Thibaut Lavril, Thomas Wang, Timothée Lacroix, and William El Sayed. Mistral 7b, 2023. URL https://arxiv.org/abs/2310.06825.

Xisen Jin, Xiang Ren, Daniel Preotiuc-Pietro, and Pengxiang Cheng. Dataless knowledge fusion by merging weights of language models. In *The Eleventh International Conference on Learning Representations*, 2023. URL https://openreview.net/forum?id=FCnohuR6AnM.

Tero Karras, Samuli Laine, Miika Aittala, Janne Hellsten, Jaakko Lehtinen, and Timo Aila. Analyzing and improving the image quality of stylegan, 2020. URL https://arxiv.org/abs/1912.04958.

Prakhar Kaushik, Alex Gain, Adam Kortylewski, and Alan Yuille. Understanding catastrophic forgetting and remembering in continual learning with optimal relevance mapping, 2021. URL https://arxiv.org/abs/2102.11343.

Prakhar Kaushik, Adam Kortylewski, and Alan Yuille. A bayesian approach to ood robustness in image classification. In *Proceedings of the IEEE/CVF Conference on Computer Vision and Pattern Recognition (CVPR)*, pp. 22988–22997, June 2024a.

Prakhar Kaushik, Aayush Mishra, Adam Kortylewski, and Alan L. Yuille. Source-free and image-only unsupervised domain adaptation for category level object pose estimation. *ArXiv*, abs/2401.10848, 2024b. URL https://api.semanticscholar.org/CorpusID:267060973.

Prakhar Kaushik, Ankit Vaidya, Shravan Chaudhari, and Alan Yuille. Eigenlorax: Recycling adapters to find principal subspaces for resource-efficient adaptation and inference. In *2025 IEEE/CVF Conference on Computer Vision and Pattern Recognition Workshops (CVPRW)*, pp. 649–659, 2025. doi: 10.1109/CVPRW67362.2025.00070.

Prakhar Kaushik, Ankit Vaidya, Shravan Chaudhari, Rama Chellappa, and Alan Yuille. Shared lora subspaces for almost strict continual learning. In Paolo Favaro, Zuzana Kukelova, Atsuto Maki, Anna Rohrbach, Konrad Schindler, and Federico Tombari (eds.), *Computer Vision – ECCV 2026*, pp. 480–497, Cham, 2026. Springer Nature Switzerland. ISBN 978-3-032-37574-2.

Dawid Jan Kopiczko, Tijmen Blankevoort, and Yuki M. Asano. VeRA: Vector-based Random Matrix Adaptation. October 2023. URL https://openreview.net/forum?id=NjNfLdxr3A.

Jonathan Krause, Michael Stark, Jia Deng, and Li Fei-Fei. 3d object representations for fine-grained categorization. In *4th International IEEE Workshop on 3D Representation and Recognition (3dRR-13)*, Sydney, Australia, 2013.

Alex Krizhevsky, Vinod Nair, and Geoffrey Hinton. Cifar-100 (canadian institute for advanced research). 2009. URL http://www.cs.toronto.edu/~kriz/cifar.html.

Alex Krizhevsky, Ilya Sutskever, and Geoffrey E Hinton. Imagenet classification with deep convolutional neural networks. In F. Pereira, C.J. Burges, L. Bottou, and K.Q. Weinberger (eds.), *Advances in Neural Information Processing Systems*, volume 25. Curran Associates, Inc., 2012. URL https://proceedings.neurips.cc/paper_files/paper/2012/file/c399862d3b9d6b76c8436e924a68c45b-Paper.pdf.

Yann LeCun, Corinna Cortes, and CJ Burges. Mnist handwritten digit database. *ATT Labs [Online]. Available: http://yann.lecun.com/exdb/mnist*, 2, 2010.

Wei Ma and Jun Lu. An equivalence of fully connected layer and convolutional layer, 2017. URL https://arxiv.org/abs/1712.01252.

Jialin Mao, Itay Griniasty, Han Kheng Teoh, Rahul Ramesh, Rubing Yang, Mark K. Transtrum, James P. Sethna, and Pratik Chaudhari. The training process of many deep networks explores the same low-dimensional manifold. *Proceedings of the National Academy of Sciences*, 121(12), March 2024. ISSN 1091-6490. doi: 10.1073/pnas.2310002121. URL http://dx.doi.org/10.1073/pnas.2310002121.

Charles Martin, Tongsu Peng, and Michael Mahoney. Predicting trends in the quality of state-of-the-art neural networks without access to training or testing data. *Nature Communications*, 12: 4122, 07 2021. doi: 10.1038/s41467-021-24025-8.

Charles H Martin and Christopher Hinrichs. Setol: A semi-empirical theory of (deep) learning, 2025. URL https://arxiv.org/abs/2507.17912.

Colin McDiarmid. *On the method of bounded differences*, pp. 148–188. London Mathematical Society Lecture Note Series. Cambridge University Press, 1989.

Yuval Netzer, Tao Wang, Adam Coates, Alessandro Bissacco, Bo Wu, and Andrew Y. Ng. Reading digits in natural images with unsupervised feature learning. In *NIPS Workshop on Deep Learning and Unsupervised Feature Learning 2011*, 2011. URL http://ufldl.stanford.edu/housenumbers/nips2011_housenumbers.pdf.

Maria-Elena Nilsback and Andrew Zisserman. Automated flower classification over a large number of classes. In *Indian Conference on Computer Vision, Graphics and Image Processing*, Dec 2008.

Chris Olah, Nick Cammarata, Ludwig Schubert, Gabriel Goh, Michael Petrov, and Shan Carter. Zoom in: An introduction to circuits. *Distill*, 2020. doi: 10.23915/distill.00024.001. https://distill.pub/2020/circuits/zoom-in.

Guillermo Ortiz-Jimenez, Alessandro Favero, and Pascal Frossard. Task arithmetic in the tangent space: Improved editing of pre-trained models. In *Thirty-seventh Conference on Neural Information Processing Systems*, 2023. URL `https://openreview.net/forum?id=0A9f2jZDGW`.

Omkar M. Parkhi, Andrea Vedaldi, Andrew Zisserman, and C. V. Jawahar. Cats and dogs. In *IEEE Conference on Computer Vision and Pattern Recognition*, 2012.

Dustin Podell, Zion English, Kyle Lacey, Andreas Blattmann, Tim Dockhorn, Jonas Müller, Joe Penna, and Robin Rombach. Sdxl: Improving latent diffusion models for high-resolution image synthesis, 2023. URL `https://arxiv.org/abs/2307.01952`.

Andrew M. Saxe, James L. McClelland, and Surya Ganguli. A mathematical theory of semantic development in deep neural networks. *Proceedings of the National Academy of Sciences*, 116 (23):11537–11546, May 2019. ISSN 1091-6490. doi: 10.1073/pnas.1820226116. URL `http://dx.doi.org/10.1073/pnas.1820226116`.

Konstantin Sch"urholt, Michael W. Mahoney, and Damian Borth. Towards scalable and versatile weight space learning. In *Proceedings of the 41st International Conference on Machine Learning (ICML)*. PMLR, 2024.

Pratyusha Sharma, Jordan T. Ash, and Dipendra Misra. The Truth is in There: Improving Reasoning in Language Models with Layer-Selective Rank Reduction, December 2023. URL `http://arxiv.org/abs/2312.13558`. arXiv:2312.13558 [cs].

Johannes Stallkamp, Marc Schlipsing, Jan Salmen, and Christian Igel. The German Traffic Sign Recognition Benchmark: A multi-class classification competition. In *IEEE International Joint Conference on Neural Networks*, pp. 1453–1460, 2011.

George Stoica, Pratik Ramesh, Boglarka Ecsedi, Leshem Choshen, and Judy Hoffman. Model merging with SVD to tie the knots. In *The Thirteenth International Conference on Learning Representations*, 2025. URL `https://openreview.net/forum?id=67X93aZHII`.

Joel A. Tropp. User-friendly tail bounds for sums of random matrices. *Foundations of Computational Mathematics*, 12(4):389–434, August 2011. ISSN 1615-3383. doi: 10.1007/s10208-011-9099-z. URL `http://dx.doi.org/10.1007/s10208-011-9099-z`.

M. Alex O. Vasilescu and Demetri Terzopoulos. Multilinear analysis of image ensembles: Tensorfaces. In Anders Heyden, Gunnar Sparr, Mads Nielsen, and Peter Johansen (eds.), *Computer Vision — ECCV 2002*, pp. 447–460, Berlin, Heidelberg, 2002. Springer Berlin Heidelberg. ISBN 978-3-540-47969-7.

M.A.O. Vasilescu and D. Terzopoulos. Multilinear independent components analysis. In *2005 IEEE Computer Society Conference on Computer Vision and Pattern Recognition (CVPR'05)*, volume 1, pp. 547–553 vol. 1, 2005. doi: 10.1109/CVPR.2005.240.

Patrick von Platen, Suraj Patil, Anton Lozhkov, Pedro Cuenca, Nathan Lambert, Kashif Rasul, Mishig Davaadorj, Dhruv Nair, Sayak Paul, William Berman, Yiyi Xu, Steven Liu, and Thomas Wolf. Diffusers: State-of-the-art diffusion models. https://github.com/huggingface/diffusers, 2022.

Alex Wang, Amanpreet Singh, Julian Michael, Felix Hill, Omer Levy, and Samuel R. Bowman. Glue: A multi-task benchmark and analysis platform for natural language understanding, 2019. URL https://arxiv.org/abs/1804.07461.

Yizhong Wang, Swaroop Mishra, Pegah Alipoormolabashi, Yeganeh Kordi, Amirreza Mirzaei, Atharva Naik, Arjun Ashok, Arut Selvan Dhanasekaran, Anjana Arunkumar, David Stap, Eshaan Pathak, Giannis Karamanolakis, Haizhi Lai, Ishan Purohit, Ishani Mondal, Jacob Anderson, Kirby Kuznia, Krima Doshi, Kuntal Kumar Pal, Maitreya Patel, Mehrad Moradshahi, Mihir Parmar, Mirali Purohit, Neeraj Varshney, Phani Rohitha Kaza, Pulkit Verma, Ravsehaj Singh Puri, Rushang Karia, Savan Doshi, Shailaja Keyur Sampat, Siddhartha Mishra, Sujan Reddy A, Sumanta Patro, Tanay Dixit, and Xudong Shen. Super-NaturalInstructions: Generalization via declarative instructions on 1600+ NLP tasks. In Yoav Goldberg, Zornitsa Kozareva, and Yue Zhang (eds.), *Proceedings of the 2022 Conference on Empirical Methods in Natural Language Processing*, pp. 5085–5109, Abu Dhabi, United Arab Emirates, December 2022. Association for Computational Linguistics. doi: 10.18653/v1/2022.emnlp-main.340. URL https://aclanthology.org/2022.emnlp-main.340/.

Colin Wei, Jason D. Lee, Qiang Liu, and Tengyu Ma. *Regularization matters: generalization and optimization of neural nets v.s. their induced kernel*. Curran Associates Inc., Red Hook, NY, USA, 2019.

J. Xiao, J. Hays, K. A. Ehinger, A. Oliva, and A. Torralba. Sun database: Large-scale scene recognition from abbey to zoo. In *2010 IEEE Computer Society Conference on Computer Vision and Pattern Recognition*, pp. 3485–3492, June 2010. doi: 10.1109/CVPR.2010.5539970.

Prateek Yadav, Derek Tam, Leshem Choshen, Colin Raffel, and Mohit Bansal. TIES-merging: Resolving interference when merging models. In *Thirty-seventh Conference on Neural Information Processing Systems*, 2023. URL https://openreview.net/forum?id=xtaX3WyCj1.

Le Yu, Bowen Yu, Haiyang Yu, Fei Huang, and Yongbin Li. Language models are super mario: Absorbing abilities from homologous models as a free lunch. In *ICML*, 2024. URL https://openreview.net/forum?id=fq0NaiU8Ex.

Yi Yu, Tengyao Wang, and Richard J. Samworth. A useful variant of the davis–kahan theorem for statisticians, 2014. URL https://arxiv.org/abs/1405.0680.

Biao Zhang, Jing Ren, and Peter Wonka. Geometry distributions. In *Proceedings of the IEEE/CVF International Conference on Computer Vision (ICCV)*, pp. 1495–1505, October 2025.

Appendix contents

A Appendix A **22**

A.1 Theoretical Analysis 23

A.2 A sufficient condition for weight-subspace agreement 26

B Appendix B **29**

B.1 A data-free suitability metric for universal subspace approximations 29

B.2 Additional Details for ResNet50 Universal-Subspace Experiments 30

B.3 Additional StyleGAN2 Universal-Subspace Experiments 32

B.4 Geometry Distributions: Scratch-Trained 3D Generation 32

B.5 Lower rank shared universal subspaces within low rank adaptation (LoRA) models . 34

B.6 Low rank shared universal subspaces in classical weights 41

B.7 Ablating number of models and subspace effectiveness 50

C Appendix C **53**

C.1 Related Work 53

C.2 Model Merging and Reuse via Universal Subspaces 54

C.3 Universal Subspace Analysis 54

C.4 Finding universal subspaces and applying them to future tasks 55

C.5 Discussion and Broader Impact 55

C.6 Limitations and Future Work 56

A Appendix A

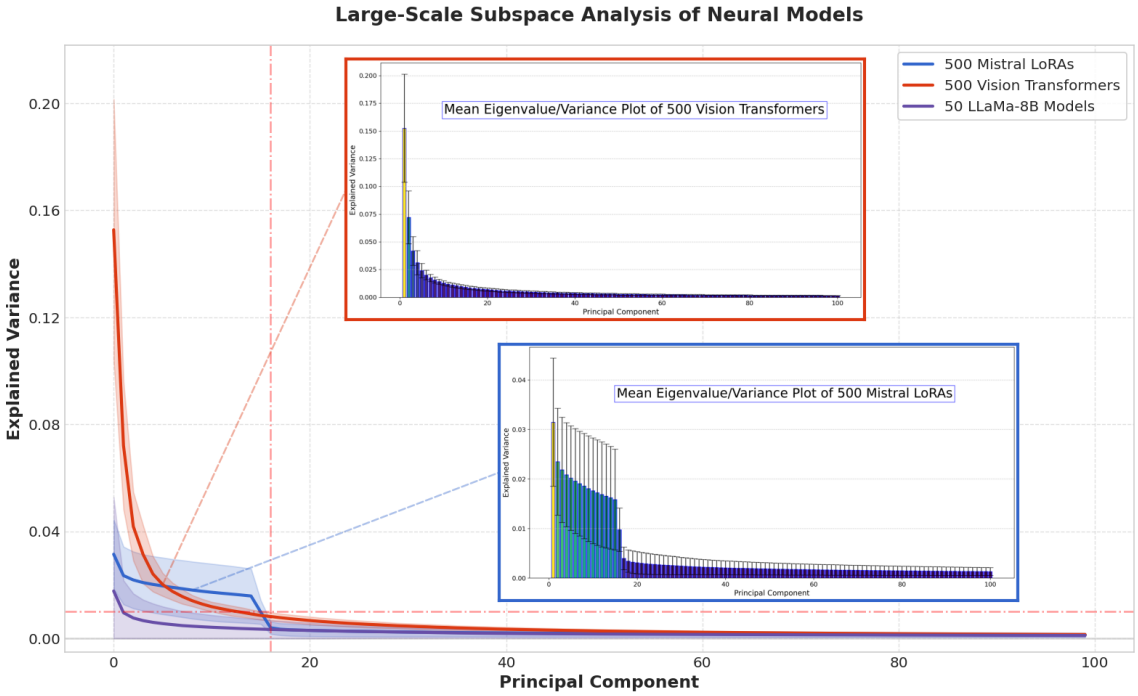


Figure 7: **Empirical Evidence for (Universal) Joint Weight Subspaces.** This figure illustrates the existence of joint low-dimensional subspaces across models trained on diverse tasks. We plot the average explained variance of the top few principal components of weight matrices from 500 Mistral-7B LoRAs, 500 Vision Transformers, and 50 LLaMA-8B models. Despite differences in modality, data, and training objective, all models exhibit rapid spectral decay - indicating that a small number of directions dominate across layers and settings. This consistent structure provides strong evidence for the presence of joint/universal subspaces, supporting our hypothesis that deep networks systematically reuse a common representational basis. Often, this shared subspace can be seen distinctly. The presence of the subspace has significant implications for deep learning. Not only can large number of models be compressed into a single, lighter Universal model with difference represented as lightweight coefficients, training on future tasks simply becomes tuning those coefficients. Since the basis are fixed, training becomes simpler and quicker. However, this convergence to similar subspace raises few important questions - is it possible to recover the "true" Universal Subspace without learning with huge amounts of data? Is this lack of diversity a bottleneck from current family of deep models?

Table 5: Notation reference.

Notation	Description
$\mathcal{H}$	Separable Hilbert space with inner product $\langle\cdot,\cdot\rangle$, norm $\|\cdot\|$.
$a \otimes b$	Rank-one operator $g \mapsto \langle b, g\rangle a$, $\|a \otimes b\|_{\mathrm{op}} = \|a\|\,\|b\|$.
T	Number of tasks.
$\mathcal{T}$	Distribution over tasks.
D_t	Data distribution for task t.
$S_t = \{(x_{t,i}, y_{t,i})\}_{i=1}^{n_t}$	Dataset of size n_t for task t.
$f_t^\star \in \mathcal{H}$	Ground-truth predictor for task t.
$\hat{f}_t \in \mathcal{H}$	Learned predictor for task t.
B	Uniform bound: $\|f_t^\star\| \le B$ almost surely.
η_t	Per-task error bound: $\Pr(\|\hat{f}_t - f_t^\star\| \le \eta_t) \ge 1 - \delta_t$ (Assumption 3.4).
$\bar{\eta}$	Average error: $\frac{1}{T}\sum_{t=1}^{T} \eta_t$.
$\overline{\eta^2}$	Average squared error: $\frac{1}{T}\sum_{t=1}^{T} \eta_t^2$.
$\mathcal{S}$	Population operator: $\mathcal{S} = \mathbb{E}_{t\sim\mathcal{T}}[f_t^\star \otimes f_t^\star]$.
$\hat{\mathcal{S}}$	Empirical operator (true predictors): $\frac{1}{T}\sum_{t=1}^{T} f_t^\star \otimes f_t^\star$.
$\tilde{\mathcal{S}}$	Empirical operator (learned predictors): $\frac{1}{T}\sum_{t=1}^{T} \hat{f}_t \otimes \hat{f}_t$.
$\lambda_1 \ge \lambda_2 \ge \dots$	Eigenvalues of $\mathcal{S}$.
ϕ_i	Orthonormal eigenvectors of $\mathcal{S}$.
P_k	Projector onto top-k eigenspace of $\mathcal{S}$.
$\tilde{P}_k$	Projector onto top-k eigenspace of $\tilde{\mathcal{S}}$.
γ_k	Eigengap: $\gamma_k := \lambda_k - \lambda_{k+1} > 0$.
$\|A\|_{\mathrm{op}}$	Operator (spectral) norm.
$\|A\|_{HS}$	Hilbert–Schmidt norm.
$\delta, \delta_t, \delta_T$	Failure probabilities (global, per-task, across-task).

A.1 Theoretical Analysis

We apply a standard generalization bound over the squared error between the task function and its projection onto the shared subspace:

$$\ell(f_t, x) = \|f_t(x) - f_{t,k}(x)\|^2$$

To justify the application of PAC-style bounds, we verify that this loss is bounded. We assume that each task predictor f_t lies in a Reproducing Kernel Hilbert Space (RKHS) with norm bounded by B, i.e., $\|f_t\|_{\mathcal{H}} \le B$, and that the projection $f_{t,k}$ onto the learned shared subspace $\hat{\mathcal{H}}_k$ also satisfies $\|f_{t,k}\|_{\mathcal{H}} \le B$.

Using the reproducing property and assuming a kernel bound $\kappa^2 = \sup_{x\in\mathcal{X}} \|\phi(x)\|^2$, we have for any x:

$$\|f_t(x)\| \le \kappa B \quad \text{and} \quad \|f_{t,k}(x)\| \le \kappa B$$

Thus, the pointwise squared loss is bounded as:

$$\|f_t(x) - f_{t,k}(x)\|^2 \le (\|f_t(x)\| + \|f_{t,k}(x)\|)^2 \le (2\kappa B)^2 = 4\kappa^2 B^2$$

Therefore, the loss function is bounded in $[0, 4\kappa^2 B^2]$, satisfying the conditions required for PAC-style generalization bounds to hold.

Statements of Lemmas 3.5–3.6, Corollaries 3.8 and 3.11, and Proposition 3.9 are given in Section 3; we provide their proofs here.

Proof of Lemma 3.5. Let $Y_t := f_t^\star \otimes f_t^\star$, so that $\hat{\mathcal{S}} - \mathcal{S} = \frac{1}{T}\sum_{t=1}^{T}(Y_t - \mathcal{S})$ with $\mathcal{S} = \mathbb{E}[Y_t]$. Since $\|f_t^\star\| \le B$ a.s., $\|Y_t\|_{HS} = \|f_t^\star\|^2 \le B^2$, so the Y_t and $\mathcal{S}$ lie in the Hilbert space of Hilbert–Schmidt operators on $\mathcal{H}$.

Expectation. The $Y_t - \mathcal{S}$ are i.i.d. and mean-zero, so the cross terms vanish and

$$\mathbb{E}\left\|\hat{\mathcal{S}} - \mathcal{S}\right\|_{HS}^2 = \frac{1}{T}\,\mathbb{E}\,\|Y_1 - \mathcal{S}\|_{HS}^2 = \frac{1}{T}\left(\mathbb{E}\,\|Y_1\|_{HS}^2 - \|\mathcal{S}\|_{HS}^2\right) \le \frac{B^4}{T}.$$

By Jensen's inequality, $\mathbb{E}\left\|\hat{\mathcal{S}} - \mathcal{S}\right\|_{HS} \le B^2/\sqrt{T}$.

Bounded differences. Let $g(f_1^\star, \ldots, f_T^\star) := \left\|\hat{\mathcal{S}} - \mathcal{S}\right\|_{HS}$. Replacing $f_t^\star$ by any f_t' with $\|f_t'\| \le B$ changes $\hat{\mathcal{S}}$ by $(f_t^\star \otimes f_t^\star - f_t' \otimes f_t')/T$, whose Hilbert–Schmidt norm is at most $2B^2/T$; by the triangle inequality, g changes by at most $2B^2/T$. McDiarmid's inequality (McDiarmid, 1989) then gives, for every $\epsilon > 0$,

$$\Pr\left(g - \mathbb{E}g \ge \epsilon\right) \le \exp\!\left(-\frac{2\epsilon^2}{T\,(2B^2/T)^2}\right) = \exp\!\left(-\frac{T\epsilon^2}{2B^4}\right).$$

Setting the right-hand side equal to δ_T, with probability at least $1 - \delta_T$,

$$\left\|\hat{\mathcal{S}} - \mathcal{S}\right\|_{HS} \le \frac{B^2}{\sqrt{T}} + B^2\sqrt{\frac{2\ln(1/\delta_T)}{T}}.$$

The claim follows since $\|A\|_{\mathrm{op}} \le \|A\|_{HS}$. □

Theorem A.1 (Restating Two-level convergence to the shared subspace theorem)**.** *Assume 3.3–3.4. There exist absolute constants $c_1, c_2 > 0$ (e.g., $c_1 = 3$, $c_2 = 2$) such that the following holds. For any $\delta \in (0,1)$, choose $\delta_t = \delta/(2T)$ and set $\delta_T = \delta/2$. With probability at least $1 - \delta$ (over tasks and all per-task samples),*

$$\left\|\tilde{\mathcal{S}} - \mathcal{S}\right\|_{\mathrm{op}} \;\le\; c_1 B^2\sqrt{\frac{\ln(c_2/\delta)}{T}} \;+\; (2B\bar{\eta} + \overline{\eta^2}) \tag{3}$$

If moreover $\gamma_k > 0$, then

$$\left\|\tilde{P}_k - P_k\right\|_{\mathrm{op}} \;\le\; \frac{2}{\gamma_k}\left(c_1 B^2\sqrt{\frac{\ln(c_2/\delta)}{T}} + (2B\bar{\eta} + \overline{\eta^2})\right). \tag{4}$$

where $\bar{\eta} = \frac{1}{T}\sum_{t=1}^{T}\eta_t$, $\overline{\eta^2} = \frac{1}{T}\sum_{t=1}^{T}\eta_t^2$, and η_t is as in Assumption 3.4.

Proof of Theorem 3.7. **(i) Triangle split.** $\left\|\tilde{\mathcal{S}} - \mathcal{S}\right\|_{\mathrm{op}} \le \left\|\tilde{\mathcal{S}} - \hat{\mathcal{S}}\right\|_{\mathrm{op}} + \left\|\hat{\mathcal{S}} - \mathcal{S}\right\|_{\mathrm{op}}$.

(ii) Within-task term. We know that,

$$\begin{aligned}\left\|\hat{f}_t \otimes \hat{f}_t - f_t^\star \otimes f_t^\star\right\|_{\mathrm{op}} &\le \left\|\hat{f}_t - f_t^\star\right\| \left(\left\|\hat{f}_t\right\| + \|f_t^\star\|\right) \\ &\le \|\hat{f}_t - f_t^\star\|(\|\hat{f}_t\| + \|f_t^\star\|) \\ &\le \eta_t\,(2B + \eta_t) \qquad (\text{since } \|\hat{f}_t\| \le \|f_t^\star\| + \|\hat{f}_t - f_t^\star\| \le B + \eta_t) \\ &= 2B\,\eta_t + \eta_t^2.\end{aligned}$$

Averaging and using the triangle inequality for operator norms,

$$\left\|\tilde{\mathcal{S}} - \hat{\mathcal{S}}\right\|_{\mathrm{op}} \le 2B\,\bar{\eta} + \overline{\eta^2}$$

This holds on the event $\bigcap_{t=1}^{T}\{\left\|\hat{f}_t - f_t^\star\right\| \le \eta_t\}$, whose probability is at least $1 - \sum_t \delta_t = 1 - \delta/2$.

(iii) Across-task term. Lemma 3.5 with $\delta_T = \delta/2$ yields, with probability at least $1 - \delta/2$,

$$\left\|\hat{\mathcal{S}} - \mathcal{S}\right\|_{\mathrm{op}} \le \frac{B^2}{\sqrt{T}}\left(1 + \sqrt{2\ln(2/\delta)}\right) \le 3B^2\sqrt{\frac{\ln(2/\delta)}{T}},$$

where the last step uses $\ln(2/\delta) \ge \ln 2$, so that $1 + \sqrt{2\ln(2/\delta)} \le \left(1/\sqrt{\ln 2} + \sqrt{2}\right)\sqrt{\ln(2/\delta)} \le 3\sqrt{\ln(2/\delta)}$. This is the across-task term of equation 1 with $c_1 = 3$ and $c_2 = 2$.

(iv) Union bound and Davis–Kahan. Combining (ii)–(iii) with a union bound gives equation 1. Lemma 3.6 then implies equation 2. □

Substituting explicit per-task bounds $\eta_t(n_t, \delta_t)$ from Assumption 3.4 gives the corresponding finite-sample rate through $\bar{\eta}$ and $\overline{\eta^2}$. In particular, when the per-task estimation errors vanish, the remaining across-task error decreases as $O(T^{-1/2})$ up to logarithmic factors.

Proof of Corollary 3.8. Since $\tilde{\mathcal{C}} = \tilde{\mathcal{S}} - \bar{f} \otimes \bar{f}$ and $\mathcal{C} = \mathcal{S} - m \otimes m$,

$$\left\|\tilde{\mathcal{C}} - \mathcal{C}\right\|_{\mathrm{op}} \le \left\|\tilde{\mathcal{S}} - \hat{\mathcal{S}}\right\|_{\mathrm{op}} + \left\|\hat{\mathcal{S}} - \mathcal{S}\right\|_{\mathrm{op}} + \left\|\bar{f} \otimes \bar{f} - m \otimes m\right\|_{\mathrm{op}}.$$

On the per-task event of step (ii) in the proof of Theorem 3.7 (probability at least $1 - \delta/2$), the first term is at most $2B\bar{\eta} + \overline{\eta^2}$. Let $r := \sqrt{\ln(4/\delta)/T}$. By Lemma 3.5 with $\delta_T = \delta/4$ and the argument of step (iii) (now using $\ln(4/\delta) \ge \ln 4$), the second term is at most $3B^2 r$ with probability at least $1 - \delta/4$. For the third term, $\bar{f} \otimes \bar{f} - m \otimes m = \bar{f} \otimes (\bar{f} - m) + (\bar{f} - m) \otimes m$, so it is at most $\left\|\bar{f} - m\right\|\left(\left\|\bar{f}\right\| + \|m\|\right) \le (2B + \bar{\eta})\left\|\bar{f} - m\right\|$, using $\left\|\hat{f}_t\right\| \le B + \eta_t$ and $\|m\| \le B$. Moreover, $\left\|\bar{f} - m\right\| \le \bar{\eta} + \left\|\bar{f}^\star - m\right\|$ with $\bar{f}^\star := \frac{1}{T}\sum_t f_t^\star$. The proof of Lemma 3.5, applied to the vectors $f_t^\star \in \mathcal{H}$ instead of the operators Y_t (now $\mathbb{E}\left\|\bar{f}^\star - m\right\|^2 \le B^2/T$ and the bounded differences are $2B/T$), gives $\left\|\bar{f}^\star - m\right\| \le 3Br$ with probability at least $1 - \delta/4$. Collecting terms, using $\bar{\eta}^2 \le \overline{\eta^2}$, and taking a union bound over the three events gives the claim. □

Proof of Proposition 3.9. (i) $\Phi u = 0$ iff $u \perp \phi(x)$ for all x, so $\ker \Phi = V^\perp$ and $\Phi u = \Phi u'$ iff $P_V u = P_V u'$. Hence $\langle \Phi u, \Phi v \rangle' := \langle P_V u, P_V v \rangle$ is a well-defined inner product on $\Phi(\mathbb{R}^p)$, under which $\Phi|_V$ is an isometry onto $\Phi(\mathbb{R}^p)$. Since $K(\cdot, x) = \Phi\phi(x)$ and $\phi(x) \in V$, we have $\langle \Phi u, K(\cdot, x) \rangle' = \langle P_V u, \phi(x) \rangle = \langle u, \phi(x) \rangle = (\Phi u)(x)$. Thus K reproduces this space, which is therefore $\mathcal{H}$ by uniqueness of the RKHS of K.

(ii) The reference terms cancel: $f_{\theta_t} - \bar{f} = \Phi(\theta_t - \bar{\theta}) = \Phi u_t$ with $u_t := P_V(\theta_t - \bar{\theta})$. For $g \in \mathcal{H}$, $(\Phi u_t \otimes \Phi u_t)g = \langle \Phi u_t, g \rangle_{\mathcal{H}}\, \Phi u_t = \Phi\, u_t u_t^\top \Phi^* g$; averaging over t gives the identity, and the population case is identical with expectations. By (i), $\Phi|_V$ is unitary from V onto $\mathcal{H}$, Φ^* maps $\mathcal{H}$ into V and inverts $\Phi|_V$, and $\hat{\Sigma}_V$ vanishes on $V^\perp$. Hence $\Phi\hat{\Sigma}_V\Phi^*$ is unitarily similar to $\hat{\Sigma}_V|_V$, which gives the spectral statement.

(iii) If $\theta_t - \theta_0 \in V$ for all t, then $\theta_t - \bar{\theta} \in V$, on which P_V is the identity. For the linearized model, the gradient of any loss $\sum_i \ell(f_\theta(x_i), y_i)$ is $\sum_i \partial_1 \ell(f_\theta(x_i), y_i)\, \phi(x_i) \in V$, so gradient steps from θ_0 stay in $\theta_0 + V$. □

Proof of Corollary 3.11. Optimality of P_k gives $\mathcal{R}(\mathcal{H}_k^\star) = \sum_{i>k} \lambda_i$. Moreover,

$$\mathcal{R}(\tilde{\mathcal{H}}_k) - \mathcal{R}(\mathcal{H}_k^\star) = \mathbb{E}\left\langle f_t^\star, (P_k - \tilde{P}_k) f_t^\star \right\rangle \le \left\|\tilde{P}_k - P_k\right\|_{\mathrm{op}} \mathbb{E}\left\|f_t^\star\right\|^2 = \mathrm{tr}(\mathcal{S})\, \left\|\tilde{P}_k - P_k\right\|_{\mathrm{op}}.$$

Apply equation 2. □

Remark A.2 (Instantiating the per-task bound). Assumption 3.4 is a property of the learning procedure used for each task, and we do not derive it here. Rademacher-complexity bounds (Bartlett & Mendelson, 2003) control the excess prediction risk of $\hat{f}_t$, which does not by itself bound the $\mathcal{H}$-norm distance $\left\|\hat{f}_t - f_t^\star\right\|$; obtaining such a bound requires additional assumptions on the procedure and on $f_t^\star$. For any procedure with an available bound $\eta_t(n_t, \delta_t)$, substituting it into $\bar{\eta}$ and $\overline{\eta^2}$ makes the rate in Theorem 3.7 explicit in the per-task sample sizes.

A.2 A sufficient condition for weight-subspace agreement

We give a sufficient-condition result that formalizes one possible mechanism behind universal weight subspaces. The result does not claim that general nonlinear networks necessarily satisfy these conditions. Rather, it isolates the assumptions under which independently trained networks must select nearby layer-wise subspaces.

Let two networks A and B have the same architecture and be trained on independent samples of size N from a common distribution $\mathcal{D}_{\mathrm{world}}$. For layer ℓ, let $\widehat{\Sigma}_M^{(\ell)}$ denote the empirical covariance of the layer inputs in model $M \in \{A, B\}$, and let $\Sigma_M^{(\ell)}$ be its population counterpart. Write $\mathcal{U}_M^{(\ell)}$ for the dominant k-dimensional weight subspace selected at that layer. For two k-dimensional subspaces $\mathcal{U}$ and $\mathcal{V}$, define

$$d(\mathcal{U}, \mathcal{V}) := \|P_{\mathcal{U}} - P_{\mathcal{V}}\|_{\mathrm{op}},$$

where $P_{\mathcal{U}}$ and $P_{\mathcal{V}}$ are the corresponding orthogonal projectors.

Assumption A.3 (Layer-wise spectral selection)**.** *For each layer ℓ and model M, the training dynamics select a dominant weight subspace $\mathcal{U}_M^{(\ell)}$ equal to the top-k eigenspace of $\widehat{\Sigma}_M^{(\ell)}$.*

This is the substantive modeling assumption. The piecewise-affine structure of ReLU networks gives an exact local linear representation (Balestriero & Baraniuk, 2018), while results for matrix factorization and deep linear networks show that gradient-based optimization can favor low-rank, mode-wise structure in such regimes (Gunasekar et al., 2017; Arora et al., 2019; Saxe et al., 2019). These results motivate Assumption A.3, but do not establish it for arbitrary nonlinear networks.

Assumption A.4 (Concentration, eigengap, and stability)**.** *For each layer ℓ and model M, suppose that, with probability at least $1-\eta$,*

$$\|\widehat{\Sigma}_M^{(\ell)} - \Sigma_M^{(\ell)}\|_{\mathrm{op}} \le \varepsilon_\ell(N,\eta).$$

Assume that both population covariances have a top-k eigengap of at least $\delta_\ell > 0$. For $\ell \ge 2$, assume further that

$$\|\Sigma_A^{(\ell)} - \Sigma_B^{(\ell)}\|_{\mathrm{op}} \le L_\ell \, d(\mathcal{U}_A^{(\ell-1)}, \mathcal{U}_B^{(\ell-1)})$$

for some $L_\ell \ge 0$.

For a fixed feature map and independent samples, standard matrix concentration results apply under appropriate boundedness or tail conditions (Tropp, 2011). For learned features, we assume the stated concentration bound. The final inequality requires the layer-input covariance to change smoothly with the preceding dominant subspace; it is stated explicitly because this property need not hold for every architecture or training regime.

Theorem A.5 (Layer-wise weight-subspace agreement)**.** *Under Assumptions A.3–A.4, for each layer $\ell \ge 2$, the following bound holds with probability at least $1-2\eta$:*

$$d(\mathcal{U}_A^{(\ell)}, \mathcal{U}_B^{(\ell)}) \le \frac{2}{\delta_\ell}\left(2\varepsilon_\ell(N,\eta) + L_\ell d(\mathcal{U}_A^{(\ell-1)}, \mathcal{U}_B^{(\ell-1)})\right) \tag{5}$$

At the first layer, where the two models have the same population input covariance, the following bound holds with the same probability:

$$d(\mathcal{U}_A^{(1)}, \mathcal{U}_B^{(1)}) \le \frac{4\varepsilon_1(N,\eta)}{\delta_1}.$$

Consequently, for any fixed depth, if $\varepsilon_\ell(N,\eta) \to 0$ as $N \to \infty$, then the corresponding dominant layer-wise subspaces of the two independently trained networks agree asymptotically. If $\rho_\ell := 2L_\ell/\delta_\ell < 1$, the recursion is contractive up to the finite-sample error floor.

Proof. Let $\mathcal{E}_M^{(\ell)}$ be the top-k eigenspace of $\Sigma_M^{(\ell)}$. By the population-gap form of the Davis–Kahan theorem (Yu et al., 2014), covariance concentration gives

$$d(\mathcal{U}_M^{(\ell)}, \mathcal{E}_M^{(\ell)}) \le \frac{2\varepsilon_\ell(N,\eta)}{\delta_\ell}$$

for each model. A second application of Davis–Kahan and Assumption A.4 gives

$$d(\mathcal{E}_A^{(\ell)}, \mathcal{E}_B^{(\ell)}) \le \frac{2L_\ell}{\delta_\ell} d(\mathcal{U}_A^{(\ell-1)}, \mathcal{U}_B^{(\ell-1)}).$$

The triangle inequality for orthogonal projectors yields Equation (5); a union bound gives probability at least $1-2\eta$. At the first layer, $\Sigma_A^{(1)} = \Sigma_B^{(1)} = \Sigma_{\mathrm{world}}$, so the middle population-subspace term vanishes. Iterating the recursion proves the final statements. □

The theorem separates three effects: finite-sample covariance error, the spectral separation δ_ℓ, and the propagation of earlier subspace differences through L_ℓ. It provides a qualified explanation for why common data statistics and architecture-specific transformations can lead independent training runs to nearby dominant weight subspaces. Establishing Assumption A.3 for broad classes of nonlinear networks remains an open problem.

B Appendix B

B.1 A data-free suitability metric for universal subspace approximations

Since a good approximation to the universal subspace requires a large, diverse, and well-trained set of models (in our case) equivalently, an ideal algorithm and an ideal set of data to train the models on, we propose a data-free suitability metric to assess the quality of the source models before fitting the HOSVD basis. This metric is based on the heavy-tail exponent of the weight matrices, which has been shown to correlate with generalization and model quality. The fundamental idea is that we want to figure out how close the universal subspace is to an ideal universal subspace for a specific architecture. However, this is a difficult problem to solve because we do not have access to the said ideal universal surface. So instead, we come up with a metric which tells us relatively how good an extracted universal space is from a set of available pre-trained models. The higher the metric, the better the relative quality is the universal space approximation. We use this score as a heuristic indicator of source-model suitability, rather than a direct measure of subspace approximation error.

For a layer l and source model m, we estimate the heavy-tail exponent $\alpha_{l,m}$ by fitting a power law to the tail of the empirical spectral density of $W_{l,m}^{\top} W_{l,m}$, following the Heavy-Tailed Self-Regularization analysis of neural weights (Martin et al., 2021; Martin & Hinrichs, 2025). This statistic provides a data-free description of the correlations in a trained weight matrix. It does not measure subspace alignment directly. We use it to assess the source models before fitting the HOSVD basis.

For N_l valid estimates at layer l, let σ_l be their standard deviation. We define

$$q_l = \left(1 - e^{-N_l/\kappa}\right) \left(\frac{1}{N_l} \sum_{m=1}^{N_l} \mathbf{1}[2 \le \alpha_{l,m} \le 6] e^{-\eta(\alpha_{l,m}-2)} \right) e^{-\lambda \sigma_l}. \tag{6}$$

The three factors respectively account for the number of available models, the fraction and position of exponents in the preferred range, and agreement across models. Unless stated otherwise, we use $\kappa = 20$, $\eta = 0.5$, and $\lambda = 1$. We first require the layer mean to lie in $[2, 6]$, its standard deviation to be at most 1, and at least half of its valid estimates to lie in $[2, 6]$; among these layers, we would like to retain those with $q_l \ge 0.2$. Any experiment-specific relaxation of these thresholds is reported with that experiment.

We summarize a family before filtering by

$$q_{\text{all}} = \exp\left(\frac{1}{L} \sum_{l=1}^{L} \log \max(q_l, \epsilon) \right), \tag{7}$$

and summarize the retained set $\mathcal{L}_{\text{keep}}$ by

$$q_{\text{arch}} = \exp\left(\frac{1}{|\mathcal{L}_{\text{keep}}|} \sum_{l \in \mathcal{L}_{\text{keep}}} \log \max(q_l, \epsilon) \right), \tag{8}$$

where $\epsilon = 10^{-12}$; we set $q_{\text{arch}} = 0$ if no layer is retained. The geometric mean prevents a few high-scoring layers from obscuring consistently weak layers. The scores are coarse diagnostics of

whether the available model collection is sufficiently large and of good quality for estimating a shared subspace approximation.

Importantly, this line of research may help investigate the idea of the ideal neural architecture, but this remains out of scope for current work and is open to future research.

B.2 Additional Details for ResNet50 Universal-Subspace Experiments

For the ResNet-50 experiment, all models are independently trained from scratch with random initialization. We use nine models trained on ImageNet-1K, ImageNet-21K, Places365, iNaturalist, RadImageNet, VGGFace2, CIFAR-10, CIFAR-100, and SVHN. These datasets are largely disjoint and span substantially different visual domains, including natural images, scenes, fine-grained species, medical radiology, faces, objects, and digits, providing a strong test of whether a shared subspace emerges across independently learned representations.

Table 6 reports **out-of-domain (OOD)** results on five datasets: ImageNet-1K, Places365, CIFAR-10, CIFAR-100, and SVHN. For each OOD evaluation, the Universal Subspace is constructed using all models *except* the model trained on the target dataset being evaluated. Thus, the reported performance measures how well a subspace learned entirely from other models can approximate the held-out target model. For a convolution tensor $W_l \in \mathbb{R}^{C_{\text{out}} \times C_{\text{in}} \times k \times k}$, we reshape each spatial kernel into a row of length k^2 and stack all $C_{\text{out}} C_{\text{in}}$ kernels from all source models before fitting a shared SVD/PCA basis.

For each shared weight tensor, we compute a heavy-tail exponent α and the layer suitability score described in Section B.1. Across the 52 common convolution tensors, $q_{\text{all}} = 0.0183$. So this analysis experiment essentially shows how a very small number of models, which are often trained from scratch, may not be sufficient for a universal subspace analysis. We however keep the experiment as a stress test for our hypothesis: the metric is shown in Figure 8, and the reconstruction results should be interpreted under this low-suitability caveat, as more like a lower bound for the performance of the universal space model. The fact that a model which is a relatively poor approximation of the universal space for this specific architecture still performs adequately well and gets very close to the performance of the original fully fine-tuned models, suggests that the universal subspace hypothesis is indeed valid and can be extended to other architectures and model families.

Evaluation and calibration protocols. We evaluate the Universal Subspace under both **IID** and **OOD** settings, first through direct parameter reconstruction and then through lightweight coefficient adaptation. In the IID setting, the shared basis is constructed from the full model pool, including the target model; this tests whether models corresponding to already observed tasks lie within the recovered Universal Subspace. In the OOD setting, we perform leave-one-model-out construction, excluding the target model entirely when estimating the basis. This provides a stronger test of whether a model from a likely unseen, or future task also lies within the same subspace.

Table 6 evaluates direct reconstruction on five target datasets, with *no task-specific optimization or fine-tuning*. Despite the relatively crude approximation of the Universal Subspace in this small-model setting, both IID and OOD reconstructions recover models whose performance remains close to their independently fully trained counterparts. This provides direct evidence that independently

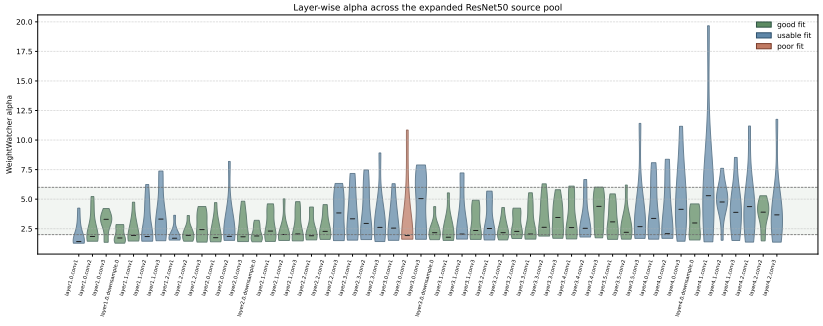


Figure 8: Layer-wise suitability diagnostics for the randomly initialized and trained from scratch ResNet-50 models. The strict metric reports $q_{\text{all}} = 0.0183$ reflecting the relatively poor quality of the universal space extractors due to the small number and diversity of models available. However, as our experiments have shown, our hypothesis still stands and and for universal space approximation still performs adequately.

learned model weights, including those excluded from subspace construction, can be well represented within the recovered linear subspace.

Table 7 further evaluates CIFAR-10, CIFAR-100, and SVHN by optimizing the lightweight coefficients within the fixed Universal Subspace. This is equivalent to restricting optimization to the recovered linear subspace rather than updating the full model parameters. With this minimal adaptation, both IID and OOD models approach the performance of full training, despite the imperfect basis estimate. We adapt the subspace coefficients while keeping the shared bases fixed; OOD adaptation additionally trains the classifier head. This lightweight adaptation brings both IID and OOD models close to full-training performance.

Table 6: **Direct reconstruction of scratch-trained ResNet-50 models.** Mean accuracy across five evaluated targets: ImageNet-1K, Places365, CIFAR-10, CIFAR-100, and SVHN. Models are reconstructed directly from the Universal Subspace without any task-specific fine-tuning. Variance Threshold denotes the fraction of spectral variance retained when constructing the subspace.

Protocol	**Variance Threshold**	**Original Acc.**	**Reconstructed Acc.**
IID	60%	81.00	62.71
IID	70%	81.00	71.56
IID	80%	81.00	78.26
IID	85%	81.00	79.86
IID	90%	81.00	80.45
IID	95%	81.00	80.85
OOD	60%	81.00	56.69
OOD	70%	81.00	69.97
OOD	80%	81.00	77.91
OOD	85%	81.00	79.80
OOD	90%	81.00	80.41
OOD	95%	81.00	80.85

Table 7: **Lightweight coefficient adaptation within the Universal Subspace.** Mean accuracy across CIFAR-10, CIFAR-100, and SVHN. IID optimizes only subspace coefficients; OOD additionally adapts the classifier head. Coefficient parameters exclude the classifier head.

Protocol	Variance Threshold	Original Acc.	Reconstructed Acc.	Adapted Acc.	Coeff. Params
IID	60%	90.63	70.52	86.25	1.28M
IID	70%	90.63	80.98	87.63	1.64M
IID	80%	90.63	88.07	88.76	2.10M
OOD	60%	90.59	69.82	86.74	1.28M
OOD	70%	90.59	79.82	87.86	1.64M
OOD	80%	90.59	87.06	88.87	2.10M

B.3 Additional StyleGAN2 Universal-Subspace Experiments

We additionally test the Universal Subspace hypothesis on StyleGAN2, providing a substantially different setting from the discriminative models considered elsewhere in the paper. We use 20 publicly available StyleGAN2 checkpoints, spanning highly diverse domains including faces, animals, scenes, artwork, textures, maps, and other specialized datasets. Some models are trained from scratch, while a small number are fine-tuned.

This setting is particularly challenging because only 20 models are available for estimating the shared subspace. Consistent with this limitation, the full model set obtains a relatively low suitability score of $q_{\text{all}} = 0.0572$. Applying a strict layer-quality filter would therefore discard most usable layers. We instead use a conservative threshold that retains 9 of the 13 common 3×3 synthesis convolution layers, yielding a retained-layer suitability score of $q_{\text{arch}} = 0.0907$. We emphasize that this remains an intentionally difficult setting and comparatively low-quality approximation of the Universal Subspace.

For each retained layer, we treat its kernels as spatial vectors, construct the corresponding shared spectral basis across the source models, and retain the smallest number of components explaining 90% of the variance. The Universal Subspace model is obtained by replacing each retained target-model layer with its projection onto the corresponding shared spatial basis, while leaving non-retained layers unchanged. We follow the same IID/OOD protocols used in the preceding experiments: IID includes the target model when constructing the shared basis, whereas OOD excludes it entirely.

Despite the limited model pool and relatively weak estimated subspace, reconstruction remains remarkably close to the original models. Across the 18 models for which reconstruction could be evaluated, the mean change in Inception Score is only -0.0041 for IID and -0.0040 for OOD, while paired reconstruction achieves approximately 20 dB PSNR in both settings. Thus, even for a complex adversarial generative model with a substantially different training mechanism, the learned weights remain well approximated by a shared low-dimensional subspace.

B.4 Geometry Distributions: Scratch-Trained 3D Generation

We further test the Universal Subspace hypothesis on Geometry Distributions (GeomDist) (Zhang et al., 2025), a 3D generative model that represents shapes as distributions over coordinates. This

Table 8: **StyleGAN2 reconstruction from the Universal Subspace.** Mean results across 18 evaluated generators. IID includes the target model during basis construction, whereas OOD excludes it.

Protocol	Original IS	Reconstructed IS	ΔIS	PSNR (dB)
IID	3.208 ± 1.273	3.204 ± 1.167	-0.0041 ± 0.2620	19.98 ± 2.25
OOD	3.208 ± 1.273	3.204 ± 1.166	-0.0040 ± 0.2626	19.92 ± 2.28



Figure 9: StyleGAN2 samples from the original models (top) and their Universal Subspace reconstructions (bottom), using matched latent seeds. Each target model is excluded when estimating its reconstruction basis (OOD).

provides another substantially different setting from both discriminative networks and image generators. We use 20 models, each randomly initialized and trained independently from scratch for 1000 epochs on a different 3D primitive.

Despite the relatively small number of available models, the models obtain suitability scores of $q_{\text{all}} = 0.1501$ and $q_{\text{arch}} = 0.1977$, retaining 18 of the 22 compatible matrix-valued layers. For each retained layer, we construct the shared spectral basis across models and project the target weights onto this Universal Subspace.

As shown in Table 9, the reconstructed models using the Universal subspace retain the geometry learned by the independently trained generative models: the mean pairwise Chamfer distance between samples from the original and reconstructed models is only 0.0250 - the reconstructed models remain close to their original counterparts without any fine-tuning. Together with the qualitative reconstructions in Figure 10, this extends the Universal Subspace hypothesis to independently trained 3D generative models with a fundamentally different architecture, training objective, and output domain. This experiment provides strong evidence to the generalizability of the Universal Subspace hypothesis across a wide range of model families and tasks, including discriminative, generative, and 3D models, especially in the case of classical weights like MLP or transformer-like models, which usually require huge amounts of data to train and are hard to analyze for the universal hypothesis.

Table 9: **Geometry Distributions reconstruction from the Universal Subspace.** Reconstruction uses a 95% explained-variance threshold with no fine-tuning. Chamfer distance (CD) is lower-is-better.

Model	GT CD	Pair CD
Original	0.0506 ± 0.0070	–
Universal reconstruction	0.0867 ± 0.0802	0.0250 ± 0.0724

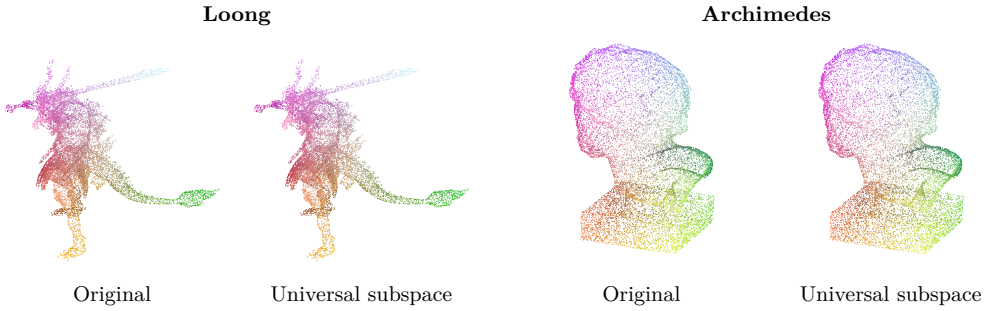


Figure 10: Geometry Distributions samples from the original models and their Universal Subspace reconstructions (IID), shown in pairs for Loong and Archimedes. Colors encode coordinates, not predicted texture.

B.5 Lower rank shared universal subspaces within low rank adaptation (LoRA) models

Spectral Decomposition is employed to extract the top `k` principal directions for each of the LoRA matrices `B` and `A`, which are concatenated across all available models. Subsequently, the top `k` principal directions are selected to define the low-rank subspace shared among the LoRA matrices. This process is conducted separately for each layer of the model to derive a low-rank approximated shared subspace for every individual layer. In practice, for every layer, the rank vectors of all available LoRA matrices are extracted and concatenated into a single matrix. This matrix is then normalized by subtracting the feature-wise mean from each vector, after which principal directions are extracted. The order-1 variant of our method (a single decomposed mode in Algorithm 1) is mathematically equivalent to Principal Component Analysis (PCA), hence we can use `torch.pca_lowrank` or `sklearn.decomposition.PCA` to extract the principal directions. The data matrix corresponding to a specific layer for 500 LoRA models is structured as $500r \times d$, where r denotes the rank of each LoRA and d specifies the dimension of each rank vector. Spectral decomposition is applied separately to the stored LoRA factors A and B for each layer. For a given factor, rank vectors from all available adapters are concatenated, zero-centered using the feature-wise mean, and decomposed to extract the dominant shared directions. This yields a layer-wise low-dimensional basis for the LoRA parameterization produced by standard training.

We note that the LoRA factorization is not unique: for any invertible R, $BA = (BR)(R^{-1}A)$. Our analysis therefore characterizes recurring structure in the learned and stored LoRA parameterization, rather than a gauge-invariant property of the equivalent full update $\Delta W = BA$. A gauge-invariant alternative would perform the same analysis directly on ΔW.

Universal Mistral-7B/Lots of LoRAs experiment details In our first experimental analysis, we use 500 LoRA models trained on distinct Natural Instructions (Wang et al., 2022) using Mistral-7B-Instruct-v0.2 (Jiang et al., 2023) as the base (Brüel-Gabrielsson et al., 2024). Please refer to Brüel-Gabrielsson et al. (2024) for more details on how the LoRA models were trained.

Table 10: Models from HuggingFace for the Universal Mistral LoRA. Models in blue indicate the OOD models and the ones in red are the IID models used for evaluation.

Lots-of-LoRAs/Mistral-7B-Instruct-v0.2-4b-r16-task391	Lots-of-LoRAs/Mistral-7B-Instruct-v0.2-4b-r16-task290
Lots-of-LoRAs/Mistral-7B-Instruct-v0.2-4b-r16-task442	Lots-of-LoRAs/Mistral-7B-Instruct-v0.2-4b-r16-task1598
Lots-of-LoRAs/Mistral-7B-Instruct-v0.2-4b-r16-task039	

Lots-of-LoRAs/Mistral-7B-Instruct-v0.2-4b-r16-task076	Lots-of-LoRAs/Mistral-7B-Instruct-v0.2-4b-r16-task627
Lots-of-LoRAs/Mistral-7B-Instruct-v0.2-4b-r16-task664	Lots-of-LoRAs/Mistral-7B-Instruct-v0.2-4b-r16-task819
Lots-of-LoRAs/Mistral-7B-Instruct-v0.2-4b-r16-task1631	
Lots-of-LoRAs/Mistral-7B-Instruct-v0.2-4b-r16-task190	Lots-of-LoRAs/Mistral-7B-Instruct-v0.2-4b-r16-task1391
Lots-of-LoRAs/Mistral-7B-Instruct-v0.2-4b-r16-task1342	Lots-of-LoRAs/Mistral-7B-Instruct-v0.2-4b-r16-task620
Lots-of-LoRAs/Mistral-7B-Instruct-v0.2-4b-r16-task769	Lots-of-LoRAs/Mistral-7B-Instruct-v0.2-4b-r16-task1448
Lots-of-LoRAs/Mistral-7B-Instruct-v0.2-4b-r16-task247	Lots-of-LoRAs/Mistral-7B-Instruct-v0.2-4b-r16-task513
Lots-of-LoRAs/Mistral-7B-Instruct-v0.2-4b-r16-task875	Lots-of-LoRAs/Mistral-7B-Instruct-v0.2-4b-r16-task515
Lots-of-LoRAs/Mistral-7B-Instruct-v0.2-4b-r16-task1534	Lots-of-LoRAs/Mistral-7B-Instruct-v0.2-4b-r16-task1551
Lots-of-LoRAs/Mistral-7B-Instruct-v0.2-4b-r16-task583	Lots-of-LoRAs/Mistral-7B-Instruct-v0.2-4b-r16-task1431
Lots-of-LoRAs/Mistral-7B-Instruct-v0.2-4b-r16-task270	Lots-of-LoRAs/Mistral-7B-Instruct-v0.2-4b-r16-task1487
Lots-of-LoRAs/Mistral-7B-Instruct-v0.2-4b-r16-task679	Lots-of-LoRAs/Mistral-7B-Instruct-v0.2-4b-r16-task456
Lots-of-LoRAs/Mistral-7B-Instruct-v0.2-4b-r16-task385	Lots-of-LoRAs/Mistral-7B-Instruct-v0.2-4b-r16-task1607
Lots-of-LoRAs/Mistral-7B-Instruct-v0.2-4b-r16-task278	Lots-of-LoRAs/Mistral-7B-Instruct-v0.2-4b-r16-task022
Lots-of-LoRAs/Mistral-7B-Instruct-v0.2-4b-r16-task210	Lots-of-LoRAs/Mistral-7B-Instruct-v0.2-4b-r16-task137
Lots-of-LoRAs/Mistral-7B-Instruct-v0.2-4b-r16-task574	Lots-of-LoRAs/Mistral-7B-Instruct-v0.2-4b-r16-task629
Lots-of-LoRAs/Mistral-7B-Instruct-v0.2-4b-r16-task1378	Lots-of-LoRAs/Mistral-7B-Instruct-v0.2-4b-r16-task1194
Lots-of-LoRAs/Mistral-7B-Instruct-v0.2-4b-r16-task1529	Lots-of-LoRAs/Mistral-7B-Instruct-v0.2-4b-r16-task453
Lots-of-LoRAs/Mistral-7B-Instruct-v0.2-4b-r16-task102	Lots-of-LoRAs/Mistral-7B-Instruct-v0.2-4b-r16-task460
Lots-of-LoRAs/Mistral-7B-Instruct-v0.2-4b-r16-task1204	Lots-of-LoRAs/Mistral-7B-Instruct-v0.2-4b-r16-task1384
Lots-of-LoRAs/Mistral-7B-Instruct-v0.2-4b-r16-task1572	Lots-of-LoRAs/Mistral-7B-Instruct-v0.2-4b-r16-task699
Lots-of-LoRAs/Mistral-7B-Instruct-v0.2-4b-r16-task1722	Lots-of-LoRAs/Mistral-7B-Instruct-v0.2-4b-r16-task580
Lots-of-LoRAs/Mistral-7B-Instruct-v0.2-4b-r16-task605	Lots-of-LoRAs/Mistral-7B-Instruct-v0.2-4b-r16-task1152
Lots-of-LoRAs/Mistral-7B-Instruct-v0.2-4b-r16-task1283	Lots-of-LoRAs/Mistral-7B-Instruct-v0.2-4b-r16-task637
Lots-of-LoRAs/Mistral-7B-Instruct-v0.2-4b-r16-task723	Lots-of-LoRAs/Mistral-7B-Instruct-v0.2-4b-r16-task084
Lots-of-LoRAs/Mistral-7B-Instruct-v0.2-4b-r16-task201	Lots-of-LoRAs/Mistral-7B-Instruct-v0.2-4b-r16-task956
Lots-of-LoRAs/Mistral-7B-Instruct-v0.2-4b-r16-task167	Lots-of-LoRAs/Mistral-7B-Instruct-v0.2-4b-r16-task1192
Lots-of-LoRAs/Mistral-7B-Instruct-v0.2-4b-r16-task300	Lots-of-LoRAs/Mistral-7B-Instruct-v0.2-4b-r16-task1714
Lots-of-LoRAs/Mistral-7B-Instruct-v0.2-4b-r16-task388	Lots-of-LoRAs/Mistral-7B-Instruct-v0.2-4b-r16-task516
Lots-of-LoRAs/Mistral-7B-Instruct-v0.2-4b-r16-task127	Lots-of-LoRAs/Mistral-7B-Instruct-v0.2-4b-r16-task362
Lots-of-LoRAs/Mistral-7B-Instruct-v0.2-4b-r16-task1158	Lots-of-LoRAs/Mistral-7B-Instruct-v0.2-4b-r16-task322
Lots-of-LoRAs/Mistral-7B-Instruct-v0.2-4b-r16-task697	Lots-of-LoRAs/Mistral-7B-Instruct-v0.2-4b-r16-task1566
Lots-of-LoRAs/Mistral-7B-Instruct-v0.2-4b-r16-task1451	Lots-of-LoRAs/Mistral-7B-Instruct-v0.2-4b-r16-task1135
Lots-of-LoRAs/Mistral-7B-Instruct-v0.2-4b-r16-task341	Lots-of-LoRAs/Mistral-7B-Instruct-v0.2-4b-r16-task267
Lots-of-LoRAs/Mistral-7B-Instruct-v0.2-4b-r16-task1720	Lots-of-LoRAs/Mistral-7B-Instruct-v0.2-4b-r16-task1452
Lots-of-LoRAs/Mistral-7B-Instruct-v0.2-4b-r16-task131	Lots-of-LoRAs/Mistral-7B-Instruct-v0.2-4b-r16-task685
Lots-of-LoRAs/Mistral-7B-Instruct-v0.2-4b-r16-task727	Lots-of-LoRAs/Mistral-7B-Instruct-v0.2-4b-r16-task1590
Lots-of-LoRAs/Mistral-7B-Instruct-v0.2-4b-r16-task1731	Lots-of-LoRAs/Mistral-7B-Instruct-v0.2-4b-r16-task047
Lots-of-LoRAs/Mistral-7B-Instruct-v0.2-4b-r16-task929	Lots-of-LoRAs/Mistral-7B-Instruct-v0.2-4b-r16-task1592
Lots-of-LoRAs/Mistral-7B-Instruct-v0.2-4b-r16-task1326	Lots-of-LoRAs/Mistral-7B-Instruct-v0.2-4b-r16-task615
Lots-of-LoRAs/Mistral-7B-Instruct-v0.2-4b-r16-task1216	Lots-of-LoRAs/Mistral-7B-Instruct-v0.2-4b-r16-task689
Lots-of-LoRAs/Mistral-7B-Instruct-v0.2-4b-r16-task1156	Lots-of-LoRAs/Mistral-7B-Instruct-v0.2-4b-r16-task1657
Lots-of-LoRAs/Mistral-7B-Instruct-v0.2-4b-r16-task833	Lots-of-LoRAs/Mistral-7B-Instruct-v0.2-4b-r16-task1206
Lots-of-LoRAs/Mistral-7B-Instruct-v0.2-4b-r16-task1151	Lots-of-LoRAs/Mistral-7B-Instruct-v0.2-4b-r16-task244
Lots-of-LoRAs/Mistral-7B-Instruct-v0.2-4b-r16-task1562	Lots-of-LoRAs/Mistral-7B-Instruct-v0.2-4b-r16-task043
Lots-of-LoRAs/Mistral-7B-Instruct-v0.2-4b-r16-task044	Lots-of-LoRAs/Mistral-7B-Instruct-v0.2-4b-r16-task722
Lots-of-LoRAs/Mistral-7B-Instruct-v0.2-4b-r16-task183	Lots-of-LoRAs/Mistral-7B-Instruct-v0.2-4b-r16-task563
Lots-of-LoRAs/Mistral-7B-Instruct-v0.2-4b-r16-task155	Lots-of-LoRAs/Mistral-7B-Instruct-v0.2-4b-r16-task353
Lots-of-LoRAs/Mistral-7B-Instruct-v0.2-4b-r16-task616	Lots-of-LoRAs/Mistral-7B-Instruct-v0.2-4b-r16-task1724
Lots-of-LoRAs/Mistral-7B-Instruct-v0.2-4b-r16-task288	Lots-of-LoRAs/Mistral-7B-Instruct-v0.2-4b-r16-task092
Lots-of-LoRAs/Mistral-7B-Instruct-v0.2-4b-r16-task707	Lots-of-LoRAs/Mistral-7B-Instruct-v0.2-4b-r16-task577
Lots-of-LoRAs/Mistral-7B-Instruct-v0.2-4b-r16-task742	Lots-of-LoRAs/Mistral-7B-Instruct-v0.2-4b-r16-task706
Lots-of-LoRAs/Mistral-7B-Instruct-v0.2-4b-r16-task1401	Lots-of-LoRAs/Mistral-7B-Instruct-v0.2-4b-r16-task1393
Lots-of-LoRAs/Mistral-7B-Instruct-v0.2-4b-r16-task1198	Lots-of-LoRAs/Mistral-7B-Instruct-v0.2-4b-r16-task966
Lots-of-LoRAs/Mistral-7B-Instruct-v0.2-4b-r16-task219	Lots-of-LoRAs/Mistral-7B-Instruct-v0.2-4b-r16-task1211
Lots-of-LoRAs/Mistral-7B-Instruct-v0.2-4b-r16-task050	Lots-of-LoRAs/Mistral-7B-Instruct-v0.2-4b-r16-task494
Lots-of-LoRAs/Mistral-7B-Instruct-v0.2-4b-r16-task1379	Lots-of-LoRAs/Mistral-7B-Instruct-v0.2-4b-r16-task176
Lots-of-LoRAs/Mistral-7B-Instruct-v0.2-4b-r16-task068	Lots-of-LoRAs/Mistral-7B-Instruct-v0.2-4b-r16-task566
Lots-of-LoRAs/Mistral-7B-Instruct-v0.2-4b-r16-task333	Lots-of-LoRAs/Mistral-7B-Instruct-v0.2-4b-r16-task593
Lots-of-LoRAs/Mistral-7B-Instruct-v0.2-4b-r16-task667	Lots-of-LoRAs/Mistral-7B-Instruct-v0.2-4b-r16-task1670
Lots-of-LoRAs/Mistral-7B-Instruct-v0.2-4b-r16-task733	Lots-of-LoRAs/Mistral-7B-Instruct-v0.2-4b-r16-task472
Lots-of-LoRAs/Mistral-7B-Instruct-v0.2-4b-r16-task1168	Lots-of-LoRAs/Mistral-7B-Instruct-v0.2-4b-r16-task075
Lots-of-LoRAs/Mistral-7B-Instruct-v0.2-4b-r16-task148	Lots-of-LoRAs/Mistral-7B-Instruct-v0.2-4b-r16-task683
Lots-of-LoRAs/Mistral-7B-Instruct-v0.2-4b-r16-task1315	Lots-of-LoRAs/Mistral-7B-Instruct-v0.2-4b-r16-task121
Lots-of-LoRAs/Mistral-7B-Instruct-v0.2-4b-r16-task370	Lots-of-LoRAs/Mistral-7B-Instruct-v0.2-4b-r16-task856
Lots-of-LoRAs/Mistral-7B-Instruct-v0.2-4b-r16-task891	Lots-of-LoRAs/Mistral-7B-Instruct-v0.2-4b-r16-task140
Lots-of-LoRAs/Mistral-7B-Instruct-v0.2-4b-r16-task609	Lots-of-LoRAs/Mistral-7B-Instruct-v0.2-4b-r16-task344
Lots-of-LoRAs/Mistral-7B-Instruct-v0.2-4b-r16-task1703	Lots-of-LoRAs/Mistral-7B-Instruct-v0.2-4b-r16-task070
Lots-of-LoRAs/Mistral-7B-Instruct-v0.2-4b-r16-task072	Lots-of-LoRAs/Mistral-7B-Instruct-v0.2-4b-r16-task504
Lots-of-LoRAs/Mistral-7B-Instruct-v0.2-4b-r16-task695	Lots-of-LoRAs/Mistral-7B-Instruct-v0.2-4b-r16-task1434
Lots-of-LoRAs/Mistral-7B-Instruct-v0.2-4b-r16-task095	Lots-of-LoRAs/Mistral-7B-Instruct-v0.2-4b-r16-task346
Lots-of-LoRAs/Mistral-7B-Instruct-v0.2-4b-r16-task274	Lots-of-LoRAs/Mistral-7B-Instruct-v0.2-4b-r16-task1325
Lots-of-LoRAs/Mistral-7B-Instruct-v0.2-4b-r16-task1190	Lots-of-LoRAs/Mistral-7B-Instruct-v0.2-4b-r16-task568
Lots-of-LoRAs/Mistral-7B-Instruct-v0.2-4b-r16-task1482	Lots-of-LoRAs/Mistral-7B-Instruct-v0.2-4b-r16-task924
Lots-of-LoRAs/Mistral-7B-Instruct-v0.2-4b-r16-task761	Lots-of-LoRAs/Mistral-7B-Instruct-v0.2-4b-r16-task596
Lots-of-LoRAs/Mistral-7B-Instruct-v0.2-4b-r16-task382	Lots-of-LoRAs/Mistral-7B-Instruct-v0.2-4b-r16-task926
Lots-of-LoRAs/Mistral-7B-Instruct-v0.2-4b-r16-task065	Lots-of-LoRAs/Mistral-7B-Instruct-v0.2-4b-r16-task1421
Lots-of-LoRAs/Mistral-7B-Instruct-v0.2-4b-r16-task323	Lots-of-LoRAs/Mistral-7B-Instruct-v0.2-4b-r16-task1310
Lots-of-LoRAs/Mistral-7B-Instruct-v0.2-4b-r16-task110	Lots-of-LoRAs/Mistral-7B-Instruct-v0.2-4b-r16-task1288
Lots-of-LoRAs/Mistral-7B-Instruct-v0.2-4b-r16-task1503	Lots-of-LoRAs/Mistral-7B-Instruct-v0.2-4b-r16-task269
Lots-of-LoRAs/Mistral-7B-Instruct-v0.2-4b-r16-task821	Lots-of-LoRAs/Mistral-7B-Instruct-v0.2-4b-r16-task565
Lots-of-LoRAs/Mistral-7B-Instruct-v0.2-4b-r16-task867	Lots-of-LoRAs/Mistral-7B-Instruct-v0.2-4b-r16-task755
Lots-of-LoRAs/Mistral-7B-Instruct-v0.2-4b-r16-task378	Lots-of-LoRAs/Mistral-7B-Instruct-v0.2-4b-r16-task518
Lots-of-LoRAs/Mistral-7B-Instruct-v0.2-4b-r16-task195	Lots-of-LoRAs/Mistral-7B-Instruct-v0.2-4b-r16-task618
Lots-of-LoRAs/Mistral-7B-Instruct-v0.2-4b-r16-task638	Lots-of-LoRAs/Mistral-7B-Instruct-v0.2-4b-r16-task1217

Lots-of-LoRAs/Mistral-7B-Instruct-v0.2-4b-r16-task118	Lots-of-LoRAs/Mistral-7B-Instruct-v0.2-4b-r16-task1564
Lots-of-LoRAs/Mistral-7B-Instruct-v0.2-4b-r16-task1429	Lots-of-LoRAs/Mistral-7B-Instruct-v0.2-4b-r16-task687
Lots-of-LoRAs/Mistral-7B-Instruct-v0.2-4b-r16-task640	Lots-of-LoRAs/Mistral-7B-Instruct-v0.2-4b-r16-task1328
Lots-of-LoRAs/Mistral-7B-Instruct-v0.2-4b-r16-task1311	Lots-of-LoRAs/Mistral-7B-Instruct-v0.2-4b-r16-task285
Lots-of-LoRAs/Mistral-7B-Instruct-v0.2-4b-r16-task1341	Lots-of-LoRAs/Mistral-7B-Instruct-v0.2-4b-r16-task1603
Lots-of-LoRAs/Mistral-7B-Instruct-v0.2-4b-r16-task162	Lots-of-LoRAs/Mistral-7B-Instruct-v0.2-4b-r16-task063
Lots-of-LoRAs/Mistral-7B-Instruct-v0.2-4b-r16-task686	Lots-of-LoRAs/Mistral-7B-Instruct-v0.2-4b-r16-task1483
Lots-of-LoRAs/Mistral-7B-Instruct-v0.2-4b-r16-task146	Lots-of-LoRAs/Mistral-7B-Instruct-v0.2-4b-r16-task1729
Lots-of-LoRAs/Mistral-7B-Instruct-v0.2-4b-r16-task852	Lots-of-LoRAs/Mistral-7B-Instruct-v0.2-4b-r16-task1622
Lots-of-LoRAs/Mistral-7B-Instruct-v0.2-4b-r16-task1704	Lots-of-LoRAs/Mistral-7B-Instruct-v0.2-4b-r16-task145
Lots-of-LoRAs/Mistral-7B-Instruct-v0.2-4b-r16-task648	Lots-of-LoRAs/Mistral-7B-Instruct-v0.2-4b-r16-task151
Lots-of-LoRAs/Mistral-7B-Instruct-v0.2-4b-r16-task1212	Lots-of-LoRAs/Mistral-7B-Instruct-v0.2-4b-r16-task045
Lots-of-LoRAs/Mistral-7B-Instruct-v0.2-4b-r16-task893	Lots-of-LoRAs/Mistral-7B-Instruct-v0.2-4b-r16-task936
Lots-of-LoRAs/Mistral-7B-Instruct-v0.2-4b-r16-task1425	Lots-of-LoRAs/Mistral-7B-Instruct-v0.2-4b-r16-task1533
Lots-of-LoRAs/Mistral-7B-Instruct-v0.2-4b-r16-task093	Lots-of-LoRAs/Mistral-7B-Instruct-v0.2-4b-r16-task389
Lots-of-LoRAs/Mistral-7B-Instruct-v0.2-4b-r16-task670	Lots-of-LoRAs/Mistral-7B-Instruct-v0.2-4b-r16-task461
Lots-of-LoRAs/Mistral-7B-Instruct-v0.2-4b-r16-task113	Lots-of-LoRAs/Mistral-7B-Instruct-v0.2-4b-r16-task066
Lots-of-LoRAs/Mistral-7B-Instruct-v0.2-4b-r16-task497	Lots-of-LoRAs/Mistral-7B-Instruct-v0.2-4b-r16-task343
Lots-of-LoRAs/Mistral-7B-Instruct-v0.2-4b-r16-task908	Lots-of-LoRAs/Mistral-7B-Instruct-v0.2-4b-r16-task1606
Lots-of-LoRAs/Mistral-7B-Instruct-v0.2-4b-r16-task381	Lots-of-LoRAs/Mistral-7B-Instruct-v0.2-4b-r16-task355
Lots-of-LoRAs/Mistral-7B-Instruct-v0.2-4b-r16-task850	Lots-of-LoRAs/Mistral-7B-Instruct-v0.2-4b-r16-task1557
Lots-of-LoRAs/Mistral-7B-Instruct-v0.2-4b-r16-task356	Lots-of-LoRAs/Mistral-7B-Instruct-v0.2-4b-r16-task1394
Lots-of-LoRAs/Mistral-7B-Instruct-v0.2-4b-r16-task1428	Lots-of-LoRAs/Mistral-7B-Instruct-v0.2-4b-r16-task087
Lots-of-LoRAs/Mistral-7B-Instruct-v0.2-4b-r16-task582	Lots-of-LoRAs/Mistral-7B-Instruct-v0.2-4b-r16-task770
Lots-of-LoRAs/Mistral-7B-Instruct-v0.2-4b-r16-task035	Lots-of-LoRAs/Mistral-7B-Instruct-v0.2-4b-r16-task1317
Lots-of-LoRAs/Mistral-7B-Instruct-v0.2-4b-r16-task1203	Lots-of-LoRAs/Mistral-7B-Instruct-v0.2-4b-r16-task1444
Lots-of-LoRAs/Mistral-7B-Instruct-v0.2-4b-r16-task1585	Lots-of-LoRAs/Mistral-7B-Instruct-v0.2-4b-r16-task1508
Lots-of-LoRAs/Mistral-7B-Instruct-v0.2-4b-r16-task740	Lots-of-LoRAs/Mistral-7B-Instruct-v0.2-4b-r16-task429
Lots-of-LoRAs/Mistral-7B-Instruct-v0.2-4b-r16-task1427	Lots-of-LoRAs/Mistral-7B-Instruct-v0.2-4b-r16-task328
Lots-of-LoRAs/Mistral-7B-Instruct-v0.2-4b-r16-task955	Lots-of-LoRAs/Mistral-7B-Instruct-v0.2-4b-r16-task130
Lots-of-LoRAs/Mistral-7B-Instruct-v0.2-4b-r16-task161	Lots-of-LoRAs/Mistral-7B-Instruct-v0.2-4b-r16-task507
Lots-of-LoRAs/Mistral-7B-Instruct-v0.2-4b-r16-task1502	Lots-of-LoRAs/Mistral-7B-Instruct-v0.2-4b-r16-task505
Lots-of-LoRAs/Mistral-7B-Instruct-v0.2-4b-r16-task633	Lots-of-LoRAs/Mistral-7B-Instruct-v0.2-4b-r16-task1645
Lots-of-LoRAs/Mistral-7B-Instruct-v0.2-4b-r16-task1486	Lots-of-LoRAs/Mistral-7B-Instruct-v0.2-4b-r16-task1146
Lots-of-LoRAs/Mistral-7B-Instruct-v0.2-4b-r16-task1380	Lots-of-LoRAs/Mistral-7B-Instruct-v0.2-4b-r16-task1088
Lots-of-LoRAs/Mistral-7B-Instruct-v0.2-4b-r16-task033	Lots-of-LoRAs/Mistral-7B-Instruct-v0.2-4b-r16-task085
Lots-of-LoRAs/Mistral-7B-Instruct-v0.2-4b-r16-task1294	Lots-of-LoRAs/Mistral-7B-Instruct-v0.2-4b-r16-task080
Lots-of-LoRAs/Mistral-7B-Instruct-v0.2-4b-r16-task489	Lots-of-LoRAs/Mistral-7B-Instruct-v0.2-4b-r16-task1721
Lots-of-LoRAs/Mistral-7B-Instruct-v0.2-4b-r16-task1713	Lots-of-LoRAs/Mistral-7B-Instruct-v0.2-4b-r16-task721
Lots-of-LoRAs/Mistral-7B-Instruct-v0.2-4b-r16-task1403	Lots-of-LoRAs/Mistral-7B-Instruct-v0.2-4b-r16-task746
Lots-of-LoRAs/Mistral-7B-Instruct-v0.2-4b-r16-task728	Lots-of-LoRAs/Mistral-7B-Instruct-v0.2-4b-r16-task889
Lots-of-LoRAs/Mistral-7B-Instruct-v0.2-4b-r16-task1583	Lots-of-LoRAs/Mistral-7B-Instruct-v0.2-4b-r16-task1665
Lots-of-LoRAs/Mistral-7B-Instruct-v0.2-4b-r16-task708	Lots-of-LoRAs/Mistral-7B-Instruct-v0.2-4b-r16-task1419
Lots-of-LoRAs/Mistral-7B-Instruct-v0.2-4b-r16-task963	Lots-of-LoRAs/Mistral-7B-Instruct-v0.2-4b-r16-task454
Lots-of-LoRAs/Mistral-7B-Instruct-v0.2-4b-r16-task308	Lots-of-LoRAs/Mistral-7B-Instruct-v0.2-4b-r16-task828
Lots-of-LoRAs/Mistral-7B-Instruct-v0.2-4b-r16-task579	Lots-of-LoRAs/Mistral-7B-Instruct-v0.2-4b-r16-task753
Lots-of-LoRAs/Mistral-7B-Instruct-v0.2-4b-r16-task1404	Lots-of-LoRAs/Mistral-7B-Instruct-v0.2-4b-r16-task1201
Lots-of-LoRAs/Mistral-7B-Instruct-v0.2-4b-r16-task901	Lots-of-LoRAs/Mistral-7B-Instruct-v0.2-4b-r16-task1567
Lots-of-LoRAs/Mistral-7B-Instruct-v0.2-4b-r16-task1319	Lots-of-LoRAs/Mistral-7B-Instruct-v0.2-4b-r16-task858
Lots-of-LoRAs/Mistral-7B-Instruct-v0.2-4b-r16-task1200	Lots-of-LoRAs/Mistral-7B-Instruct-v0.2-4b-r16-task492
Lots-of-LoRAs/Mistral-7B-Instruct-v0.2-4b-r16-task675	Lots-of-LoRAs/Mistral-7B-Instruct-v0.2-4b-r16-task094
Lots-of-LoRAs/Mistral-7B-Instruct-v0.2-4b-r16-task1506	Lots-of-LoRAs/Mistral-7B-Instruct-v0.2-4b-r16-task694
Lots-of-LoRAs/Mistral-7B-Instruct-v0.2-4b-r16-task614	Lots-of-LoRAs/Mistral-7B-Instruct-v0.2-4b-r16-task1390
Lots-of-LoRAs/Mistral-7B-Instruct-v0.2-4b-r16-task1355	Lots-of-LoRAs/Mistral-7B-Instruct-v0.2-4b-r16-task714
Lots-of-LoRAs/Mistral-7B-Instruct-v0.2-4b-r16-task457	Lots-of-LoRAs/Mistral-7B-Instruct-v0.2-4b-r16-task1565
Lots-of-LoRAs/Mistral-7B-Instruct-v0.2-4b-r16-task834	Lots-of-LoRAs/Mistral-7B-Instruct-v0.2-4b-r16-task642
Lots-of-LoRAs/Mistral-7B-Instruct-v0.2-4b-r16-task732	Lots-of-LoRAs/Mistral-7B-Instruct-v0.2-4b-r16-task1605
Lots-of-LoRAs/Mistral-7B-Instruct-v0.2-4b-r16-task326	Lots-of-LoRAs/Mistral-7B-Instruct-v0.2-4b-r16-task1292
Lots-of-LoRAs/Mistral-7B-Instruct-v0.2-4b-r16-task716	Lots-of-LoRAs/Mistral-7B-Instruct-v0.2-4b-r16-task1479
Lots-of-LoRAs/Mistral-7B-Instruct-v0.2-4b-r16-task1147	Lots-of-LoRAs/Mistral-7B-Instruct-v0.2-4b-r16-task153
Lots-of-LoRAs/Mistral-7B-Instruct-v0.2-4b-r16-task1495	Lots-of-LoRAs/Mistral-7B-Instruct-v0.2-4b-r16-task1196
Lots-of-LoRAs/Mistral-7B-Instruct-v0.2-4b-r16-task1489	Lots-of-LoRAs/Mistral-7B-Instruct-v0.2-4b-r16-task294
Lots-of-LoRAs/Mistral-7B-Instruct-v0.2-4b-r16-task157	Lots-of-LoRAs/Mistral-7B-Instruct-v0.2-4b-r16-task147
Lots-of-LoRAs/Mistral-7B-Instruct-v0.2-4b-r16-task1197	Lots-of-LoRAs/Mistral-7B-Instruct-v0.2-4b-r16-task754
Lots-of-LoRAs/Mistral-7B-Instruct-v0.2-4b-r16-task1599	Lots-of-LoRAs/Mistral-7B-Instruct-v0.2-4b-r16-task1420
Lots-of-LoRAs/Mistral-7B-Instruct-v0.2-4b-r16-task1285	Lots-of-LoRAs/Mistral-7B-Instruct-v0.2-4b-r16-task587
Lots-of-LoRAs/Mistral-7B-Instruct-v0.2-4b-r16-task1338	Lots-of-LoRAs/Mistral-7B-Instruct-v0.2-4b-r16-task116
Lots-of-LoRAs/Mistral-7B-Instruct-v0.2-4b-r16-task713	Lots-of-LoRAs/Mistral-7B-Instruct-v0.2-4b-r16-task431
Lots-of-LoRAs/Mistral-7B-Instruct-v0.2-4b-r16-task067	Lots-of-LoRAs/Mistral-7B-Instruct-v0.2-4b-r16-task934
Lots-of-LoRAs/Mistral-7B-Instruct-v0.2-4b-r16-task617	Lots-of-LoRAs/Mistral-7B-Instruct-v0.2-4b-r16-task696
Lots-of-LoRAs/Mistral-7B-Instruct-v0.2-4b-r16-task846	Lots-of-LoRAs/Mistral-7B-Instruct-v0.2-4b-r16-task933
Lots-of-LoRAs/Mistral-7B-Instruct-v0.2-4b-r16-task865	Lots-of-LoRAs/Mistral-7B-Instruct-v0.2-4b-r16-task671
Lots-of-LoRAs/Mistral-7B-Instruct-v0.2-4b-r16-task1398	Lots-of-LoRAs/Mistral-7B-Instruct-v0.2-4b-r16-task1518
Lots-of-LoRAs/Mistral-7B-Instruct-v0.2-4b-r16-task628	Lots-of-LoRAs/Mistral-7B-Instruct-v0.2-4b-r16-task1286
Lots-of-LoRAs/Mistral-7B-Instruct-v0.2-4b-r16-task1596	Lots-of-LoRAs/Mistral-7B-Instruct-v0.2-4b-r16-task298
Lots-of-LoRAs/Mistral-7B-Instruct-v0.2-4b-r16-task645	Lots-of-LoRAs/Mistral-7B-Instruct-v0.2-4b-r16-task903
Lots-of-LoRAs/Mistral-7B-Instruct-v0.2-4b-r16-task594	Lots-of-LoRAs/Mistral-7B-Instruct-v0.2-4b-r16-task413
Lots-of-LoRAs/Mistral-7B-Instruct-v0.2-4b-r16-task719	Lots-of-LoRAs/Mistral-7B-Instruct-v0.2-4b-r16-task672
Lots-of-LoRAs/Mistral-7B-Instruct-v0.2-4b-r16-task1418	Lots-of-LoRAs/Mistral-7B-Instruct-v0.2-4b-r16-task475
Lots-of-LoRAs/Mistral-7B-Instruct-v0.2-4b-r16-task357	Lots-of-LoRAs/Mistral-7B-Instruct-v0.2-4b-r16-task1387
Lots-of-LoRAs/Mistral-7B-Instruct-v0.2-4b-r16-task1711	Lots-of-LoRAs/Mistral-7B-Instruct-v0.2-4b-r16-task304
Lots-of-LoRAs/Mistral-7B-Instruct-v0.2-4b-r16-task750	Lots-of-LoRAs/Mistral-7B-Instruct-v0.2-4b-r16-task1320
Lots-of-LoRAs/Mistral-7B-Instruct-v0.2-4b-r16-task034	Lots-of-LoRAs/Mistral-7B-Instruct-v0.2-4b-r16-task692
Lots-of-LoRAs/Mistral-7B-Instruct-v0.2-4b-r16-task1406	Lots-of-LoRAs/Mistral-7B-Instruct-v0.2-4b-r16-task119
Lots-of-LoRAs/Mistral-7B-Instruct-v0.2-4b-r16-task211	Lots-of-LoRAs/Mistral-7B-Instruct-v0.2-4b-r16-task363

Lots-of-LoRAs/Mistral-7B-Instruct-v0.2-4b-r16-task1087	Lots-of-LoRAs/Mistral-7B-Instruct-v0.2-4b-r16-task083
Lots-of-LoRAs/Mistral-7B-Instruct-v0.2-4b-r16-task1385	Lots-of-LoRAs/Mistral-7B-Instruct-v0.2-4b-r16-task1308
Lots-of-LoRAs/Mistral-7B-Instruct-v0.2-4b-r16-task1656	Lots-of-LoRAs/Mistral-7B-Instruct-v0.2-4b-r16-task892
Lots-of-LoRAs/Mistral-7B-Instruct-v0.2-4b-r16-task499	Lots-of-LoRAs/Mistral-7B-Instruct-v0.2-4b-r16-task1409
Lots-of-LoRAs/Mistral-7B-Instruct-v0.2-4b-r16-task1207	Lots-of-LoRAs/Mistral-7B-Instruct-v0.2-4b-r16-task564
Lots-of-LoRAs/Mistral-7B-Instruct-v0.2-4b-r16-task325	Lots-of-LoRAs/Mistral-7B-Instruct-v0.2-4b-r16-task206
Lots-of-LoRAs/Mistral-7B-Instruct-v0.2-4b-r16-task890	Lots-of-LoRAs/Mistral-7B-Instruct-v0.2-4b-r16-task1520
Lots-of-LoRAs/Mistral-7B-Instruct-v0.2-4b-r16-task703	Lots-of-LoRAs/Mistral-7B-Instruct-v0.2-4b-r16-task318
Lots-of-LoRAs/Mistral-7B-Instruct-v0.2-4b-r16-task366	Lots-of-LoRAs/Mistral-7B-Instruct-v0.2-4b-r16-task335
Lots-of-LoRAs/Mistral-7B-Instruct-v0.2-4b-r16-task600	Lots-of-LoRAs/Mistral-7B-Instruct-v0.2-4b-r16-task477
Lots-of-LoRAs/Mistral-7B-Instruct-v0.2-4b-r16-task138	Lots-of-LoRAs/Mistral-7B-Instruct-v0.2-4b-r16-task291
Lots-of-LoRAs/Mistral-7B-Instruct-v0.2-4b-r16-task074	Lots-of-LoRAs/Mistral-7B-Instruct-v0.2-4b-r16-task1389
Lots-of-LoRAs/Mistral-7B-Instruct-v0.2-4b-r16-task192	Lots-of-LoRAs/Mistral-7B-Instruct-v0.2-4b-r16-task316
Lots-of-LoRAs/Mistral-7B-Instruct-v0.2-4b-r16-task1609	Lots-of-LoRAs/Mistral-7B-Instruct-v0.2-4b-r16-task296
Lots-of-LoRAs/Mistral-7B-Instruct-v0.2-4b-r16-task666	Lots-of-LoRAs/Mistral-7B-Instruct-v0.2-4b-r16-task1582
Lots-of-LoRAs/Mistral-7B-Instruct-v0.2-4b-r16-task1728	Lots-of-LoRAs/Mistral-7B-Instruct-v0.2-4b-r16-task701
Lots-of-LoRAs/Mistral-7B-Instruct-v0.2-4b-r16-task275	Lots-of-LoRAs/Mistral-7B-Instruct-v0.2-4b-r16-task107
Lots-of-LoRAs/Mistral-7B-Instruct-v0.2-4b-r16-task079	Lots-of-LoRAs/Mistral-7B-Instruct-v0.2-4b-r16-task1157
Lots-of-LoRAs/Mistral-7B-Instruct-v0.2-4b-r16-task1167	Lots-of-LoRAs/Mistral-7B-Instruct-v0.2-4b-r16-task403
Lots-of-LoRAs/Mistral-7B-Instruct-v0.2-4b-r16-task359	Lots-of-LoRAs/Mistral-7B-Instruct-v0.2-4b-r16-task517
Lots-of-LoRAs/Mistral-7B-Instruct-v0.2-4b-r16-task351	Lots-of-LoRAs/Mistral-7B-Instruct-v0.2-4b-r16-task964
Lots-of-LoRAs/Mistral-7B-Instruct-v0.2-4b-r16-task904	Lots-of-LoRAs/Mistral-7B-Instruct-v0.2-4b-r16-task1148
Lots-of-LoRAs/Mistral-7B-Instruct-v0.2-4b-r16-task879	Lots-of-LoRAs/Mistral-7B-Instruct-v0.2-4b-r16-task636
Lots-of-LoRAs/Mistral-7B-Instruct-v0.2-4b-r16-task1509	Lots-of-LoRAs/Mistral-7B-Instruct-v0.2-4b-r16-task207
Lots-of-LoRAs/Mistral-7B-Instruct-v0.2-4b-r16-task228	Lots-of-LoRAs/Mistral-7B-Instruct-v0.2-4b-r16-task209
Lots-of-LoRAs/Mistral-7B-Instruct-v0.2-4b-r16-task128	Lots-of-LoRAs/Mistral-7B-Instruct-v0.2-4b-r16-task710
Lots-of-LoRAs/Mistral-7B-Instruct-v0.2-4b-r16-task1322	Lots-of-LoRAs/Mistral-7B-Instruct-v0.2-4b-r16-task163
Lots-of-LoRAs/Mistral-7B-Instruct-v0.2-4b-r16-task178	Lots-of-LoRAs/Mistral-7B-Instruct-v0.2-4b-r16-task089
Lots-of-LoRAs/Mistral-7B-Instruct-v0.2-4b-r16-task700	Lots-of-LoRAs/Mistral-7B-Instruct-v0.2-4b-r16-task1581
Lots-of-LoRAs/Mistral-7B-Instruct-v0.2-4b-r16-task927	Lots-of-LoRAs/Mistral-7B-Instruct-v0.2-4b-r16-task101
Lots-of-LoRAs/Mistral-7B-Instruct-v0.2-4b-r16-task123	Lots-of-LoRAs/Mistral-7B-Instruct-v0.2-4b-r16-task1321
Lots-of-LoRAs/Mistral-7B-Instruct-v0.2-4b-r16-task550	Lots-of-LoRAs/Mistral-7B-Instruct-v0.2-4b-r16-task129
Lots-of-LoRAs/Mistral-7B-Instruct-v0.2-4b-r16-task393	Lots-of-LoRAs/Mistral-7B-Instruct-v0.2-4b-r16-task1214
Lots-of-LoRAs/Mistral-7B-Instruct-v0.2-4b-r16-task277	Lots-of-LoRAs/Mistral-7B-Instruct-v0.2-4b-r16-task1447
Lots-of-LoRAs/Mistral-7B-Instruct-v0.2-4b-r16-task324	Lots-of-LoRAs/Mistral-7B-Instruct-v0.2-4b-r16-task455
Lots-of-LoRAs/Mistral-7B-Instruct-v0.2-4b-r16-task725	Lots-of-LoRAs/Mistral-7B-Instruct-v0.2-4b-r16-task365
Lots-of-LoRAs/Mistral-7B-Instruct-v0.2-4b-r16-task1316	Lots-of-LoRAs/Mistral-7B-Instruct-v0.2-4b-r16-task1199
Lots-of-LoRAs/Mistral-7B-Instruct-v0.2-4b-r16-task717	Lots-of-LoRAs/Mistral-7B-Instruct-v0.2-4b-r16-task245
Lots-of-LoRAs/Mistral-7B-Instruct-v0.2-4b-r16-task874	Lots-of-LoRAs/Mistral-7B-Instruct-v0.2-4b-r16-task925
Lots-of-LoRAs/Mistral-7B-Instruct-v0.2-4b-r16-task380	Lots-of-LoRAs/Mistral-7B-Instruct-v0.2-4b-r16-task1712
Lots-of-LoRAs/Mistral-7B-Instruct-v0.2-4b-r16-task1504	Lots-of-LoRAs/Mistral-7B-Instruct-v0.2-4b-r16-task619
Lots-of-LoRAs/Mistral-7B-Instruct-v0.2-4b-r16-task590	Lots-of-LoRAs/Mistral-7B-Instruct-v0.2-4b-r16-task1186
Lots-of-LoRAs/Mistral-7B-Instruct-v0.2-4b-r16-task736	Lots-of-LoRAs/Mistral-7B-Instruct-v0.2-4b-r16-task069
Lots-of-LoRAs/Mistral-7B-Instruct-v0.2-4b-r16-task377	Lots-of-LoRAs/Mistral-7B-Instruct-v0.2-4b-r16-task181
Lots-of-LoRAs/Mistral-7B-Instruct-v0.2-4b-r16-task859	Lots-of-LoRAs/Mistral-7B-Instruct-v0.2-4b-r16-task144
Lots-of-LoRAs/Mistral-7B-Instruct-v0.2-4b-r16-task632	Lots-of-LoRAs/Mistral-7B-Instruct-v0.2-4b-r16-task641
Lots-of-LoRAs/Mistral-7B-Instruct-v0.2-4b-r16-task064	Lots-of-LoRAs/Mistral-7B-Instruct-v0.2-4b-r16-task630
Lots-of-LoRAs/Mistral-7B-Instruct-v0.2-4b-r16-task1154	Lots-of-LoRAs/Mistral-7B-Instruct-v0.2-4b-r16-task390
Lots-of-LoRAs/Mistral-7B-Instruct-v0.2-4b-r16-task1188	Lots-of-LoRAs/Mistral-7B-Instruct-v0.2-4b-r16-task625
Lots-of-LoRAs/Mistral-7B-Instruct-v0.2-4b-r16-task607	Lots-of-LoRAs/Mistral-7B-Instruct-v0.2-4b-r16-task495
Lots-of-LoRAs/Mistral-7B-Instruct-v0.2-4b-r16-task1189	Lots-of-LoRAs/Mistral-7B-Instruct-v0.2-4b-r16-task398
Lots-of-LoRAs/Mistral-7B-Instruct-v0.2-4b-r16-task108	Lots-of-LoRAs/Mistral-7B-Instruct-v0.2-4b-r16-task1347
Lots-of-LoRAs/Mistral-7B-Instruct-v0.2-4b-r16-task1541	Lots-of-LoRAs/Mistral-7B-Instruct-v0.2-4b-r16-task202
Lots-of-LoRAs/Mistral-7B-Instruct-v0.2-4b-r16-task1723	Lots-of-LoRAs/Mistral-7B-Instruct-v0.2-4b-r16-task1669
Lots-of-LoRAs/Mistral-7B-Instruct-v0.2-4b-r16-task1089	Lots-of-LoRAs/Mistral-7B-Instruct-v0.2-4b-r16-task1584
Lots-of-LoRAs/Mistral-7B-Instruct-v0.2-4b-r16-task081	Lots-of-LoRAs/Mistral-7B-Instruct-v0.2-4b-r16-task329
Lots-of-LoRAs/Mistral-7B-Instruct-v0.2-4b-r16-task691	Lots-of-LoRAs/Mistral-7B-Instruct-v0.2-4b-r16-task588
Lots-of-LoRAs/Mistral-7B-Instruct-v0.2-4b-r16-task1593	Lots-of-LoRAs/Mistral-7B-Instruct-v0.2-4b-r16-task724
Lots-of-LoRAs/Mistral-7B-Instruct-v0.2-4b-r16-task149	Lots-of-LoRAs/Mistral-7B-Instruct-v0.2-4b-r16-task1449
Lots-of-LoRAs/Mistral-7B-Instruct-v0.2-4b-r16-task1313	Lots-of-LoRAs/Mistral-7B-Instruct-v0.2-4b-r16-task1453
Lots-of-LoRAs/Mistral-7B-Instruct-v0.2-4b-r16-task905	Lots-of-LoRAs/Mistral-7B-Instruct-v0.2-4b-r16-task704
Lots-of-LoRAs/Mistral-7B-Instruct-v0.2-4b-r16-task585	Lots-of-LoRAs/Mistral-7B-Instruct-v0.2-4b-r16-task1209
Lots-of-LoRAs/Mistral-7B-Instruct-v0.2-4b-r16-task249	Lots-of-LoRAs/Mistral-7B-Instruct-v0.2-4b-r16-task1386
Lots-of-LoRAs/Mistral-7B-Instruct-v0.2-4b-r16-task1400	Lots-of-LoRAs/Mistral-7B-Instruct-v0.2-4b-r16-task751
Lots-of-LoRAs/Mistral-7B-Instruct-v0.2-4b-r16-task1332	Lots-of-LoRAs/Mistral-7B-Instruct-v0.2-4b-r16-task674
Lots-of-LoRAs/Mistral-7B-Instruct-v0.2-4b-r16-task379	Lots-of-LoRAs/Mistral-7B-Instruct-v0.2-4b-r16-task243
Lots-of-LoRAs/Mistral-7B-Instruct-v0.2-4b-r16-task1318	Lots-of-LoRAs/Mistral-7B-Instruct-v0.2-4b-r16-task428
Lots-of-LoRAs/Mistral-7B-Instruct-v0.2-4b-r16-task488	Lots-of-LoRAs/Mistral-7B-Instruct-v0.2-4b-r16-task705
Lots-of-LoRAs/Mistral-7B-Instruct-v0.2-4b-r16-task698	Lots-of-LoRAs/Mistral-7B-Instruct-v0.2-4b-r16-task1601
Lots-of-LoRAs/Mistral-7B-Instruct-v0.2-4b-r16-task861	Lots-of-LoRAs/Mistral-7B-Instruct-v0.2-4b-r16-task1510
Lots-of-LoRAs/Mistral-7B-Instruct-v0.2-4b-r16-task077	Lots-of-LoRAs/Mistral-7B-Instruct-v0.2-4b-r16-task509
Lots-of-LoRAs/Mistral-7B-Instruct-v0.2-4b-r16-task734	Lots-of-LoRAs/Mistral-7B-Instruct-v0.2-4b-r16-task720
Lots-of-LoRAs/Mistral-7B-Instruct-v0.2-4b-r16-task1210	Lots-of-LoRAs/Mistral-7B-Instruct-v0.2-4b-r16-task284
Lots-of-LoRAs/Mistral-7B-Instruct-v0.2-4b-r16-task584	Lots-of-LoRAs/Mistral-7B-Instruct-v0.2-4b-r16-task105
Lots-of-LoRAs/Mistral-7B-Instruct-v0.2-4b-r16-task330	Lots-of-LoRAs/Mistral-7B-Instruct-v0.2-4b-r16-task923
Lots-of-LoRAs/Mistral-7B-Instruct-v0.2-4b-r16-task319	Lots-of-LoRAs/Mistral-7B-Instruct-v0.2-4b-r16-task400
Lots-of-LoRAs/Mistral-7B-Instruct-v0.2-4b-r16-task246	Lots-of-LoRAs/Mistral-7B-Instruct-v0.2-4b-r16-task726
Lots-of-LoRAs/Mistral-7B-Instruct-v0.2-4b-r16-task1568	Lots-of-LoRAs/Mistral-7B-Instruct-v0.2-4b-r16-task1442
Lots-of-LoRAs/Mistral-7B-Instruct-v0.2-4b-r16-task1640	Lots-of-LoRAs/Mistral-7B-Instruct-v0.2-4b-r16-task280

Figure 11 presents the aggregated results across all layers, with error bars representing the standard deviation. For reference, the eigenvalue (scree) plot from Figure 4b is also reproduced in Figure 12.

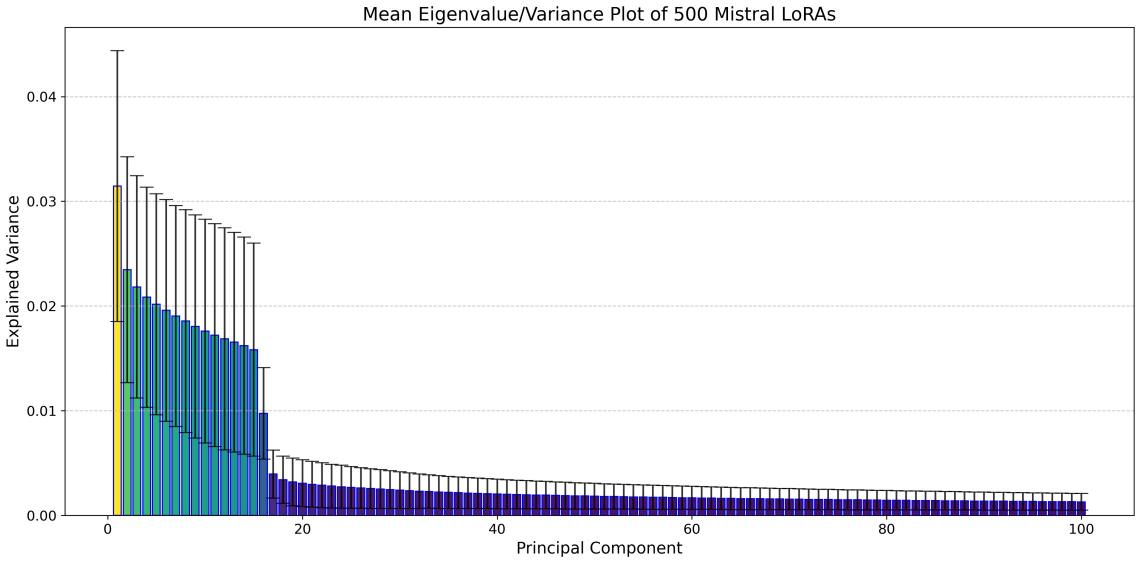


Figure 11: Spectral analysis of the Mistral-7B-Instruct-v0.2 model: Aggregated eigenvalue (scree) plot across 500 LoRA models and all layers. The plot demonstrates that the majority of the variance is consistently captured by the top few principal directions, indicating the presence of a shared low-dimensional universal subspace.

This plot depicts the proportion of variance explained by each principal component, computed across all weight matrices and layers from 500 independently trained Mistral models. The concentration of variance within the top k components reveals the presence of a consistent low-dimensional subspace, offering strong empirical support for the universal subspace hypothesis.

The individual plots provide spectral analysis results for the key, query, and value matrices from all 31 layers of all 500 Mistral models. For clarity, only the top 128 principal directions are visualized, representing a subset of the full component basis. This truncation mitigates the visual distortion caused by the long tail of near-zero eigenvalues beyond the universal subspace, which would otherwise dominate the graph without contributing meaningful information.

To test subspace expressiveness, we reconstruct LoRA weights for both 5 seen (IID) and unseen (OOD) tasks by projecting them into the universal subspace. As shown in Figure 3, the reconstructed models retain high performance in both cases. In contrast, projection into the residual *Secondary Subspace* leads to a sharp performance drop, underscoring the importance of the principal subspace. Our method is also 19× more memory efficient, as it eliminates the need to store all 500 LoRAs.

Table 11: Models from HuggingFace used for the Universal Stable Diffusion-XL subspace extraction

alphonse-mucha-style	directors-coen-brothers-style	larry-carlson-style	rene-magritte-style
beeple-mike-winkelmann-style	director-sergei-eisenstein-style	lascaux	richard-corben-style
character-design	director-sofia-coppola-style	laurel-burch-style	richard-dadd-style
director-christopher-nolan-style	director-terrence-malick-style	lawrence-alma-tadema-style	richard-hescox-style
director-lars-von-trier-style	director-tim-burton-style	leonid-afremov-style	richard-scarry-style
director-ridley-scott-style	director-wes-anderson-style	leonora-carrington-style	robert-adams-style
director-stanley-kubrick-style	director-wong-kar-wai-style	levitating-cube	robert-crumb-style

director-zhang-yimou-style	director-yorgos-lanthimos-style	liam-wong-style	robert-rauschenberg-style
olafur-eliasson-style	dixit-card-generator	lotte-reiniger-style	rodney-matthews-style
origami	dressed-animals	louis-comfort-tiffany-style	roger-ballen-style
simone-martini-style	dripping-art	lovis-corinth-style	roger-deakins-style
studio-ghibli-style	edward-gorey-style	lucas-cranach-style	romare-bearden-style
ukiyo-e-art	elizabeth-gadd-style	luc-schuiten-style	ryoji-ikeda-style
wu-guanzhong-style	erik-johansson-style	lyonel-feininger-style	sacha-goldberger-style
1987-action-figure-playset-packaging	erik-madigan-heck-style	made-of-iridescent-foil	salomon-van-ruysdael-style
aardman-animations-style	euan-uglow-style	makoto-shinkai-style	sam-spratt-style
akos-major-style	felipe-pantone-style	marc-silvestri-style	sandy-skoglund-style
albumen-print	filip-hodas-style	marianna-rothen-style	santiago-caruso-style
alec-soth-style	folk-art	maria-sibylla-merian-style	shaun-tan-style
alejandro-jodorowsky-style	gabriel-pacheco-style	mark-catesby-style	shepard-fairey-style
alessandro-gottardo-style	gemma-correll-style	mark-ryden-style	sidney-nolan-style
alex-andreev-style	george-condo-style	martin-whatson-style	simon-stalenhag-style
alex-gross-style	gilbert-garcin-style	mary-cassatt-style	skottie-young-style
alfred-augustus-glendening-style	gregory-crewdson-style	maurice-de-vlaminck-style	sofonisba-anguissola-style
alex-pardee-style	gustave-dore-style	maurice-prendergast-style	sophie-gengembre-anderson-style
alternate-realities	hasui-kawase-style	maxfield-parrish-style	stained-glass-portrait
ando-fuchs-style	hiroshi-nagai-style	maxime-maufra-style	stanley-donwood-style
andre-derain-style	infrared-photos	mike-mignola-style	stephan-martiniere-style
andrei-tarkovsky-style	isometric-cutaway	mikhail-vrubel-style	stephen-gammell-style
andrew-wyeth-style	ivan-bilibin-style	moebius-jean-giraud-style	stop-motion-animation
angus-mckie-style	james-c-christensen-style	movie-poster	surreal-collage
anna-maria-garthwaite-style	james-jean-style	moving-meditations	surreal-harmony
atey-ghailan-style	james-r-eads-style	nadav-kander-style	surreal-plate
audrey-kawasaki-style	james-turrell-style	natalia-goncharova-style	syd-mead-style
avant-garde-fashion	jan-brueghel-style	n-c-wyeth-style	synthwave-t-shirt
banksy-style	jan-svankmajer-style	needlepoint	teamlab-style
bas-relief	jan-van-eyck-style	neon-night	terry-gilliam-style
century-botanical-illustration	jan-van-goyen-style	nicolas-poussin-style	thomas-cole-style
christopher-balaskas-style	j-c-leyendecker-style	noah-bradley-style	thomas-kinkade-style
christopher-ryan-mckenney-style	jean-baptiste-camille-corot-style	ohara-koson-style	thomas-moran-style
clay-animation	jean-baptiste-monge-style	okuda-san-miguel-style	thomas-schaller-style
color-palette	jean-baptiste-simeon-chardin-style	olly-moss-style	tim-walker-style
craig-mullins-style	jean-metzinger-style	op-art	tintoretto-style
crocheted	jean-michel-basquiat-style	parralel-dimensions	todd-hido-style
daniel-arsham-style	jessie-willcox-smith-style	pascal-campion-style	tove-jansson-style
dark-fantasy	jim-mahfood-style	paul-gustav-fischer-style	tracie-grimwood-style
dave-mckean-style	john-albert-bauer-style	paul-laffoley-style	vasily-vereshchagin-style
diorama	john-berkey-style	paul-signac-style	vertical-landscapes
director-agnes-varda-style	john-blanche-style	peter-doig-style	victor-brauner-style
death-stranding	john-constable-style	peter-paul-rubens-style	victor-moscoso-style
director-akira-kurosawa-style	john-everett-millais-style	philippe-druillet-style	video-installation
director-andrei-zvyagintsev-style	john-harris-style	photographer-elena-helfrecht-style	vintage-postage-stamps
director-bong-joon-ho-style	john-james-audubon-style	photographer-flora-borsi-style	weegee-style
director-darren-aronofsky-style	john-kenn-mortensen-style	photographer-maren-klemp-style	wendy-froud-style
director-david-fincher-style	john-martin-style	photographer-martin-kimbell-style	will-eisner-style
director-david-lynch-style	john-singer-sargent-style	photographer-reuben-wu-style	willem-haenraets-style
cute-animals	john-singleton-copley-style	pierre-auguste-renoir-style	willem-van-aelst-style
ben-aronson-style	john-william-waterhouse-style	pierre-bonnard-style	william-langson-lathrop-style
director-emir-kusturica-style	joseph-wright-of-derby-style	pieter-claesz-style	william-mctaggart-style
director-gaspar-noe-style	josh-agle-style	punk-collage	william-merritt-chase-style
director-jean-pierre-jeunet-style	josh-kirby-style	quentin-blake-style	winslow-homer-style
director-krzysztof-kieslowski-style	jules-bastien-lepage-style	raimonds-staprans-style	worthington-whittredge-style
director-martin-scorsese-style	kate-greenaway-style	ralph-bakshi-style	yaacov-agam-style
director-nicolas-winding-refn-style	kay-nielsen-style	ralph-steadman-style	yoh-nagao-style
director-park-chan-wook-style	kilian-eng-style	randolph-caldecott-style	yves-klein-style
director-pedro-almodovar-style	kirigami	ray-caesar-style	zanele-muholi-style
director-quentin-tarantino-style	konstantin-korovin-style	remedios-varo-style	

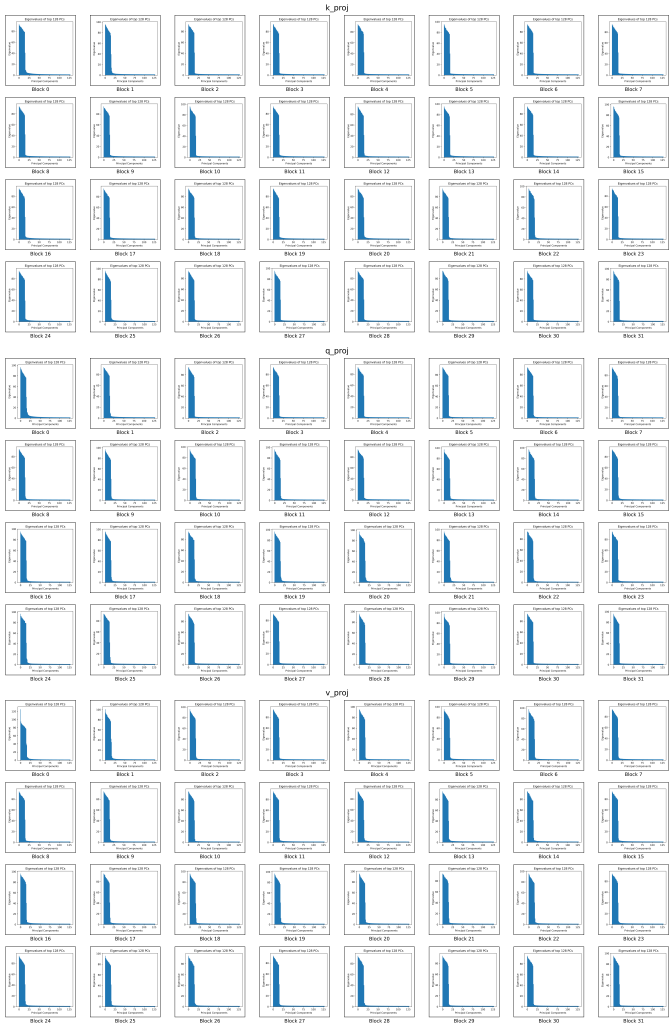


Figure 12: Layerwise Eigenvalue Plots of 500 Mistral-7B-Instruct-v0.2 models. Each layer has 3 sets of parameters - k_proj, q_proj, v_proj

Universal SDXL experiment details Our second experiment involves the complex and multimodal task of Text-to-Image generation using the Stable Diffusion-XL model Podell et al. (2023). We extract our low rank universal subspace from publicly available LoRA models on HuggingFace repository von Platen et al. (2022) - Table 11 lists all the SDXL models that we used to extract the Universal Subspace. As can be seen in Table 11, the models range wildly in styles on which they were finetuned. The fact that all these diverse models can be represented by a single low rank universal subspace model provides strong empirical support for our hypothesis. We use top 16 components and 30 denoising steps. For each experiment model shown in Table 1 and Figure 5,

that LoRA model is reconstructed using a universal subspace created using rest of the available LoRA adapters, essentially confirming the generalization capability of this subspace.

We then use this single SDXL universal subspace to generate images with similar styles to evaluate whether this subspace is capable of doing so, by projecting randomly chosen LoRA models into this subspace. Figure 5 shows that our universal subspace matches the visual quality and style nuances of individual LoRAs, resulting in significant memory savings. Table 1 shows quantitative results for our Universal subspace in terms of CLIP scores, where interestingly we can see that our Universal Subspace outperforms the individual LoRA models. The small improvement may reflect a denoising effect from low-rank spectral projection, although we do not isolate its cause here - similar to what was observed by Sharma et al. (2023). The styles used in Table 1, which are in Table 11 are (from Style 1 to Style 10) Ukiyo-e Style, Todd Hildo Style , Olly Moss Style , Needlepoint Style , Studio Ghibli Style, Surreal Harmony Style , Dressed Animal Style , Lascaux Cave Art Style , Kirigami Style , Yaacov Agam Style.

B.6 Low rank shared universal subspaces in classical weights

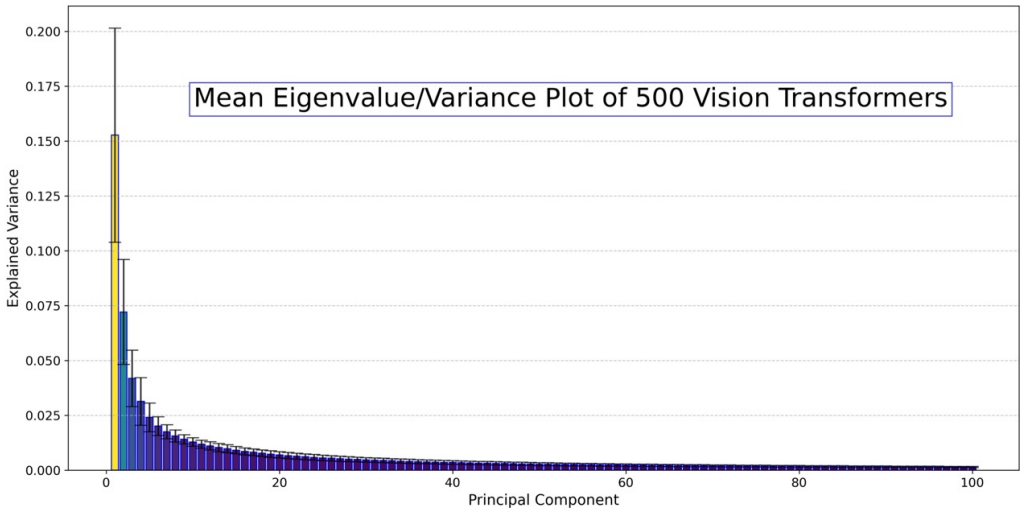


Figure 13: Spectral analysis of the Vision Transformer (ViT-base-patch16-224) model: Aggregated eigenvalue (scree) plot across 500 ViT models and all layers. The plot demonstrates that the majority of the variance is consistently captured by the top 16 principal directions, indicating the presence of a shared low-dimensional universal subspace.

We show that this universality does extend beyond adapter models to conventional weights. Convolutional weight parameters have been shown, in limited scope, to match Gabor-like filters (Krizhevsky et al., 2012). Therefore, our analysis extends to these kinds of parameters as well. However, there are a few practical differences between the low rank adapter and classical weight subspace analysis. The classical weight subspace analysis is more computationally expensive relative to the LoRA one due to high dimensionality of the parameters, but in effect, same. Additionally, the number of sufficiently well trained models is understandably fewer than LoRA

models. Further, there is also higher variance in terms of model quality in the classical weights as it is harder to optimize these models as compared to LoRA which often are optimized from a good initialization point (the pretrained base model). An outcome of this is that the universal subspace approximation that we obtain from the publicly available pretrained models are noisier than their LoRA counterparts. Despite this, our universal subspace hypothesis remains validated.

To further support our universal subspace hypothesis, we extend our analysis beyond adapter models to standard full-rank weights. We also include convolutional parameters, although they are functionally equivalent to fully connected layers under certain conditions (Ma & Lu, 2017), and their learned representations (e.g., Gabor-like filters) have been studied, in limited scope, in prior work (Krizhevsky et al., 2012). Consequently, our analysis generalizes naturally to convolutional weights as well.

There are, however, practical differences between the subspace analysis of full-rank model weights and that of low-rank adapters. First, analyzing conventional weight matrices is significantly more computationally intensive because of their higher dimensionality. Second, the availability of a large number of independently and sufficiently well-trained models is limited compared to LoRA models. Third, the classical weight models exhibit greater variance in model quality when trained from scratch, as it requires good initialization, optimization, and a sufficient amount and quality of data, unlike LoRA which builds upon a strong pretrained base.

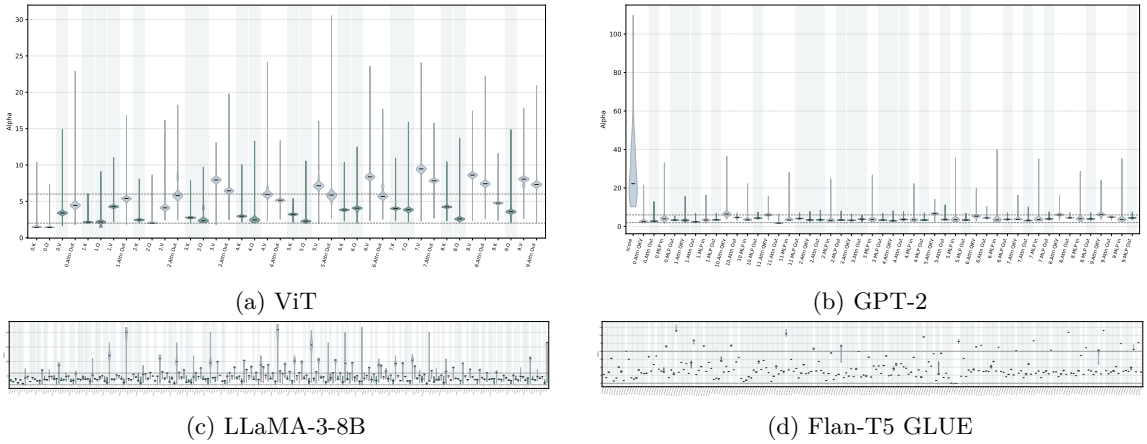
As a result, subspaces estimated from classical weights tend to be noisier than their LoRA counterparts. Despite this, we consistently observe dominant shared spectral structure, providing further empirical support for the Universal Subspace hypothesis.

Transformer suitability diagnostics. For the VIT analysis, we compute α directly from the raw weight matrices using the procedure in Section B.1. We estimate α for every available model and layer, then compute q_l, q_{all}, and q_{arch} from those estimates. The retained layers are the ones used to calculate q_{arch}.

Table 12: Suitability diagnostics for classical-transformer model families. Retained layers satisfy the statistical and q_l criteria in Section B.1.

Family	**Models**	**Mean α**	q_{all}	q_{arch}	**Retained Layers**
ViT	464	4.7066	0.0518	0.3545	18 / 40
GPT-2	177	4.0951	0.0725	0.3059	23 / 49
LLaMA-3-8B	50	5.2391	0.0940	0.3290	116 / 224
Flan-T5 GLUE	196	3.9136	0.0224	0.4850	179 / 216

Universal ViT experiment details We collect ∼500 pretrained ViT models from HuggingFace, shown in Table 13, spanning very diverse domains - many of which would be considered orthogonal to one another in terms of domain generalization. These models have been trained with varying losses, optimizers, and initializations. These models were used as-is, without curation or access to training data, to reflect real-world variability. Figure 13 shows the summarized scree plot for all relevant layers of ViT (sans first and last layers due to differences in shape and tasks) for all ~ 500 ViT models showing that the majority of variance is captured by the top 16 principal directions, revealing a highly compressible, shared subspace across layers. Only the top 100 components are visualized for clarity, although the available subspace is significantly larger, underlying the sparsity of this universal subspace. We observe this for layerwise analysis in Figure 15 as well. For the



(a) ViT (b) GPT-2

(c) LLaMA-3-8B (d) Flan-T5 GLUE

Figure 14: Per-layer alpha diagnostics for classical-transformer families. Each violin aggregates valid raw-weight alpha estimates over all available models for a fixed layer; retained layers are summarized numerically in Table 12.

experimental results presented in Table 2, we randomly choose 4-5 IID and 4-5 OOD models from Table 13 for which evaluation dataset is available, and reconstruct these model weights by projecting them into our universal subspace. For the OOD case, we ensure that the models being evaluated are not present in the subset used for creating the universal subspace approximation. As seen from the results, our extremely sparse subspace model performs competitively compared to the fully trained versions. It is likely that with more careful choice of principal directions per layer would allow for at par or even better performance.

Table 13: Finetuned Models from HuggingFace used for the Universal Vision Transformer subspace extraction (vit-base-patch16-224)

0.50-200Train-100Test-vit-base	2025-01-21-16-13-04-vit-base-patch16-224
2025-02-05-14-22-36-vit-base-patch16-224	21BAI1229
Accomodation__room__classification	adam__VitB-p16-224-1e-4-batch__16__epoch__4__classes__24
age__face__detection__base	AIvisionGuard-v2
alea	amns
AnimeCharacterClassifierMark1	autotrain-48ci8-roib9
autotrain-8oqr6-image0807-20	autotrain-ap-pass-fail-v1
autotrain-g2g80-iwcfm	autotrain-google-vit-13epoch
autotrain-ht4es-gbvmt	autotrain-image-classifier-cats-and-dogs
autotrain-pknu0-o76h9	autotrain-s0sds-erede
autotrain-test-image-classification	autotrain-vit-base-patch16-224-fog-or-smog-classification
beauty-ornot	beer-classifier
bg-classif	bigger-chord-finetuned
brain-tumor-44	ButterflyClasifModel
camera-type	Caracam
cards-vit-base-patch16-224-finetuned-v1	carmodel
cats123	cats-dogs-2024
cats-dogs-classification	CheXpert-ViT-U-MultiClass
CheXpert-ViT-U-SelfTrained	chord-final-model
chord__ViT-finetuned	cifar10-lt
city__multiclass__classification	clasificador__masas
corals__binary__classification	custom
detect__meme	dog-breeds-classification
dog-cat-demo-20240815	dog-cats-model
dummy__classification__model	dvm-cars-vit-first-5k
ecg-image-multilabel-classification	emotion
EmotionAgeModel	emotion__model
emotion-recognition	emotion__recognition
emotion__recognition__results	emotion-vit
face__age__detection__base__v2	face__age__detection__base__v3__weighted
final-run	finetune-cats
fine-tuned	finetuned-amazon
fine-tuned-augmented	finetuned-bin
finetuned-cifar10	finetuned-indian-food
fine-tuned-model	finetuned__model

Fine-Tuned__Model	Fine-Tuned__Model2
Fine-Tuned__Model3	Fine-Tuned__Model3__Transfer__learning
finetune-vit-base-patch16-224	finetune__vit__base__patch16__224__1epoch
Flowers	food
food-101-finetuned-model	Freshness-Fruit__Vegies
frost-vision-v2-google__vit-base-patch16-224	frost-vision-v2-google__vit-base-patch16-224-v2024-11-09
frost-vision-v2-google__vit-base-patch16-224-v2024-11-11	frost-vision-v2-google__vit-base-patch16-224-v2024-11-14
fruit__classification	fruits-360-16-7
ft__stable__diffusion	gender
giecom-vit-model-clasification-waste	google-vit-base-patch16-224-batch32-lr0.0005-standford-dogs
google-vit-base-patch16-224-batch32-lr0.005-standford-dogs	google-vit-base-patch16-224-batch32-lr5e-05-standford-dogs
google-vit-base-patch16-224-batch64-lr0.005-standford-dogs	google-vit-base-patch16-224-OrganicAndInorganicWaste-classification
google-vit-base-patch16-224-Waste-O-I-classification	hf__vit__format__hap__pretrained__256__128
Human-Action-Recognition-VIT-Base-patch16-224	human-actions
image-classification	image__classification
image__strawbery-peach__classifier	isa-vit__model
lixg__food__model001	Maggi-Parle-G__Classifier
mammals__multiclass__classification	MemeDetector
model	Model
model-vit-base-finetuned	MRI__vit
my__chest__xray__model	myclass
my__classification	MyPetModel
out	outputs
PagesClassificationModel	physiotheraphy-E2
plant__disease__detection-beans	pokemon__classification
pokemon__model	pokemon-vit
recaptcha	recycled__waste__classification
results	rmsprop__VitB-p16-224-1e-4-batch__16__epoch__4__classes__24
rmsprop__VitB-p16-224-2e-4-batch__16__epoch__4__classes__24	road-conditions
rose__recognition	rotated2
Ruster	S1__M1__R1__vit__42498800
S1__M1__R1__vit__42509509	S1__M1__R1__ViT__42616100
S1__M1__R2__vit__42498972	S1__M1__R2__ViT__42618476
S1__M1__R3__vit__42499444	S1__M1__R3__ViT__42618486
S2__M1__R1__vit__42499480	S2__M1__R1__ViT__42618522
S2__M1__R2__vit__42499499	S2__M1__R2__ViT__42618530
S2__M1__R3__vit__42499514	S2__M1__R3__ViT__42618549
S5__M1__fold1__vit__42499955	S5__M1__fold1__ViT__42618571
S5__M1__fold2__vit__42499968	S5__M1__fold2__ViT__42618583
S5__M1__fold3__vit__42499983	S5__M1__fold3__ViT__42618589
S5__M1__fold4__vit__42499997	S5__M1__fold4__ViT__42618593
S5__M1__fold5__vit__42500027	S5__M1__fold5__ViT__42621111
Screenshots__detection__to__classification	sign-lan-model
square__run__32__batch	square__run__age__gender
square__run__first__vote__full__pic__50	square__run__first__vote__full__pic__50__age__gender
square__run__first__vote__full__pic__75	square__run__first__vote__full__pic__75__age__gender
square__run__second__vote	square__run__second__vote__full__pic__50
square__run__second__vote__full__pic__50__age__gender	square__run__second__vote__full__pic__75
square__run__second__vote__full__pic__75__age__gender	square__run__second__vote__full__pic__age__gender
square__run__second__vote__full__pic__stratified	square__run__square__run__first__vote__full__pic__25
square__run__square__run__first__vote__full__pic__25__age	square__run__square__run__first__vote__full__pic
square__run__square__run__first__vote__full__pic__25	square__run__square__run__second__vote__full__pic__25
square__run__square__run__second__vote..nder	square__run__with__16__batch__size
square__run__with__actual__16__batch__size	stool-condition-classification
swaddling-classifier	swin-tiny-patch4-window7-224-finetuned-eurosat-kornia
tarread	telidermai
test-cifar-10	traffic-levels-image-classification
Train-Augmentation-vit-base	trainer__output
Train-Test-Augmentation-V3D-vit-base	UL__base__classification
UL__bedroom__classification	UL__exterior__classification
UL__interior__classification	vehicle__multiclass__classification
ViT__ASVspoof__DF	vit-augmentation
vit-b16-plant__village	vit__base
vit-base-1e-4-15ep	vit-base-1e-4-20ep
vit-base-1e-4-randaug	vit-base-1stGen-Pokemon-Images
vit-base-25ep	Vit-Base-30VN
vit-base-3e-5-randaug	vit-base-5e-4
vit-base-add-2-decay	vit-base-augment
vit-base-batch-32	vit-base-beans
vit-base-brain-mri	vit-base-cat__or__dog
vit-base-change-arg	vit-base-cocoa
ViT-Base-Document-Classifier	vit-base-fashion
vit-base-finetuned-cephalometric	vit-base-food101
vit-base-fruits-360	vit-base-hate-meme
vit-base-nationality	vit-base-org-plot
vit-base-oxford-brain-tumor	vit-base-oxford-brain-tumor__try__stuff
vit-base-oxford-brain-tumor__x-ray	vit-base-oxford-iiit-pets
vit-base-oxford-pets-krasuluk	vit-base-patch16-224
vit-base-patch16-224-13__model	vit-base-patch16-224-30-vit
vit-base-patch16-224-9models	vit-base-patch16-224-abhi1-finetuned

vit-base-patch16-224__augmented-v2__fft	vit-base-patch16-224__augmented-v2__tl
vit-base-patch16-224-blur__vs__clean	vit-base-patch16-224-brand
vit-base-patch16-224-classifier	vit-base-patch16-224-clothes-filter
vit-base-patch16-224-cl-v1	vit-base-patch16-224-crochets-clothes-classification
vit-base-patch16-224-Diastar	vit-base-patch16-224-Diastarallclasses
vit-base-patch16-224-dmae-va-U	vit-base-patch16-224-dmae-va-U5-100-iN
vit-base-patch16-224-dmae-va-U5-10-45-5e-05	vit-base-patch16-224-dmae-va-U5-20-45-5e-05
vit-base-patch16-224-dmae-va-U5-40-45-5e-05	vit-base-patch16-224-dmae-va-U5-42B
vit-base-patch16-224-dmae-va-U5-42C	vit-base-patch16-224-dmae-va-U5-42D
vit-base-patch16-224-ethos	vit-base-patch16-224-ethos-25
vit-base-patch16-224-ethos-8	vit-base-patch16-224-ethos-data
vit-base-patch16-224-ethosrealdata	vit-base-patch16-224-fatigue
vit-base-patch16-224-finalterm	vit-base-patch16-224-finetuned
vit-base-patch16-224-finetuned-barkley	vit-base-patch16-224-finetuned-brain-tumor-classification
vit-base-patch16-224-finetuned-Brain-Tumor-Classification	vit-base-patch16-224-finetuned-cassava-leaf-disease
vit-base-patch16-224-finetuned-cedar	vit-base-patch16-224-finetuned-cifar10
vit-base-patch16-224-finetuned-combinedSpiders	vit-base-patch16-224-finetuned-context-classifier
vit-base-patch16-224-finetuned-covid__ct__set__full	vit-base-patch16-224-finetuned-covid__ct__set__resumed
vit-base-patch16-224-finetuned-crochets-clothes	vit-base-patch16-224-finetuned-dangerousSpiders
vit-base-patch16-224-finetuned-eurosat	vit-base-patch16-224-finetuned-feature-maps-v3
vit-base-patch16-224-finetuned-feature-map-v2	vit-base-patch16-224-finetuned-fibre
vit-base-patch16-224-finetuned-flower	vit-base-patch16-224-finetuned-flower-classify
vit-base-patch16-224-finetuned-flowers	vit-base-patch16-224-finetuned-food101
vit-base-patch16-224-finetuned-food102	vit-base-patch16-224-finetuned-foveated-features
vit-base-patch16-224-finetuned-foveated-features-v2	vit-base-patch16-224-finetuned-galaxy10-decals
vit-base-patch16-224-finetuned-hateful-meme-restructured	vit-base-patch16-224-finetuned-hateful-meme-restructured-balanced
vit-base-patch16-224-finetuned-imagegpt	vit-base-patch16-224-finetuned-ind-17-imbalanced-aadhaarmask
vit-base-patch16-224-finetuned-ind-17-imbalanced-aadhaarmask-new-parameter	vit-base-patch16-224-finetuned-landscape-test
vit-base-patch16-224-finetuned-lora-oxford-pets	vit-base-patch16-224-finetuned-masked-hateful-meme-restructured
vit-base-patch16-224-finetuned-noh	vit-base-patch16-224-finetuned-original-images
vit-base-patch16-224-finetuned-pneumonia-detection	vit-base-patch16-224-finetuned-polyterrasse
vit-base-patch16-224-finetuned-skin	vit__base__patch16__224-finetuned-SkinDisease
vit-base-patch16-224-finetuned-teeth__dataset	vit-base-patch16-224-finetuned-trash-classifications-albumentations
vit-base-patch16-224-finetuned-turquoise	vit-base-patch16-224-finetuned-Visual-Emotional
vit-base-patch16-224-finetuned-vit	vit-base-patch16-224-finetune__test
vit-base-patch16-224-food101-16-7	vit-base-patch16-224-food101-24-12
vit-base-patch16-224-for-pre__evaluation	vit-base-patch16-224-fruits-360-16-7
vit-base-patch16-224-high-vit	vit-base-patch16-224-jvadlamudi2
vit-base-patch16-224-masaratti	vit-base-patch16-224-mascotas
vit-base-patch16-224-mascotas-DA	vit-base-patch16-224-MSC-dmae
vit-base-patch16-224-newly-trained	vit-base-patch16-224-oxford-pets-classification
vit-base-patch16-224-perros-y-gatos	vit-base-patch16-224-pure-ViT
vit-base-patch16-224-R1-10	vit-base-patch16-224-R1-40
vit-base-patch16-224-Rado__5	vit-base-patch16-224__rice-disease-02
vit-base-patch16-224__rice-leaf-disease-augmented__fft	vit-base-patch16-224__rice-leaf-disease-augmented__tl
vit-base-patch16-224__rice-leaf-disease-augmented-v4__fft	vit-base-patch16-224__rice-leaf-disease-augmented-v4__tl
vit-base-patch16-224__rice-leaf-disease-augmented-v4__v5__fft	vit-base-patch16-224__rice-leaf-disease-augmented-v4__v5__pft
vit-base-patch16-224-rotated-dungeons-v101	vit-base-patch16-224-rotated-dungeons-v103
vit-base-patch16-224-RU2-10	vit-base-patch16-224-RU2-40
vit-base-patch16-224-RU3-10	vit-base-patch16-224-RU3-40
vit-base-patch16-224-RU4-10	vit-base-patch16-224-RU4-40
vit-base-patch16-224-RU5-10	vit-base-patch16-224-RU5-10-8
vit-base-patch16-224-RU5-40	vit-base-patch16-224-RU9-24
vit-base-patch16-224-RX1-24	vit-base-patch16-224-RX2-12
vit-base-patch16-224-RXL1-24	vit-base-patch16-224-type
vit-base-patch16-224-U6-10	vit-base-patch16-224-U7-10
vit-base-patch16-224-U8-10	vit-base-patch16-224-U8-10b
vit-base-patch16-224-U8-10c	vit-base-patch16-224-U8-40
vit-base-patch16-224-U8-40b	vit-base-patch16-224-U8-40c
vit-base-patch16-224-U8-40d	vit-base-patch16-224-ve-b-U10-12
vit-base-patch16-224-ve-b-U10-24	vit-base-patch16-224-ve-b-U10-40
vit-base-patch16-224-ve-U10-12	vit-base-patch16-224-ve-U10-24
vit-base-patch16-224-ve-U11-12	vit-base-patch16-224-ve-U11-b-24
vit-base-patch16-224-ve-U11-b-40	vit-base-patch16-224-ve-U11-b-80
vit-base-patch16-224-ve-U12-b-24	vit-base-patch16-224-ve-U12-b-80
vit-base-patch16-224-ve-U13-b-120	vit-base-patch16-224-ve-U13-b-24
vit-base-patch16-224-ve-U13-b-80	vit-base-patch16-224-ve-U13b-80R
vit-base-patch16-224-ve-U13b-80RX	vit-base-patch16-224-ve-U13b-80RX1
vit-base-patch16-224-ve-U13b-80RX3	vit-base-patch16-224-ve-U13b-R
vit-base-patch16-224-ve-U14-b-24	vit-base-patch16-224-ve-U15-b-80
vit-base-patch16-224-ve-U16-b-80	vit-base-patch16-224-ve-Ub
vit-base-patch16-224-vit	vit-base-patch16-224-vit-base-patch16-224-vit-base-patch16-224-dogORnot
vit-base-pets	vit-base-PICAI
vit-base-seed-1e-4	vit-base-seed-3e-4
vit-base-travel-document-classification	vit-base-v1-eval-epoch-maxgrad-decay-cosine
vit-beans-classifier	vit-beta1-0.85
vit-beta1-0.88	vit-beta1-0.95

vit-beta2-0.99	vit-beta2-0.995
vit-beta2-0.9995	vit-bird
ViT__bloodmnist	ViT__bloodmnist__std__0
ViT__bloodmnist__std__15	ViT__bloodmnist__std__30
ViT__bloodmnist__std__45	ViT__bloodmnist__std__60
ViT__breastmnist	ViT__breastmnist__std__0
ViT__breastmnist__std__15	ViT__breastmnist__std__30
ViT__breastmnist__std__45	ViT__breastmnist__std__60
VIT-cats-vs-dogs	vit-cifar10-fine-tuned
vit-class-weight	vit-cxr4
vit-demo	ViT__dog__food
vit-dropout-0.2	vit-dropout-0.3
vit-dropout-0.4	vit-dropout-0.5
vit-ds-processed	vit-emotion-model
vit-epsilon-1e-7	vit-epsilon-1e-9
vit-epsilon-5e-9	vit-face-project-piyush
vit-fine-tune-classification-cats-vs-dogs	vit-finetuned-1
vit-food-classification-chrisis2	vit-geometric-shapes-base
vit-google-model-30-classes	vit__google__vehicle__classification__model
vit-historical-page	vit__Liveness__detection__v1.0
vit-lr-0.0001	vit-lr-0.001
vit-lr-0.01	vit-lr-cosine-restarts
vit-lr-cosine-warm-restarts	vit-lr-cosine-warmup
vit-lr-exponential	vit-lr-inverse-sqrt
vit-lr-linear	vit-lr-poly
vit-lr-reduce-plateau	vit-lr-step
vit-mae-base-finetuned-eurosat	vit-molecul
vit-ori-dataset-exp	vit-plant-classification
vit-plantnet300k	vit-plants
vit-real-fake-classification-v1	vit-real-fake-classification-v2
vit-real-fake-classification-v3	vit-real-fake-classification-v4
vit-skin-demo-v1	vit-skin-demo-v2
vit-skin-demo-v3	vit-skin-demo-v4
vit-skin-demo-v5	vit-spam
vit-sports-cls	vit-transfer-learning
vit__transformer__eye__disease	vit__tumor__classifier
vit-vit	vit-vit-base-patch16-224-finetuned-chest
vit-weight-decay-1e-2	vit-weight-decay-1e-3
vit-weight-decay-1e-4	vit-weight-decay-1e-5
wmc__v2__vit__base__wm811k__cls__contra__learning__0916	wmc__v2__vit__base__wm811k__cls
wmc-wmk811-v0-vit-special__map__det__0917	WS800__ViT__42820348
WS800__ViT__42895082	xraynewww
yet-another-amber-mines	zdravJEM__CV__BERT



Figure 15: Layerwise Eigenvalue Plots of 500 ViT models.

Universal LLaMA3-8B Experiment Details To further stress-test our universal subspace hypothesis on classical weight matrices, we extract a shared subspace from approximately 50 fine-tuned LLaMA3 models, each with 8 billion parameters. These models were obtained from publicly available repositories on HuggingFace. Due to their scale, we do not apply any model selection

or filtering, and instead include the entire available set - we may also use compatible layers from slightly different model architectures.

As shown in Figure 16, which presents the aggregated scree plot across all layers and all 50 models, the principal variance is concentrated in the top few components—consistent with the emergence of a low-rank universal subspace. For reference, the plot displays only the top 300 components, which represent a small fraction of the full rank, highlighting the inherently low-dimensional structure.

The models included in this analysis span a diverse range of domains, including medical applications, multilingual dialogue systems, and general-purpose assistants, as listed in Table 14. To the best of our knowledge, this is the first work to demonstrate that such a large and heterogeneous collection of high-capacity language models can be jointly represented within a single low-rank subspace.

The layerwise spectral analysis, shown in Figure 17, corroborates this finding: across all layers, the majority of eigenvalues fall below a threshold of < 0.001, indicating that most directions in parameter space contribute negligibly to variation across models. The plots are cropped to show only the leading components due to the large number of total dimensions. We recommend zooming in for clearer visualization.

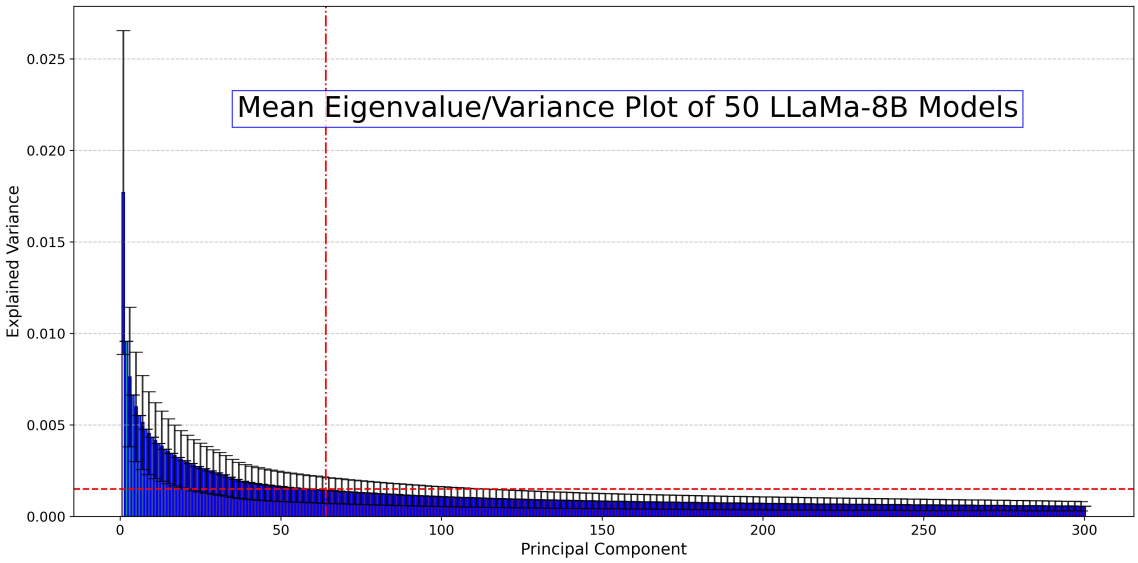


Figure 16: Spectral analysis of 50 LLaMA-3-8B model: Aggregated eigenvalue (scree) plot across 50 LlaMa-8B models and all layers. The plot demonstrates that the majority of the variance is consistently captured by few top principal directions, indicating the presence of a shared low-dimensional universal subspace.

Universal GPT-2 Experiment Details We analyze 177 public GPT-2 checkpoints over 49 matrix layers, listed in Table 15. These checkpoints cover multilingual, summarization, classification, and domain-specialized finetunes, making them a heterogeneous full-weight language-model pool. We use about 200 models for Figure 1.

Table 14: Models from HuggingFace used for the Universal LlaMa3-8B subspace extraction

Meta-Llama-3-8B-Instruct-Jailbroken	Llama-3-13B-Instruct	large_crafting_sft_success	suzume-llama-3-8B-multilingual
summary-llama3-8b-f16-full	Llama-3-13B-Instruct-v0.1	Llama-3-8B-ProLong-64k-Base	LLaMAntino-3-ANITA-8B-Inst-DPO-ITA
ai-medical-model-32bit	filtered_crafting_train_data_shorter_length	Llama-3-portuguese-Tom-cat-8b-instruct	Llama-3-MAAL-8B-Instruct-v0.1
Human-Like-LLama3-8B-Instruct	LLaMA-3-8B-Instruct-TR-DPO	CabraLlama3-8b	chartgpt-llama3
KoLlama-3-8B-Instruct	honeypot-llama3-8B	Llama-SEA-LION-v2-8B	TR
Llama3-8B-Instruct-Turkish-Finetuned	Llama-3-15B-Instruct-zeroed	Llama-3-8B-Instruct-TAR-Bio-v2	Bio-Medical-Llama-3-8B
filtered_construction_train_data	shisa-v1-llama3-8b	REFUEL-Llama-3-Armo-iter_1	llama3-instrucTrans-enko-8b
Llama-3-8B-Instruct-Ja	llama3-passthrough-chat	RoLlama3-8b-Instruct	Lloro-SQL
Summary_L3_1000steps_1e7rate_SFT2	CyberSentinel	Meta-Llama-3-8B-Instruct-function-calling-json-mode	MARS
Llama-3-8B-Instruct-Finance-RAG	LLaMA3-Instruct-8B-FR-Spec	Llama-3-8B-Japanese-Instruct	Llama3-8B-Chinese-Chat
llama-3-chinese-8b-instruct-v2	Athene-RM-8B	Llama-3-OffsetBias-RM-8B	large_cooking_sft_success
suzume-llama-3-8B-japanese	llama-3-chinese-8b-instruct-v3	Waktaverse-Llama-3-KO-8B-Instruct	llama-3-8b-gpt-4o-ru1.0
Llama-3-Aplite-Instruct-4x8B-MoE	Llama-3-8B-Instruct-DPO-v0.3		

Table 15: Models from HuggingFace used for the GPT-2 subspace extraction

openai-community/gpt2	pierreguillou/gpt2-small-portuguese
ai-forever/rugpt3small_based_on_gpt2	uer/gpt2-chinese-cluecorpussmall
axtonyao/gpt2-fp16-tflite	Xenova/gpt2
tensorblock/rakeshkiriyath_gpt2Medium_text_to_sql-GGUF	13on/gpt2-wishes
13onn/gpt2-wishes-2	13onnn/gpt2-wish
3koozy/gpt2-HxH	850886470/xxy_gpt2_chinese
AAli/gpt2-wikitext2	ARCYVILK/gpt2-bot
Akash7897/gpt2-wikitext2	Aleksandar1932/gpt2-country
Aleksandar1932/gpt2-hip-hop	Aleksandar1932/gpt2-pop
Aleksandar1932/gpt2-rock-124439808	Aleksandar1932/gpt2-soul
Aleksandar1932/gpt2-spanish-classics	Azaghast/GPT2-SCP-ContainmentProcedures
Azaghast/GPT2-SCP-Descriptions	Azaghast/GPT2-SCP-Miscellaneous
BenDavis71/GPT-2-Finetuning-AIRaid	BhanuSama/gpt2-finetuned-xsum
BigSalmon/GPT2HardandEasy	Chaewon/mnmt_decoder_en_gpt2
Chakita/gpt2_mwp	CoffeeAddict93/gpt2-call-of-the-wild
CoffeeAddict93/gpt2-modest-proposal	ComCom/gpt2
ComCom-Dev/gpt2-bible-test	DHBaek/gpt2-stackoverflow-question-contents-generator
DeepESP/gpt2-spanish	Enes3774/gpt2
Eren/gpt-2-small-the-office	Eunooeh/mnmt_gpt2
Fabby/gpt2-english-light-novel-titles	Ferch423/gpt2-small-portuguese-wikipediabio
Finnish-NLP/gpt2-finnish	Forest/gpt2-fanfic
GHP/gpt2-fine-tuned	Galuh/id-journal-gpt2
Gantenbein/ADDI-CH-GPT2	Gantenbein/ADDI-DE-GPT2
Gantenbein/ADDI-FI-GPT2	Gantenbein/ADDI-FR-GPT2
Gantenbein/ADDI-IT-GPT2	Graphcore/gpt2-medium-ipu
Graphcore/gpt2-small-ipu	GroNLP/gpt2-small-dutch-embeddings
GroNLP/gpt2-small-dutch	GroNLP/gpt2-small-italian-embeddings
GroNLP/gpt2-small-italian	HamidRezaAttar/gpt2-product-description-generator
HooshvareLab/gpt2-fa-comment	HooshvareLab/gpt2-fa-poetry
HooshvareLab/gpt2-fa	Iacopo/Shakespear-GPT2
Inkdrop/gpt2-property-classifier	JaidevShriram/gpt2-wikitext2
JasonCheung/gpt2	Jipski/gpt2-Flo-BasBoettcher-Chefkoch
Jipski/gpt2-Flo-BasBoettcher	Jipski/gpt2-FloSolo
Kup/gpt2-wikitext2	Langame/gpt2-starter-2
Langame/gpt2-starter	Langame/gpt2-waiting
Luciano/gpt2-small-portuguese-finetuned-peticoes	Luciano/gpt2-small-portuguese-finetuned-tcu-acordaos
MYX4567/gpt2-wikitext2	Madhour/gpt2-eli5
Mamatha/agri-gpt2	Mary222/GPT2_RU_GAME
Mary222/GPT2_standard	Masdfasdg/GPT2-Prompt
Micky/gpt2-wikitext2	MickyMike/0-GPT2SP-appceleratorstudio
MickyMike/0-GPT2SP-aptanastudio	MickyMike/0-GPT2SP-bamboo
MickyMike/0-GPT2SP-clover	MickyMike/0-GPT2SP-datamanagement
MickyMike/0-GPT2SP-duracloud	MickyMike/0-GPT2SP-jirasoftware
MickyMike/0-GPT2SP-mesos	MickyMike/0-GPT2SP-moodle
MickyMike/0-GPT2SP-mule	MickyMike/0-GPT2SP-mulestudio
MickyMike/0-GPT2SP-springxd	MickyMike/0-GPT2SP-talenddataquality
MickyMike/0-GPT2SP-talendesb	MickyMike/0-GPT2SP-titanium
MickyMike/0-GPT2SP-usergrid	MickyMike/00-GPT2SP-appceleratorstudio-aptanastudio
MickyMike/00-GPT2SP-appceleratorstudio-titanium	MickyMike/00-GPT2SP-aptanastudio-titanium
MickyMike/00-GPT2SP-mesos-usergrid	MickyMike/00-GPT2SP-mule-mulestudio
MickyMike/00-GPT2SP-mulestudio-mule	MickyMike/00-GPT2SP-titanium-appceleratorstudio
MickyMike/00-GPT2SP-usergrid-mesos	MickyMike/000-GPT2SP-appceleratorstudio-mule
MickyMike/000-GPT2SP-appceleratorstudio-mulestudio	MickyMike/000-GPT2SP-clover-usergrid
MickyMike/000-GPT2SP-mule-titanium	MickyMike/000-GPT2SP-mulestudio-titanium
MickyMike/000-GPT2SP-talenddataquality-appceleratorstudio	MickyMike/000-GPT2SP-talenddataquality-aptanastudio
MickyMike/000-GPT2SP-talendesb-mesos	MickyMike/1-GPT2SP-appceleratorstudio
MickyMike/1-GPT2SP-aptanastudio	MickyMike/1-GPT2SP-bamboo
MickyMike/1-GPT2SP-clover	MickyMike/1-GPT2SP-datamanagement
MickyMike/1-GPT2SP-duracloud	MickyMike/1-GPT2SP-jirasoftware
MickyMike/1-GPT2SP-mesos	MickyMike/1-GPT2SP-moodle
MickyMike/1-GPT2SP-mule	MickyMike/1-GPT2SP-mulestudio
MickyMike/1-GPT2SP-springxd	MickyMike/1-GPT2SP-talenddataquality
MickyMike/1-GPT2SP-talendesb	MickyMike/1-GPT2SP-titanium

MickyMike/1-GPT2SP-usergrid	MickyMike/11-GPT2SP-appceleratorstudio-aptanastudio
MickyMike/11-GPT2SP-appceleratorstudio-titanium	MickyMike/11-GPT2SP-aptanastudio-titanium
MickyMike/11-GPT2SP-mesos-usergrid	MickyMike/11-GPT2SP-mule-mulestudio
MickyMike/11-GPT2SP-mulestudio-mule	MickyMike/11-GPT2SP-titanium-appceleratorstudio
MickyMike/11-GPT2SP-usergrid-mesos	MickyMike/111-GPT2SP-appceleratorstudio-mule
MickyMike/111-GPT2SP-appceleratorstudio-mulestudio	MickyMike/111-GPT2SP-clover-usergrid
MickyMike/111-GPT2SP-mule-titanium	MickyMike/111-GPT2SP-mulestudio-titanium
MickyMike/111-GPT2SP-talenddataquality-appceleratorstudio	MickyMike/111-GPT2SP-talenddataquality-aptanastudio
MickyMike/111-GPT2SP-talendesb-mesos	MickyMike/2-GPT2SP-appceleratorstudio
MickyMike/2-GPT2SP-aptanastudio	MickyMike/2-GPT2SP-bamboo
MickyMike/2-GPT2SP-clover	MickyMike/2-GPT2SP-datamanagement
MickyMike/2-GPT2SP-duracloud	MickyMike/2-GPT2SP-jirasoftware
MickyMike/2-GPT2SP-mesos	MickyMike/2-GPT2SP-moodle
MickyMike/2-GPT2SP-mule	MickyMike/2-GPT2SP-mulestudio
MickyMike/2-GPT2SP-springxd	MickyMike/2-GPT2SP-talenddataquality
MickyMike/2-GPT2SP-talendesb	MickyMike/2-GPT2SP-titanium
MickyMike/2-GPT2SP-usergrid	MickyMike/22-GPT2SP-appceleratorstudio-aptanastudio
MickyMike/22-GPT2SP-appceleratorstudio-titanium	MickyMike/22-GPT2SP-aptanastudio-titanium
MickyMike/22-GPT2SP-mesos-usergrid	MickyMike/22-GPT2SP-mule-mulestudio
MickyMike/22-GPT2SP-mulestudio-mule	MickyMike/22-GPT2SP-titanium-appceleratorstudio
MickyMike/22-GPT2SP-usergrid-mesos	MickyMike/222-GPT2SP-appceleratorstudio-mule
MickyMike/222-GPT2SP-appceleratorstudio-mulestudio	MickyMike/222-GPT2SP-clover-usergrid
MickyMike/222-GPT2SP-mule-titanium	MickyMike/222-GPT2SP-mulestudio-titanium
MickyMike/222-GPT2SP-talenddataquality-appceleratorstudio	MickyMike/222-GPT2SP-talenddataquality-aptanastudio
MickyMike/222-GPT2SP-talendesb-mesos	MickyMike/6-GPT2SP-appceleratorstudio
MickyMike/6-GPT2SP-aptanastudio	MickyMike/6-GPT2SP-bamboo
MickyMike/6-GPT2SP-clover	MickyMike/6-GPT2SP-datamanagement
MickyMike/6-GPT2SP-duracloud	MickyMike/6-GPT2SP-jirasoftware
MickyMike/6-GPT2SP-mesos	MickyMike/6-GPT2SP-moodle
MickyMike/6-GPT2SP-mule	MickyMike/6-GPT2SP-mulestudio
MickyMike/6-GPT2SP-springxd	MickyMike/6-GPT2SP-talenddataquality
MickyMike/6-GPT2SP-talendesb	MickyMike/6-GPT2SP-titanium
MickyMike/6-GPT2SP-usergrid	MickyMike/66-GPT2SP-appceleratorstudio-aptanastudio
MickyMike/66-GPT2SP-appceleratorstudio-titanium	MickyMike/66-GPT2SP-aptanastudio-titanium
MickyMike/66-GPT2SP-mesos-usergrid	MickyMike/66-GPT2SP-mule-mulestudio
MickyMike/66-GPT2SP-mulestudio-mule	MickyMike/66-GPT2SP-titanium-appceleratorstudio
MickyMike/66-GPT2SP-usergrid-mesos	MickyMike/666-GPT2SP-appceleratorstudio-mule

Universal Flan-T5 Experiment Details We collected Flan-T5 models fine-tuned on individual datasets from the GLUE (Wang et al., 2019) benchmark. The alpha diagnostic is strongest among the transformer families, retaining 179 layers with $q_{\text{all}} = 0.0224$ and $q_{\text{arch}} = 0.4850$. The 90% explained-variance setting yields 85.13% savings on analyzed matrix tensors, showing that the shared subspace remains compact even across task-specialized sequence-to-sequence finetunes. The suitability diagnostics use 196 Flan-T5 models, while the subspace analysis in Figure 1 uses the eight models listed below.

Table 16: Finetuned Flan-T5 Models from HuggingFace used for the Universal Flan-T5 subspace extraction

tanganke/flan-t5-base_glue-cola	tanganke/flan-t5-base_glue-mnli
tanganke/flan-t5-base_glue-mrpc	tanganke/flan-t5-base_glue-qnli
tanganke/flan-t5-base_glue-rte	tanganke/flan-t5-base_glue-qqp
tanganke/flan-t5-base_glue-sst2	tanganke/flan-t5-base_glue-stsb

B.7 Ablating number of models and subspace effectiveness

Although this is implicitly addressed through our large-scale experiments (500 ViTs, 500 Mistral-7B and 300 Stable Diffusion LoRAs, 50 LLaMA3-8B, 177 GPT-2s, Flan-T5, and ResNet50 models) in all Figures and Tables, which demonstrate consistent behavior at different scales. Theorem 3.7 provides insight into the saturation dynamics: the finite-task estimation error decreases at the standard $O(T^{-1/2})$ rate, up to logarithmic factors, where T is the number of available tasks. Thus, increasing the number of models improves the estimated shared subspace, with diminishing returns as T grows. In practice, the minimum number of models per architecture needed to achieve saturation point depends on the quality of the trained models, the diversity of data they have been trained on, and on the architecture itself. Ablating these would require access to all the data for all

Table 17: Lots of LoRAs (Mistral-7B) OOD evaluation per increasing number of models used to extract Universal Subspace

Method	**Model Number**	**Rouge-L Score**
Normal Model	-	73.7
Universal model	50	55.8
Universal model	150	66.1
Universal model	250	71.9
Universal model	450	72.3

the models, and very careful training on every training for each data, and then running permutation with all possible combinations of models. All of this is out of reach for most researchers simply due to time, data and compute constraints. We, however, do provide an initial ablation here. For LoRA models shown in Table 10, we choose 9 random (OOD) tasks (39 ,190 ,280 ,290 ,391 ,442 ,1342 ,1391 ,1598) and extract the Universal Subspace from rest of the tasks, sampled randomly for increasing number of models. The coefficients for OOD tasks are analytically reconstructed to effectively evaluate the universal subspace created from varying number of models. Table 17 shows that the adequate principal components are quickly extracted, and increasing the number of models has diminishing returns.

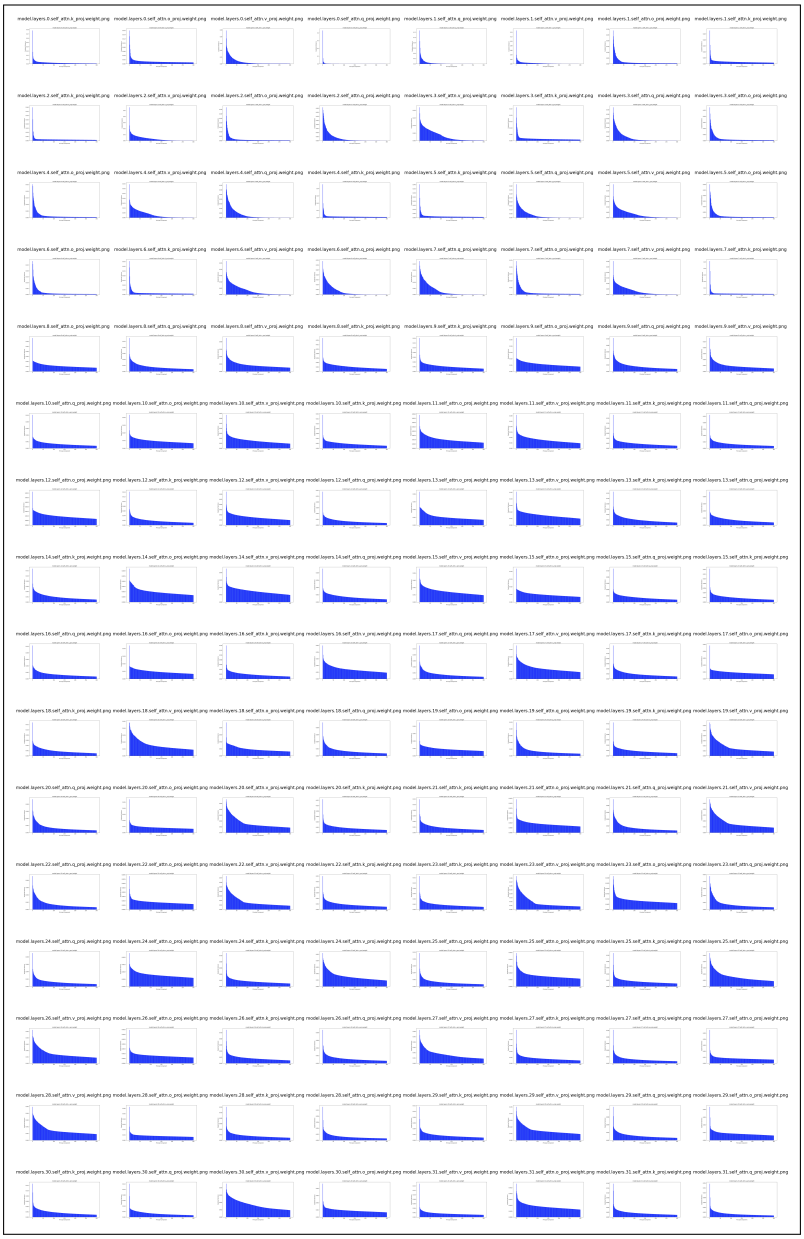


Figure 17: Layerwise Scree Plots for 50 LLaMA-3-8B Models. For enhanced clarity, each subplot presents a truncated view of the total possible principal directions. These plots consistently demonstrate that the dominant information, as represented by explained variance, resides within a small number of leading principal directions for all models. Components beyond this initial set are characterized by eigenvalues approaching zero, signifying their redundancy for the universal subspace.

C Appendix C

Table 18: Per-task results for eight ViT-B/32 models, each fine-tuned with LoRA on a different image-classification dataset. "Finetuned" reports the absolute accuracy of each task-specific model. For merging methods, we report per-task accuracy normalized by the corresponding fine-tuned model, together with the average across tasks.

Method	**Datasets**								**Avg.**
	Cars	**DTD**	**EuroSAT**	**GTSRB**	**MNIST**	**RESISC45**	**SUN397**	**SVHN**	
Per-Task Absolute Accuracies (%)									
Finetuned	74.0	58.3	99.0	92.7	99.3	88.4	64.5	96.2	84.1
Combined-Model Accuracy Normalized by Finetuned Accuracy (%)									
RegMean	80.2	71.3	37.9	47.3	43.1	70.5	93.9	43.0	60.9
TA	82.0	73.6	48.8	42.1	53.1	71.5	97.5	41.2	63.7
TIES	82.2	72.8	50.0	36.8	56.8	69.4	96.9	44.6	63.7
DARE-TIES	81.4	74.5	50.8	39.2	55.0	70.7	97.6	40.1	63.7
KnOTS-TIES	82.7	73.7	49.3	48.9	68.9	70.9	95.5	53.8	68.0
KnOTS-DARE-TIES	81.8	75.9	50.7	40.3	53.2	70.2	97.9	41.0	63.9
Ours	**88.1**	**82.3**	**65.9**	**61.3**	**88.3**	**98.1**	**98.5**	**85.1**	**83.5**

C.1 Related Work

Several lines of prior research support the core intuition behind our universal subspace hypothesis, though they do not provide a unified, scalable framework for identifying and leveraging such subspaces across architectures, tasks, and modalities. The Neural Tangent Kernel framework reinforces this idea, in the infinite-width limit, training dynamics are governed by a limiting kernel determined by the architecture and initialization distribution (Jacot et al., 2018). This result implies that training is implicitly constrained to a shared function space, suggesting the existence of low-dimensional structures that generalize across tasks. Complementing this, works in mechanistic interpretability has uncovered modular and recurring patterns that consistently re-emerge in independently trained models (Olah et al., 2020; Chughtai et al., 2023), supporting the notion of structural universality in network representations. The closest related work is (Kaushik et al., 2025), which investigates principal subspaces in low rank adapters for highly parameter efficient finetuning, and is an application of the universal subspace hypothesis presented in this work. Relatedly, Han et al. (2026) report that the functional energy of trained mixture-of-experts layers concentrates in a sharply low-rank subspace despite near-full-rank weights, and use this to add new tasks as low-rank slices of a fixed expert pool for continual multimodal multi-task learning.

While Mao et al. (2024) study low-dimensional structure in prediction space, we examine shared subspaces in model weights. Importantly, in contrast to the abstract, weak, or speculative notions of universality presented in earlier works like Chughtai et al. (2023); Olah et al. (2020) - which focus primarily on representations and are arguably easier to demonstrate due to direct data dependency - ours is the first work to provide concrete evidence and a clear universal hypothesis at the *neural parameter* level.

Empirical studies further strengthen this perspective. The lottery ticket hypothesis (Frankle & Carbin, 2019) demonstrates that overparameterized networks contain sparse subnetworks capable of matching full-model performance, implying that task-relevant information resides in a small,

structured subset of weights. Similarly, mode connectivity studies (Garipov et al., 2018) reveal that seemingly isolated optima in parameter space are often connected by low-loss paths. In convolutional models, Krizhevsky et al. (Krizhevsky et al., 2012) famously observed that early layers consistently learn Gabor-like filters, indicating a universal inductive bias in early representations. More recent works (Guth et al., 2024; Guth & Ménard, 2024) extends this observation to deeper layers, showing that certain eigendirections of trained convolutional layers recur across networks trained on different datasets.

While these studies are suggestive of shared structures in neural representations or parameters, they remain limited in their focus, application and analysis. Our work fills this critical gap by presenting a principled and empirically validated method for discovering and utilizing universal parametric subspaces that span across architectures, tasks, and modalities. By conducting large-scale spectral analyses of over large number of diverse architectures, models and tasks, we demonstrate that a small number of principal directions consistently capture the majority of task-relevant variation. We then operationalize these findings by developing a practical framework for reusing these subspaces for parameter-efficient finetuning, task adaptation, and model merging, achieving competitive performance while dramatically reducing memory and compute requirements.

C.2 Model Merging and Reuse via Universal Subspaces

We present this experiment as an illustration of model merging through shared subspaces and task-specific reuse. We extract common layer-wise bases and retain lightweight coefficients for each task, computed by projection. Evaluation uses the corresponding task's coefficients; these are not averaged or combined. This shared-basis representation is related to Brüel-Gabrielsson et al. (2024). Unlike the weight-merging baselines, our approach retains task-specific coefficients rather than producing one fixed set of weights for all tasks. Despite retaining task-specific coefficients, our shared representation can be smaller than a baseline merged model or even a single original model. A lightweight gating network or parameter could be trained to select the appropriate coefficients at inference, similar to the task-specific routers that select low-rank expert slices in Han et al. (2026); we leave this extension to future work.

C.3 Universal Subspace Analysis

Similar methodology is followed for subspace analysis for both LoRA and classical weight models. The same spectral methodology applies to both LoRA parameters and conventional weight tensors after aligning parameter shapes across models. We nevertheless evaluate both settings independently because their parameterizations and training mechanisms differ substantially. However, in order to solidify our universal subspace hypothesis, we conduct extensive experiments for both types of models. LoRA is chosen because of the recent spurt in the availability of LoRA models trained on diverse kinds of datasets and models. We do this universal subspace analysis on all weight parameters in every neural network layer except the first (or few initial) and last neural network layer. This is because these layers may differ across models due to differences in input shapes and types, loss functions, and the tasks being trained. We also focus our analysis on linear/fully-connected and matrix weights, as well as convolutional weights, as the analysis done on these are straightforward and the results observed can be extended to other types of neural parameters (Ma & Lu, 2017).

Secondary Subspace refers to the residual subspace that remains after removing the top k principal directions associated with the low-rank universal subspace. This subspace is orthogonal to the universal subspace and serves as a control for evaluating the uniqueness and effectiveness of the learned shared subspace. To make computation tractable when the residual subspace is high-dimensional, we focus on the top components beyond rank k, as computing a full SVD is often impractical. This approximation is justified, since the lower components typically capture noise, which has been shown to degrade performance (Sharma et al., 2023).

How to choose top k components? As shown in all eigenvalue (scree) plots, a trivial way to choose is a simple visual inspection, since we can see a discontinuity in the spectral analysis. Another way is to define a threshold on the explained variance, all components whose explained variance is close to zero $<.01$ are considered secondary subspace, and can be discarded. Singular-value thresholds derived for matrix denoising can also motivate heuristic rank selection for the matrix unfoldings used in HOSVD (Gavish & Donoho, 2014).

C.4 Finding universal subspaces and applying them to future tasks

In this section, we present two tasks, GLUE (Wang et al., 2019) and Image Classification. For each experiment, the joint subspace is created using all other models in subset. For Image Classification, we use $k = 4$ and train only 8 epochs using learning rate of 1e-4. Importantly, only the coefficients are trained for the experiment. It is important to note that our shared subspace model performs quite well despite using very few (4-5) models to extract the subspace. For GLUE, we use 16-32 components for our subspace, with learning rate of 4e-4, batch size of 64, and 30-80 epochs for each task. In addition, it is likely that our model might perform similarly or better if trained longer or with optimized hyperparameters.

Compute Resources We conduct all our experiments using a single A5000 GPU, and a CPU with 8 workers. For the universal subspace extraction, all calculation can be done on the CPU. However, GPU would increase the speed of calculation as the layerwise subspace extraction can be parallelized. Storage comparisons use same precision and for Universal Subspace model variants count the shared bases once together with all model-specific coefficients, excluding task-specific first and last layers from both representations.

C.5 Discussion and Broader Impact

Our findings suggest that deep neural networks trained across diverse tasks and modalities systematically converge to shared, low-dimensional subspaces within their parameter space. The existence of such universal subspaces challenges conventional assumptions about the independence and diversity of model and task-specific finetuning trajectories. Instead, it highlights a powerful regularity in the way deep models encode task-specific knowledge - one that can be exploited for significantly improved training and deployment efficiency. By leveraging these subspaces, we demonstrate that models can be adapted to new tasks by learning only a small number of coefficients, rather than retraining or storing full sets of weights. This facilitates more robust multi-task learning, model merging, and scalable fine-tuning, with theoretical guarantees and empirical validation across multiple architectures.

The broader societal impact of this work is substantial. Our approach enables large-scale models to be reused and extended with dramatically reduced computational overhead, addressing both the financial and environmental costs associated with training and deploying deep learning systems. This contributes directly to the goals of sustainable and accessible AI. By lowering the hardware and energy requirements for adaptation and inference, we empower under-resourced researchers, institutions, and communities to build upon state-of-the-art models without needing extensive compute infrastructure. Furthermore, by supporting modular model design and data-free model merging, our work lays the foundation for more interpretable, maintainable, and equitable AI systems.

C.6 Limitations and Future Work

Although we provide conclusive results towards the existence and utility of universal shared subspaces, the current analysis has scope for future research, such as limited interpretability of the shared subspace and the corresponding directions. While it is a critical area of research, it is extremely cumbersome to demonstrate interpretability of the principal directions for each layer of the network. To the best of our knowledge we are not aware of any other literature that performs such an in-depth analysis of the weight space of large models across diverse tasks, data modalities and model architectures. The current approach to approximating a universal subspace relies on pretrained task-specific models (predictors) for tasks, which may not be readily available for new tasks. An interesting direction for future research would be to explore model independent methods for learning a universal shared subspace, potentially derived directly from data. Furthermore, the conditions proposed in Ortiz-Jimenez et al. (2023) relate task arithmetic to localized kernel eigenfunctions. How these conditions interact with our shared weight-subspace formulation is unclear and warrants further investigation. As a result, performing task arithmetic within the current framework of a shared universal subspace is non-trivial and warrants further investigation. Our analysis also assumes that tasks are drawn i.i.d. from a fixed task distribution. Whether a shared subspace remains adequate under distribution shift, for example when novel classes appear while the distribution of known classes also changes (Chaudhari et al., 2026), is an open question.